

Electronics for the readout of segmented semiconductor radiation detectors with emphasis on X-ray detector systems

Part 1: Introduction to hybrid pixel detectors

Classification of technologies, limitations of hybrid pixel detectors

Part 2: Introduction to signal processing

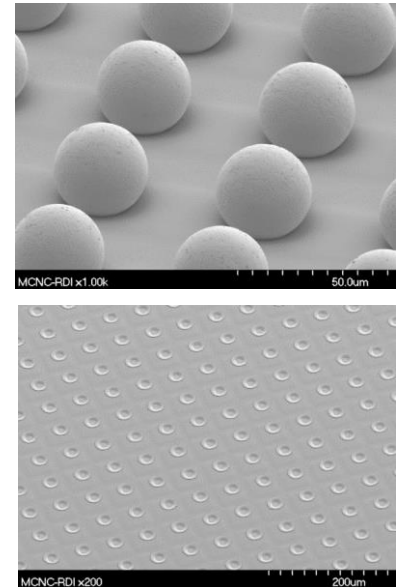
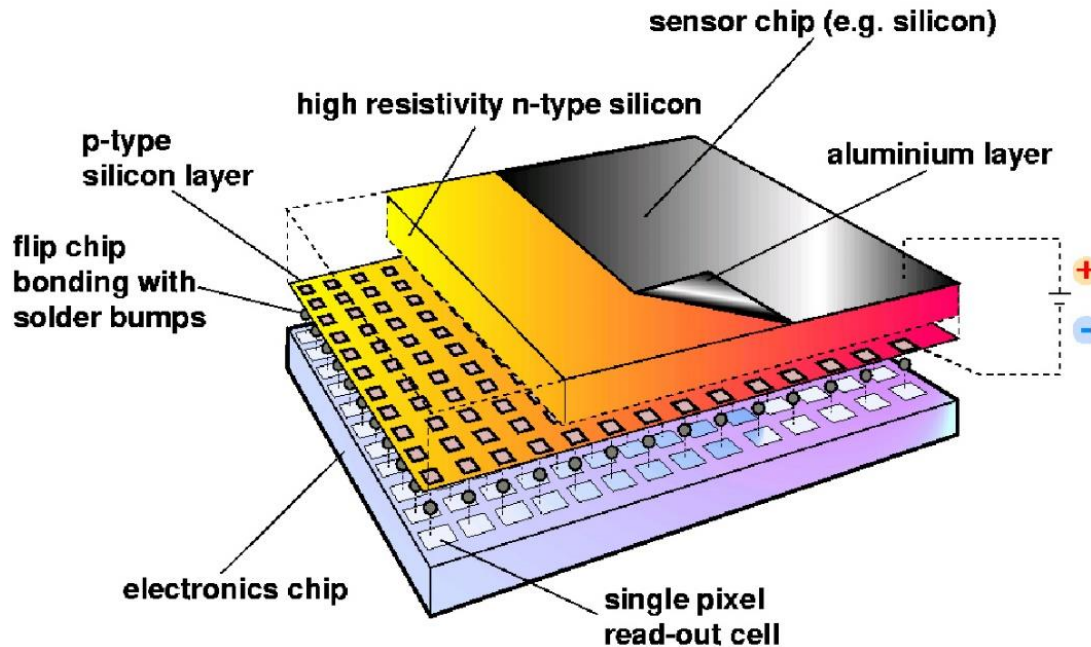
Part 3: Review of ASICs

Rafael Ballabriga Suñé

rafael.ballabriga@cern.ch

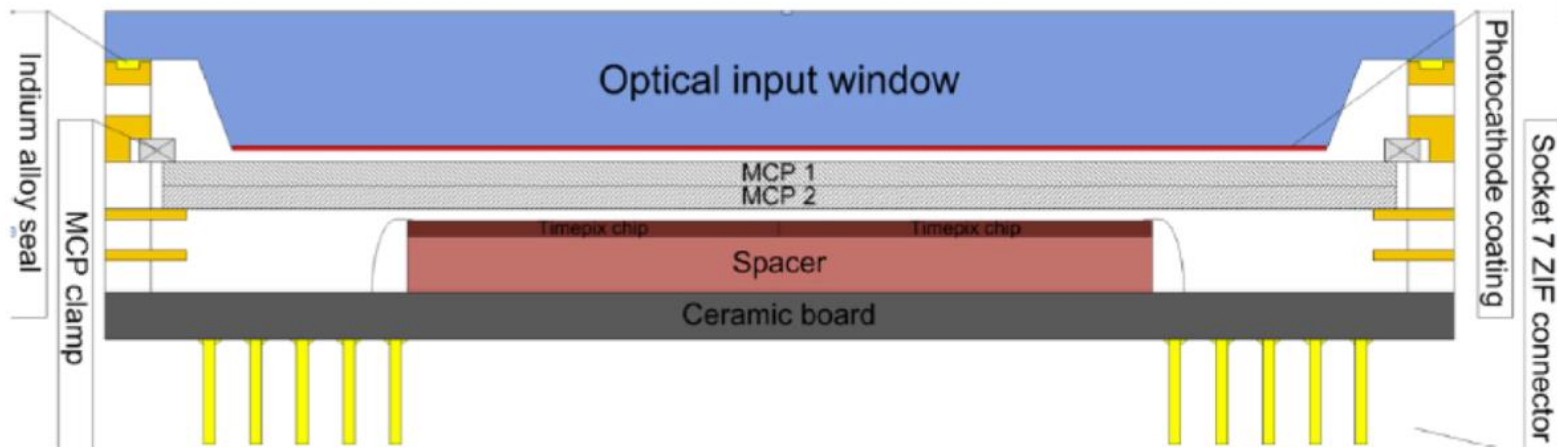
CERN Microelectronics Section

Semiconductor Hybrid Pixel Detectors



- A hybrid pixel detector is a 2-dimensional matrix of microscopic radiation-sensitive elements each of which is connected to its own pulse processing electronics.
- The sensor element and the readout electronics are implemented in different substrates i.e. can be optimized separately
 - Sensor material can be changed (Si, GaAs, CdTe)

Chips can be used to readout the signal from other detectors (e.g. MCP)



MCP-based systems can be used to detect visible light photons and soft X-rays (with photocathode) and electrons, ions or neutrons (when e.g. B doped)

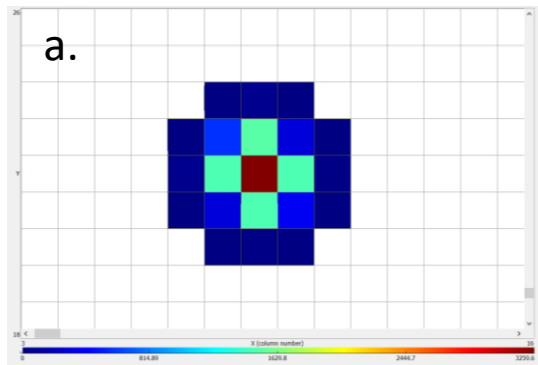
Measurements

Information from the incoming beam

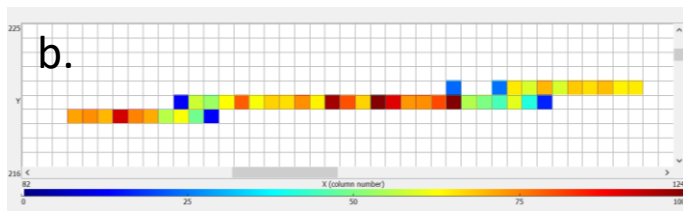
- The number of particles deposited during a given exposure time
- The energy deposited by an individual particle
- The time of arrival of the particle

Information from the incoming beam

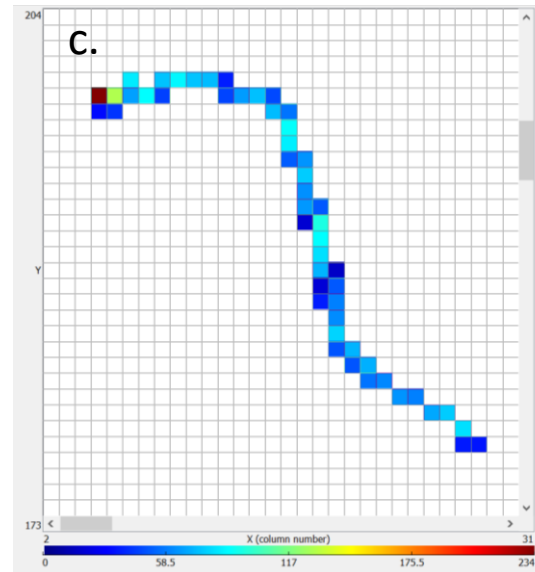
- The number of particles deposited during a given exposure time
- The energy deposited by an individual particle
- The time of arrival of the particle
- The incoming type of particle, based on the shape of the cluster of pixels responding to a single charge deposition event



~270μm



~2mm



~1.3mm

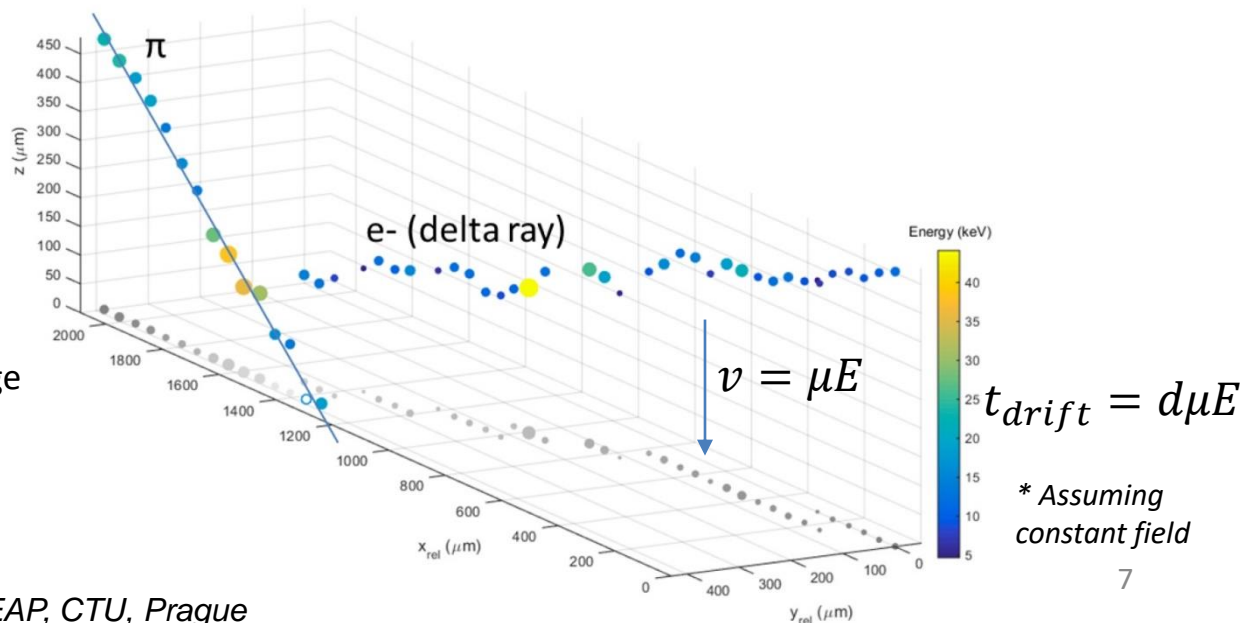
“Different particles have a different “signature” in their interaction with the detector material”

a. Alpha particle, b. Muon, c. Electron
Timepix data, 55 μm pixels

Information from the incoming beam

- The number of particles deposited during a given exposure time
- The energy deposited by an individual particle
- The time of arrival of the particle
- The incoming type of particle, based on the shape of the cluster of pixels responding to a single charge deposition event
- The angle of incidence of the incoming charged particle based on the difference in the induced signal time in the pixels

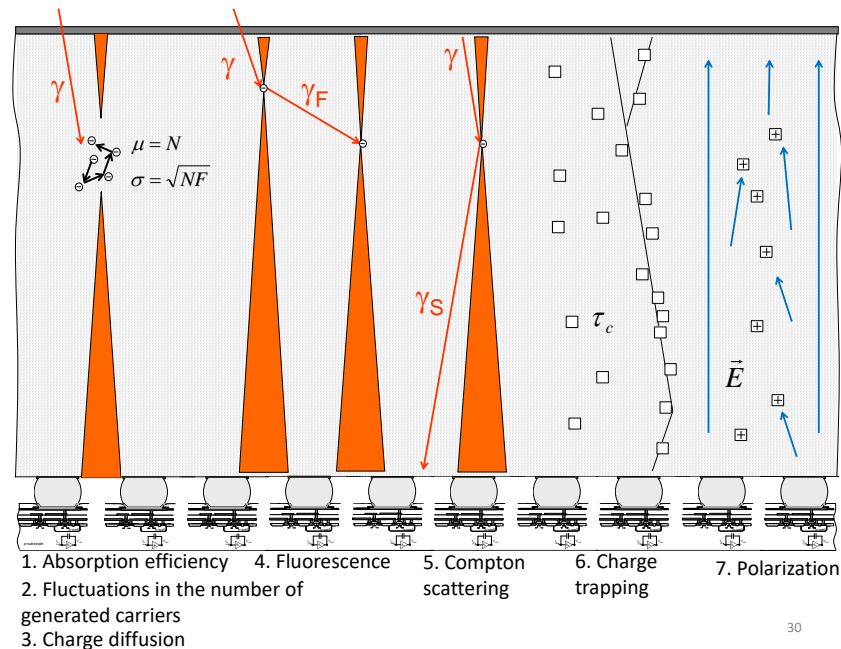
60 deg
p+ in n Si sensor, Timepix3
500 μ m thick
 $V_{\text{bias}} = 130\text{V}$
Colour (and diameter) indicate charge
Measured z resolution $\sim 50\mu\text{m}$



Outline

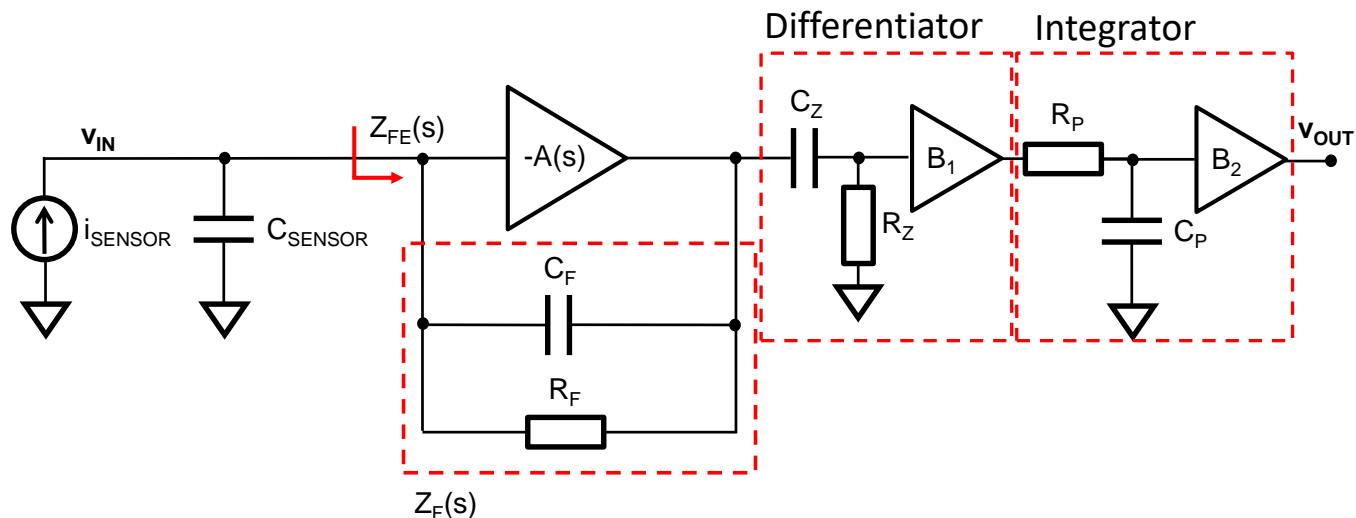
Part 1:

- Classification of X-ray detector systems
 - X-ray conversion
 - Signal processing
 - Detector geometry
- The ideal detector system
- Limiting factors in real systems



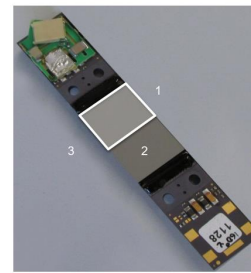
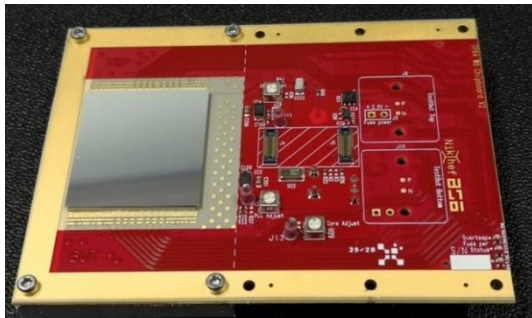
Part 2:

- Signal chain for readout electronics
- Sensor geometry modelling
- Preamplifier topologies
- The CSA/TIA
- Noise (basic introduction)
- Noise in the MOS transistor
- Noise in a cascade of amplifiers
- Transfer of noise sources to the output of the CSA
- Noise filtering
- CR-RC shaper

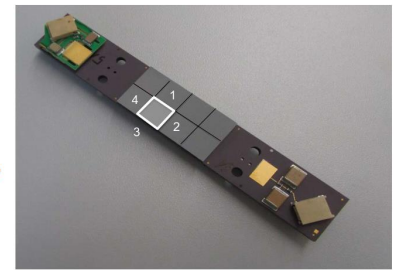


Part 3:

- Review of ASICs (full picture)
- Review of ASICs (details)
- Techniques for increasing the count rate
- Techniques for allowing spectroscopic information at fine pixel pitch
- Towards large area detectors
- Summary and conclusions



3 side buttable

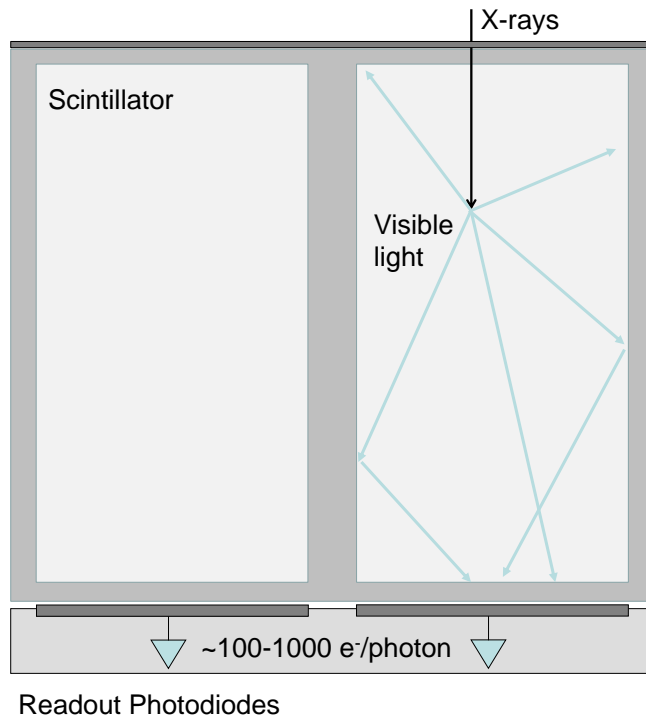


4 side buttable

Classification of detector systems: X-ray conversion to electrical signal

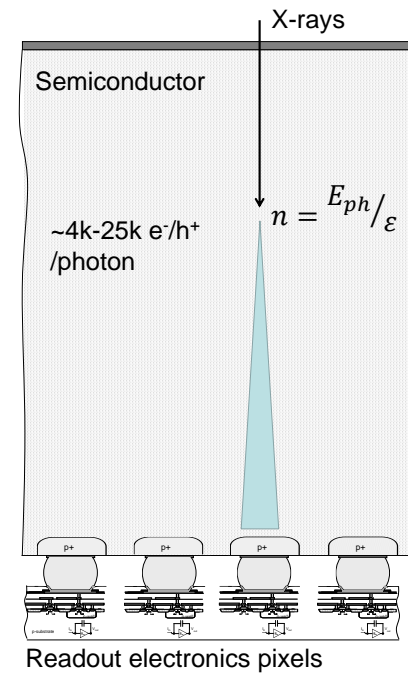
X-ray imaging technologies classification: conversion of X-rays

Indirect conversion



- 100-1000 e^- generated in the diode (Interaction depth dependent)
- Degraded energy and spatial resolution
- Cheaper

Direct Conversion

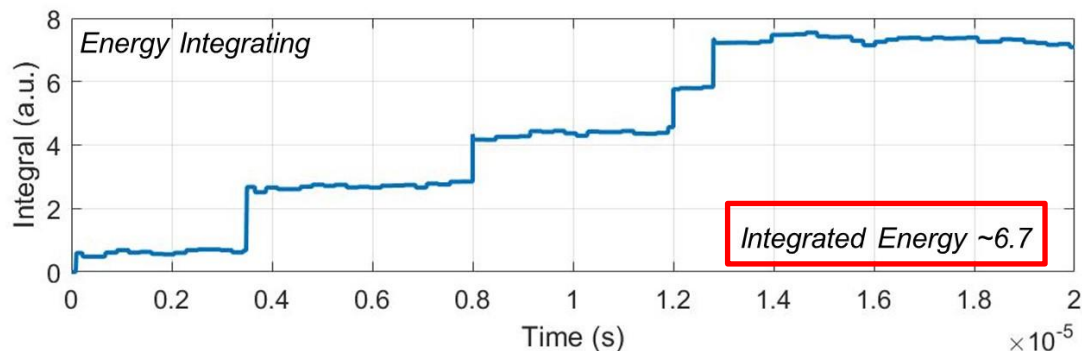
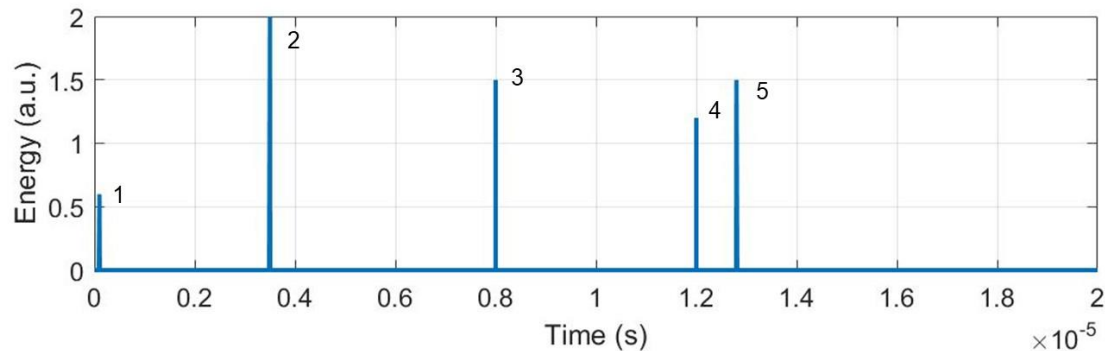


- 4000-25000 e^- induced (Medical radiography range) (reproducible)

Classification of detector systems: signal processing

Signal processing in the readout electronics: integrating vs pulse processing

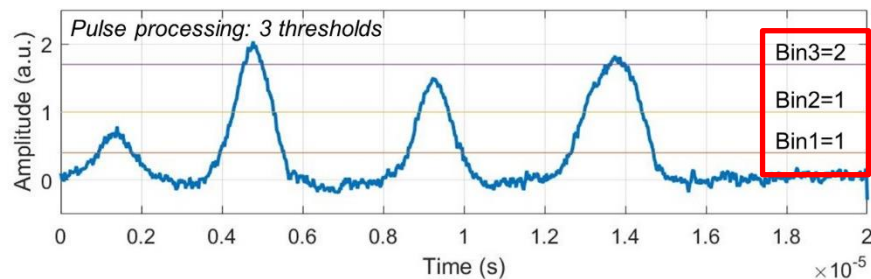
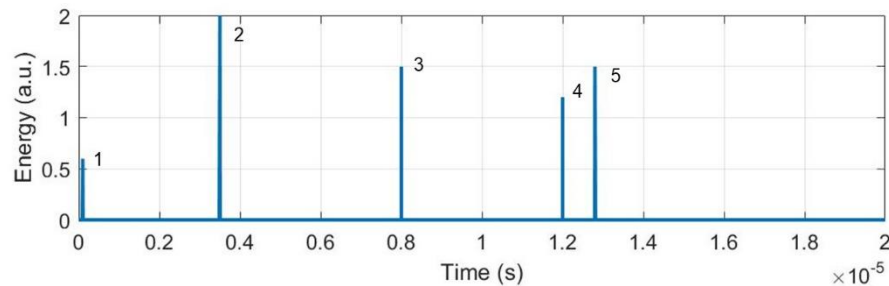
- Energy integration
 - The signal deposited in the sensor is integrated (together with the noise)
 - The weight of each photon in the image is proportional to its energy
 - The system does not suffer from pile up

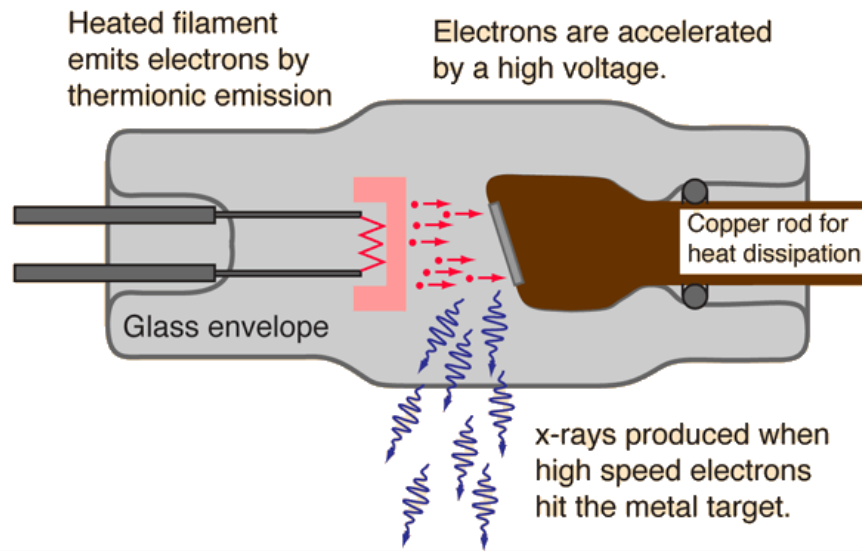


Signal processing in the readout electronics

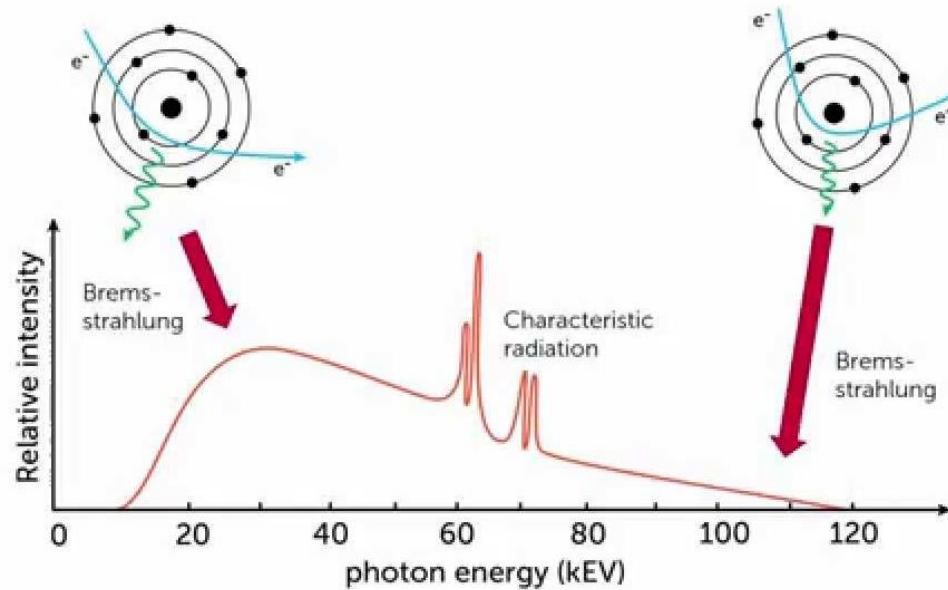
- Single Quantum Processing (*See presentation E. Heijne*)
 - Signal from each individual photon is treated on an event-by-event basis
 - Signal attributed to a particle only when it exceeds a threshold (suppression of random electronics noise)
 - Possible measurements: Particle hit, Energy (Amplitude/ToT), Time of Arrival
 - With one threshold level: The weight of each photon in the image is one (photon counting)
 - With multiple thresholds: Spectral imaging (energy resolved information)

Spectral photon
counting X-ray
imaging

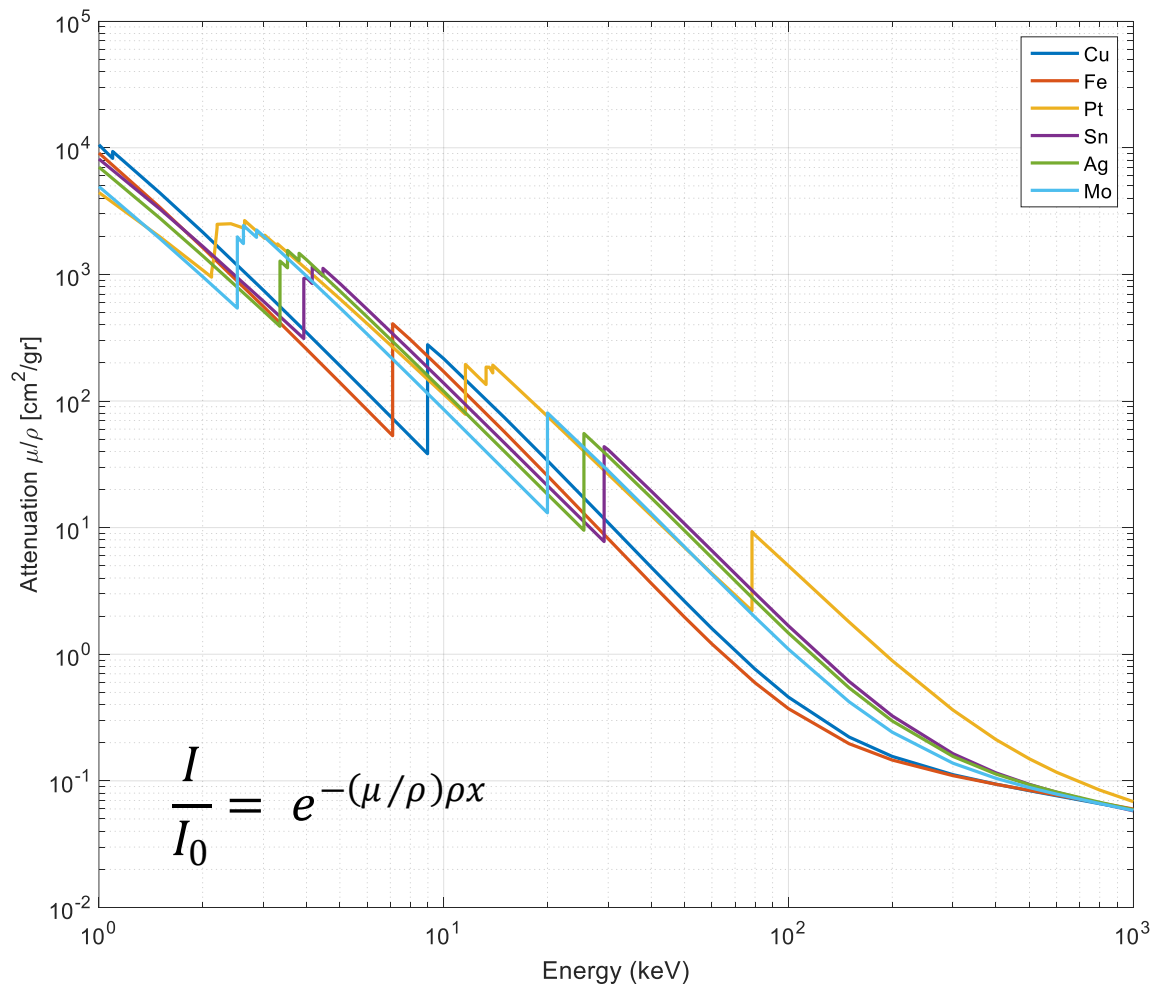




X-ray generation - spectrum

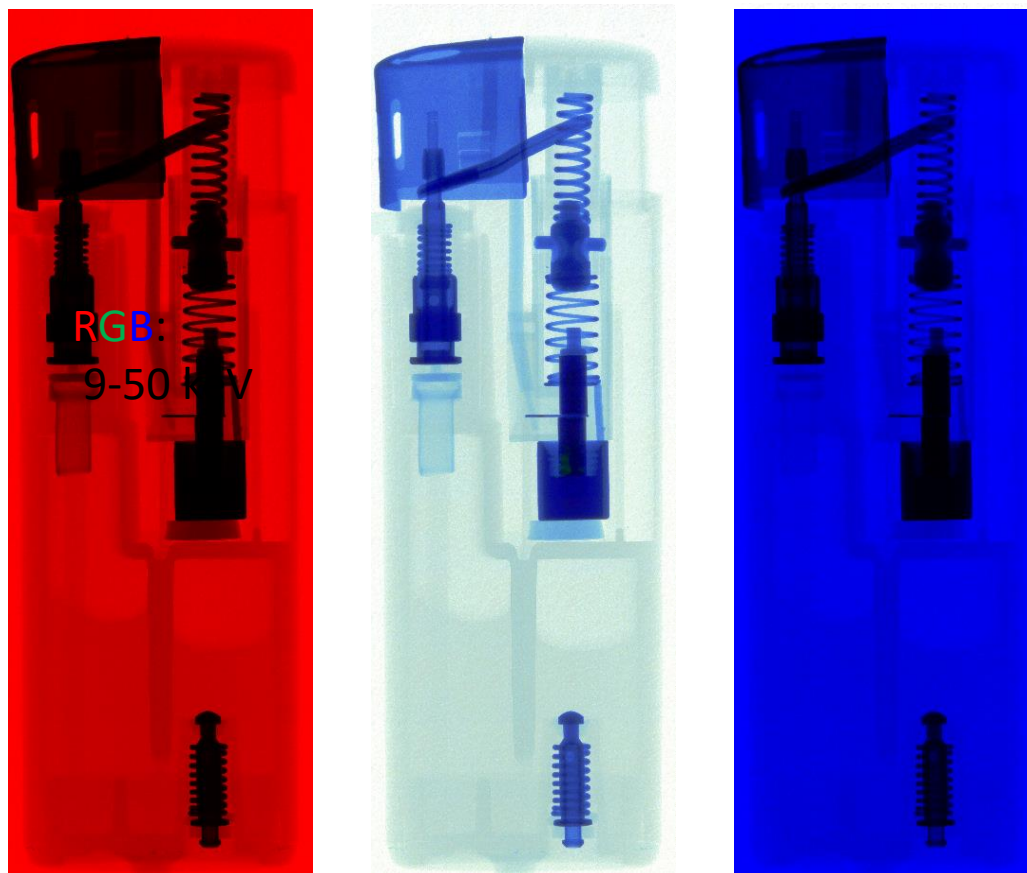


Due to the nature of how X-rays are generated in an X-ray tube, the beam that we obtain is polychromatic



$$\frac{I}{I_0} = e^{-(\mu/\rho)\rho x}$$

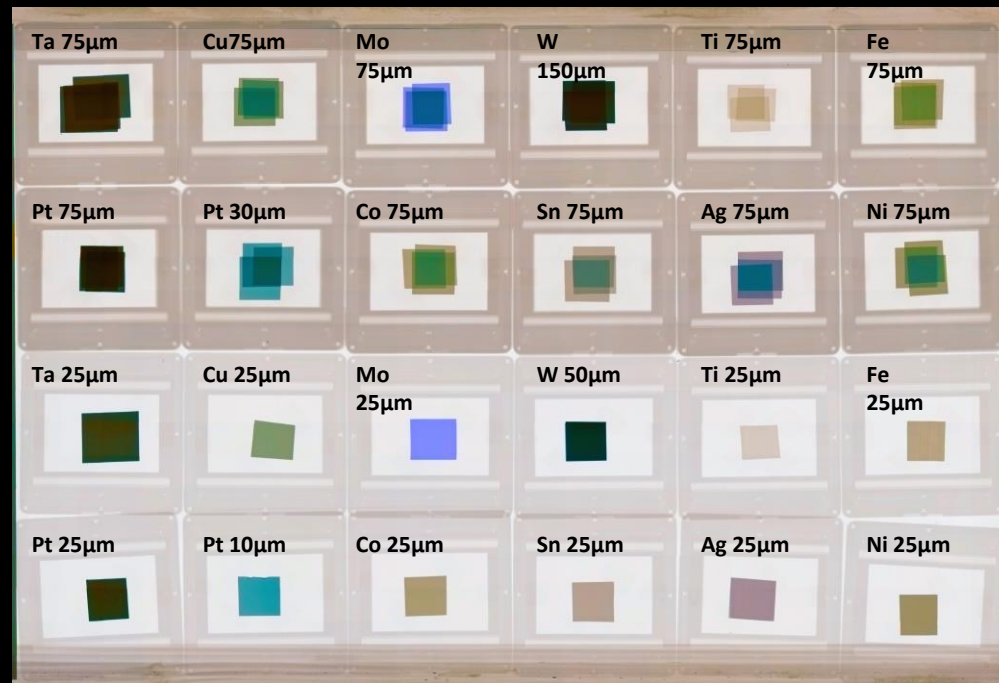
The energy dependent attenuation is a signature of a material



Courtesy: S. Procz et al.

Photons in different energy bins give complementary information

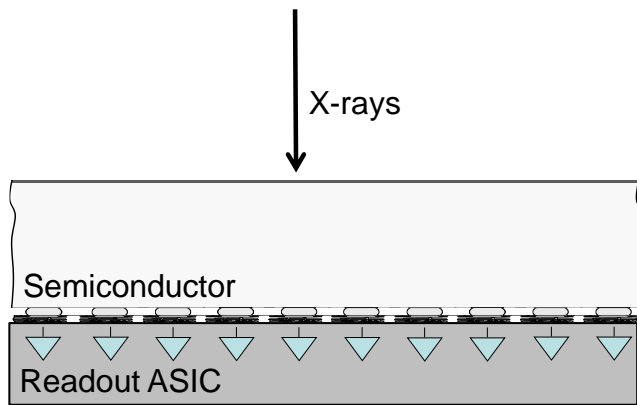
The regular vs “colour” X-ray imaging of test samples



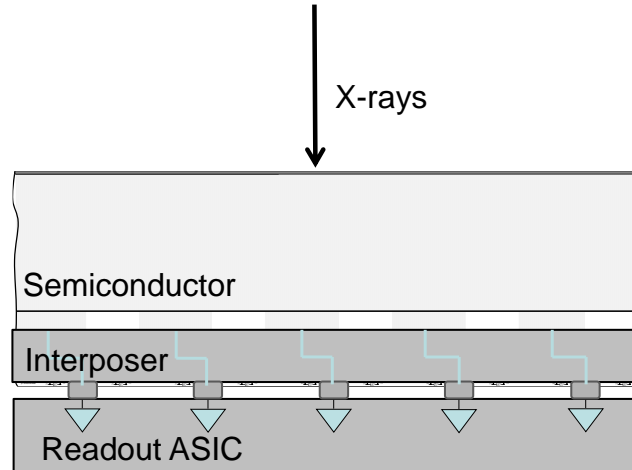
Sampling different sections of the polychromatic energy spectrum allows to identify materials in a sample

Classification of detector systems: geometry

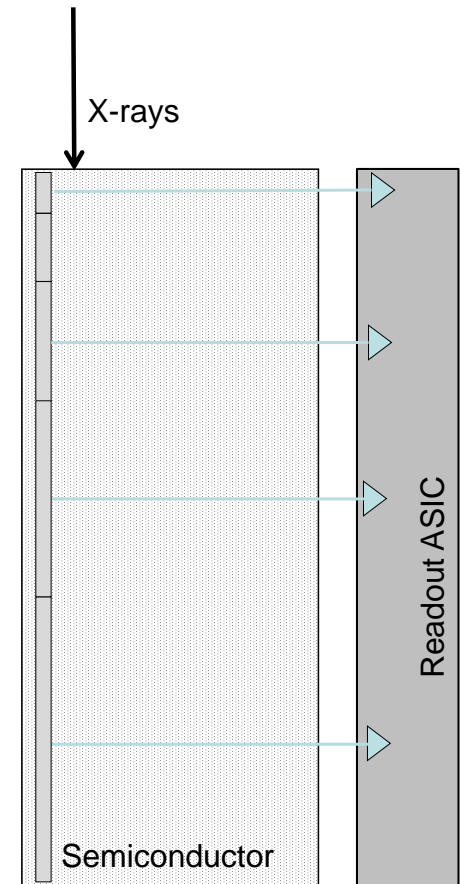
X-ray imaging direct conversion detectors geometry



Hybrid pixel detector (very fine interconnection <math><350\mu\text{m}</math>) (Face-on)



Connection of the semiconductor sensor material pixels to the ASIC through interposer (Face-on)



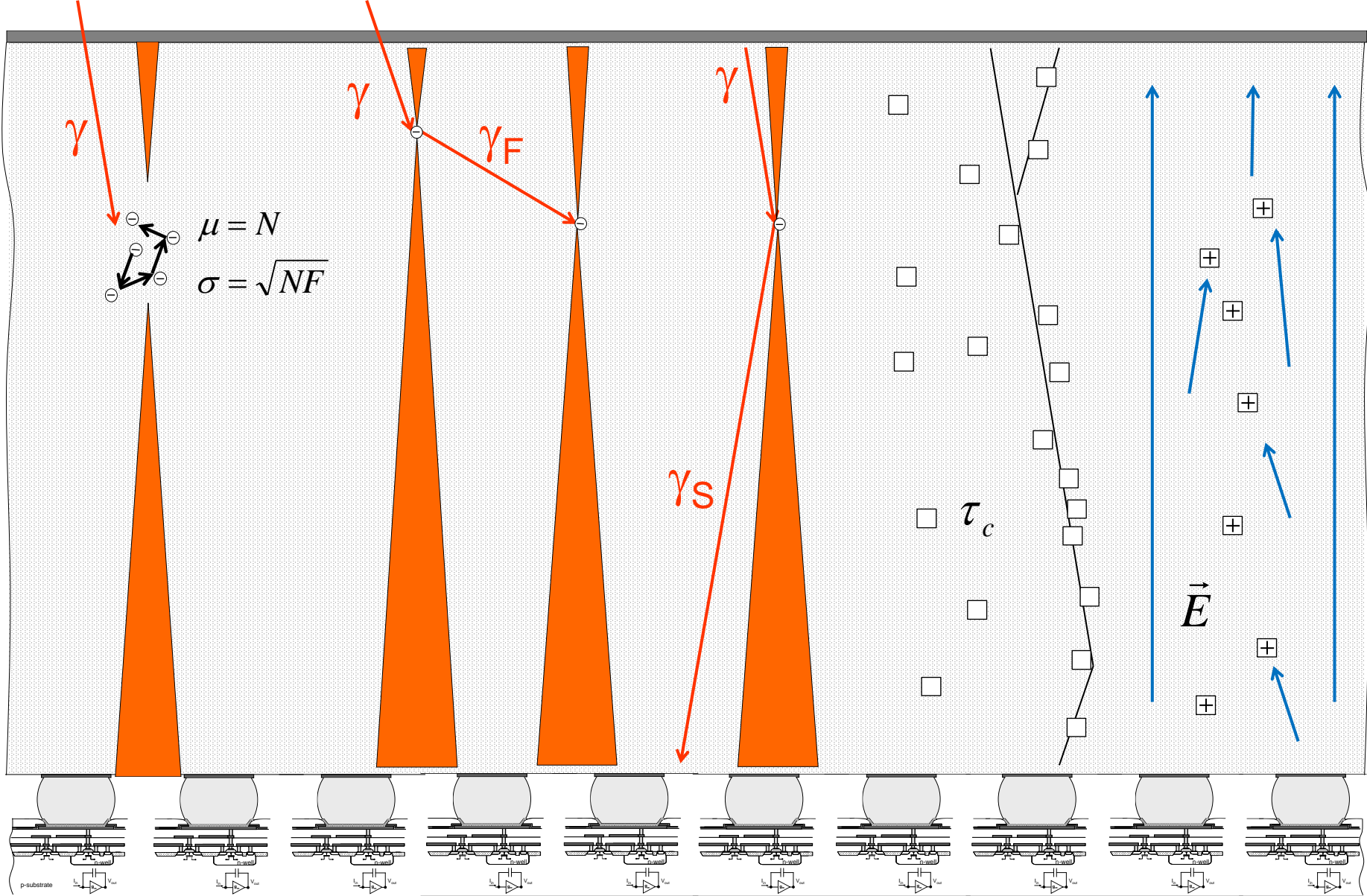
Edge-on configuration on micro strips

The ideal detector system

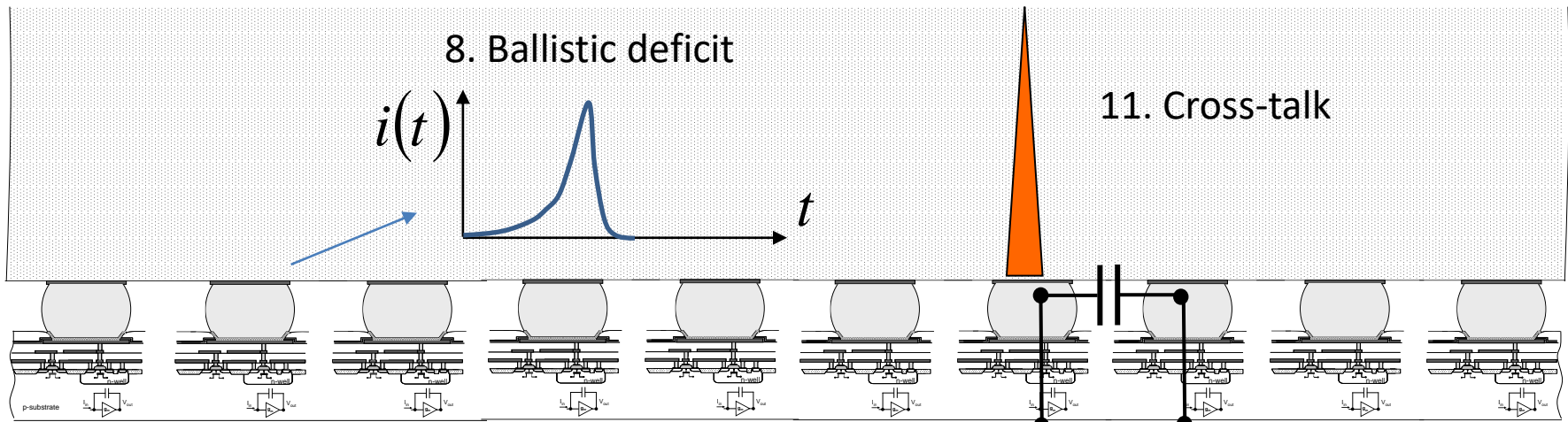
The ideal X-ray detector

- Direct detection
 - Increased and reproducible signal, improved spatial resolution
- Signal deposited by a photon should be proportional to the photon energy and localized in a small volume in the detector
- Single quantum processing
 - Photons are detected and classified in a plurality of energy bins
 - That leads to possibility to energy weighting (optimal SNR), noise rejection, perfect linear behaviour
- Zero dead time (τ)
 - Limitation of single quantum processing
 - For a given application $\tau \ll 1/r$ (τ is the dead time, r is the count rate and $1/r$ is the mean time between consecutive photons)

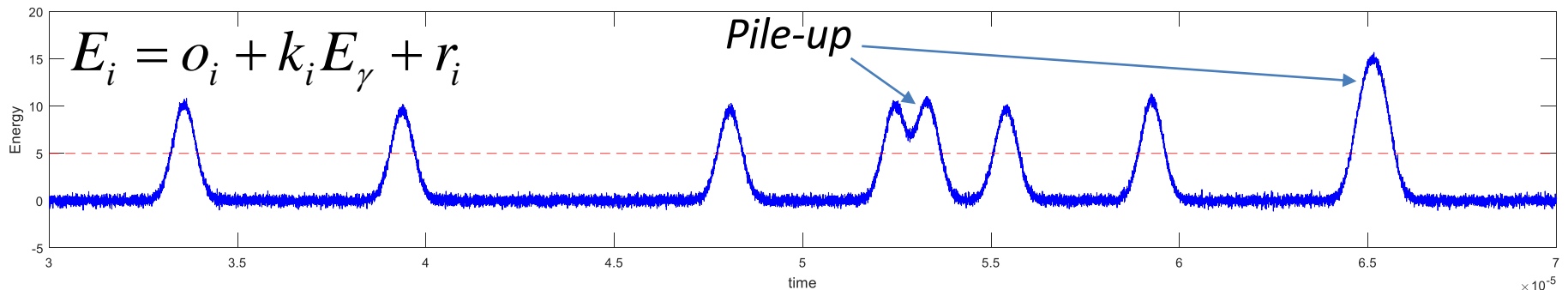
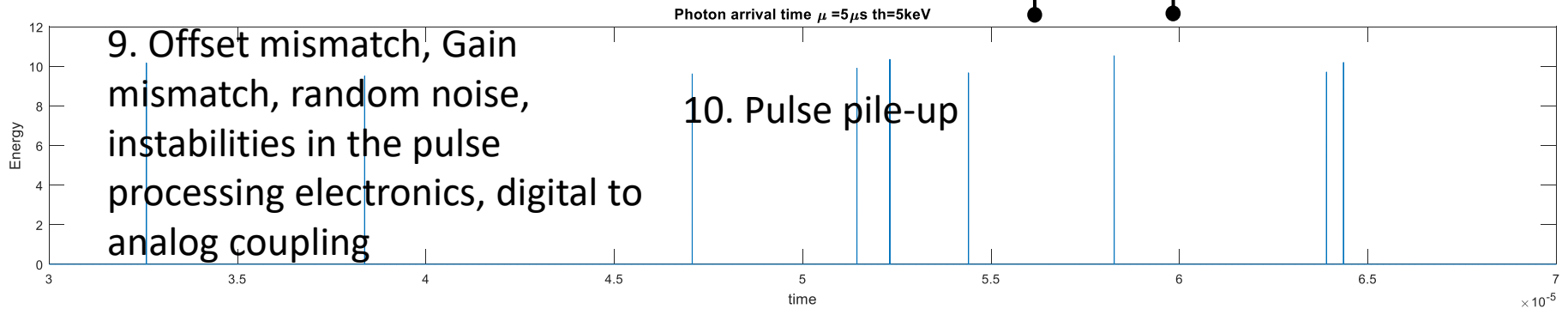
Limiting factors in real systems
degrading spatial, time and energy
resolution and count rate



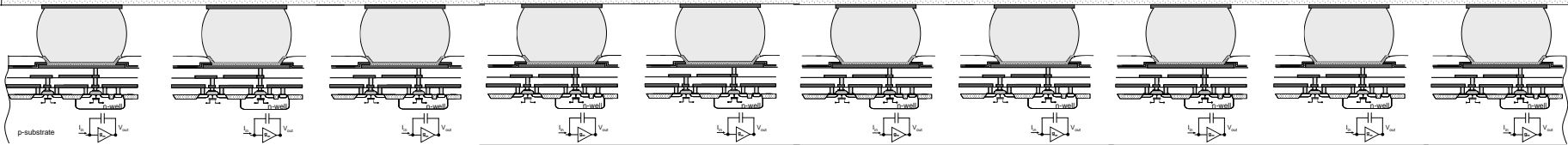
1. Absorption efficiency
2. Fluctuations in the number of generated carriers
3. Charge diffusion
4. Fluorescence
5. Compton scattering
6. Charge trapping
7. Polarization



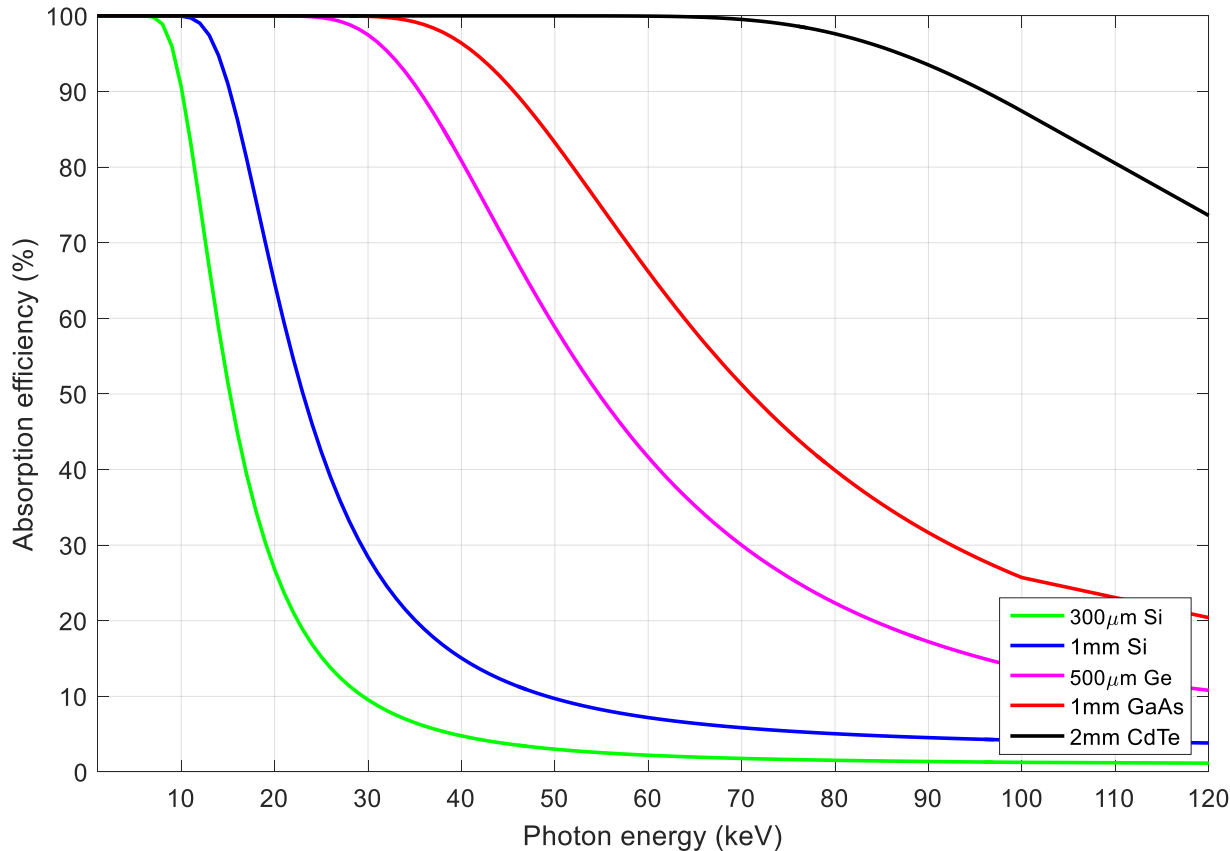
Channel i



1. Absorption efficiency



Absorption efficiency



$$100\left(1 - \frac{I}{I_0}\right) = 100\left(1 - e^{-(\mu/\rho)\rho x}\right)$$

x is the *thickness*

μ is the *linear attenuation coefficient* (units: distance⁻¹) (inverse of the mean free path)

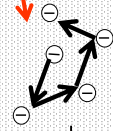
ρ is the *density* of the material

μ/ρ is the *mass attenuation coefficient*

- Silicon (Z=14) ideal for charged particle detection in many applications (homogeneity, availability, cost)
- Higher Z required above 20keV (unless edge on geometry is used)
- Ge (Z=32), GaAs (Z=31,33), CdTe (Z=48,52), CdZnTe

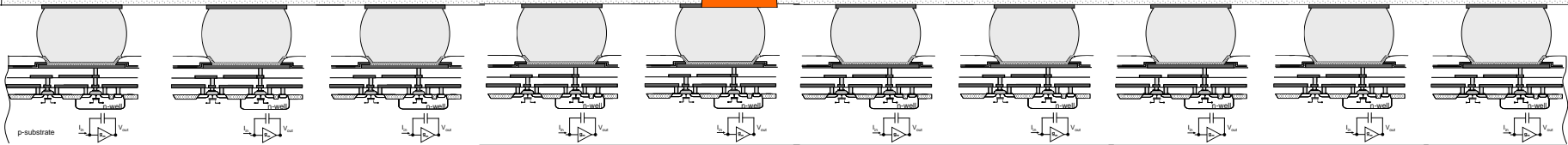
3. Charge diffusion

γ

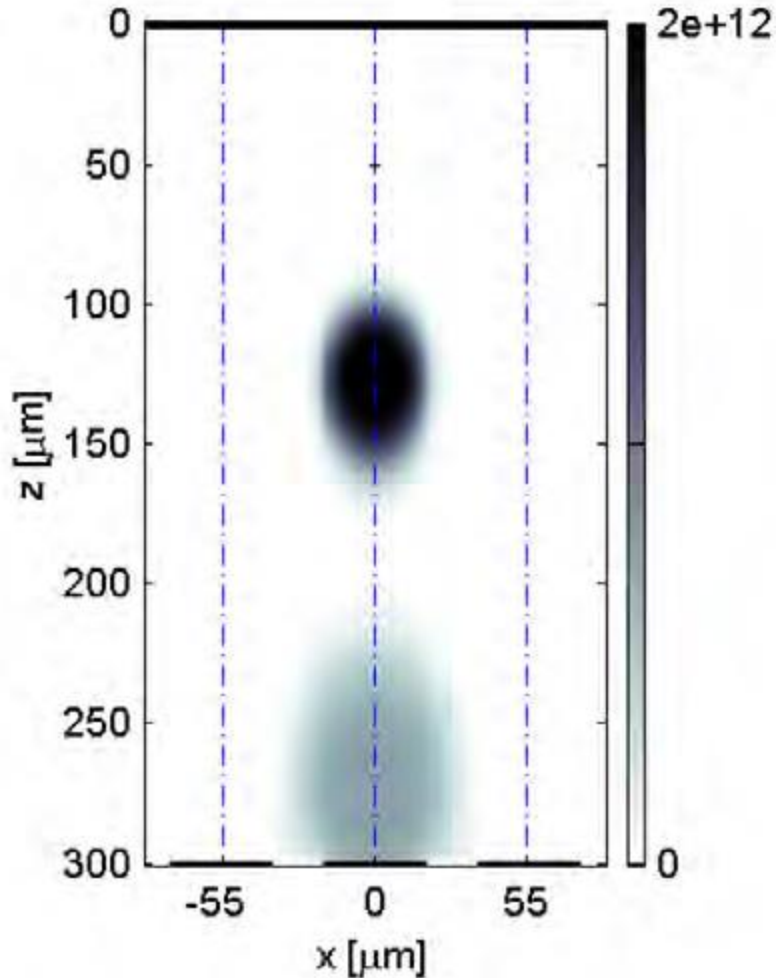


$$\mu = N$$

$$\sigma = \sqrt{NF}$$



Charge diffusion



- Diffusion occurs when there are local differences of carrier concentrations in the semiconductor
- Gaussian cross section of the distribution with standard deviation:

$$\sigma = \sqrt{\sigma_0^2 + 2Dt} \quad \begin{array}{l} D: \text{Diffusion coefficient} \\ t: \text{time} \end{array}$$

$$D = \mu \frac{KT}{q}$$

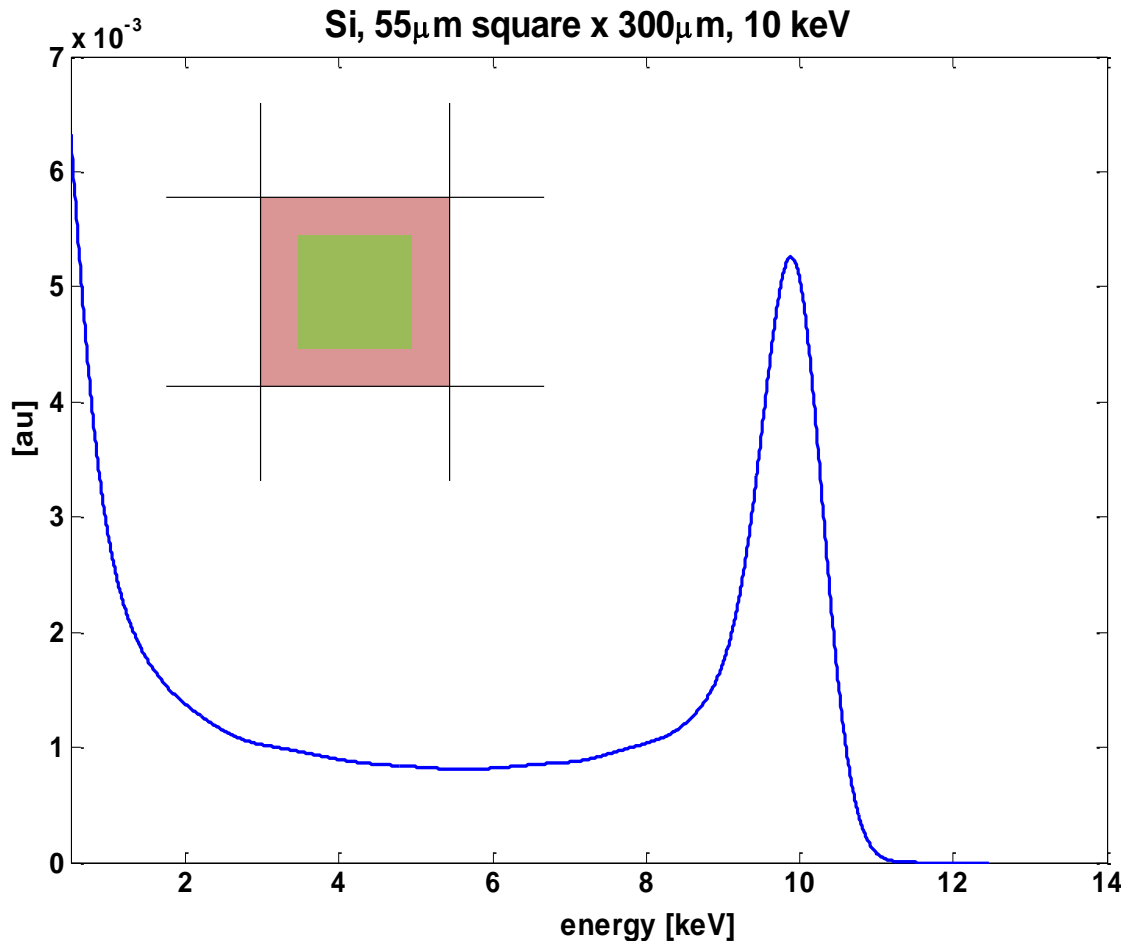
$$t = \frac{d}{\mu E}$$

- Diffusion enhanced by Coulombic repulsion¹

Charge density distribution (hole component) (Charges/cm³), Si sensor, deposition at 50μm, 4ns and 14ns after conversion (Thesis L. Tlustos)

¹X. Lai et al. "CZT modeling for photon counting computer tomography" <https://doi.org/10.1117/12.2512531>

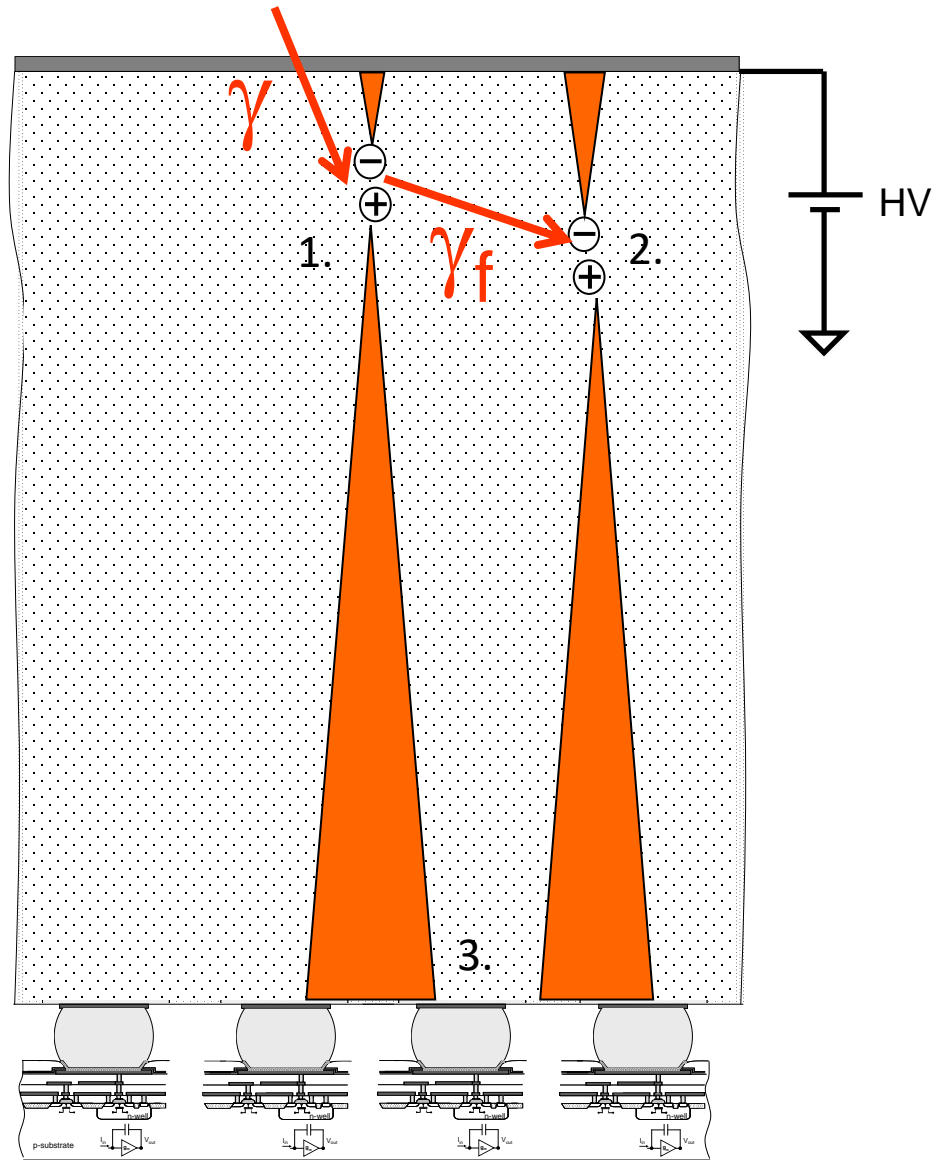
Charge diffusion



- ***Simulated Data***
- ***Si 300 μm , 55 μm pixel***
- ***100 e^- r.m.s. noise***
- ***10keV monochromatic photon beam***

- ***Distortion in the energy spectrum (charge sharing tail) increases as the pixel pitch decreases with the detector thickness***

Fluorescence



Fluorescence

Mean free path of fluorescence photon [μm]

Fluorescence yield [%]

Energy fluorescence photons [keV]

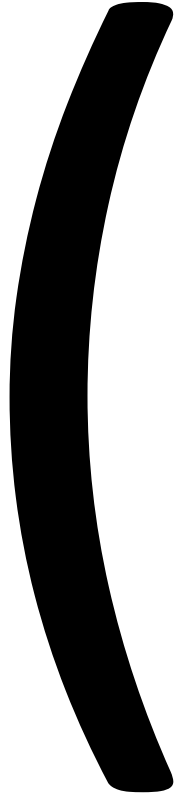
Z

Material	N	K ₁ [keV]	L ₂ [keV]	L ₃ [keV]	K _{α1} [keV]	K _{α2} [keV]	d _{α1} [μm]	d _{α2} [μm]	η[%]
Si	14	1.84	0.10	0.10	1.74	1.74	11.86	11.86	4.1
Ge	32	11.1	1.26	1.23	9.89	9.86	50.85	50.40	54.8
GaAs Ga, 48.20% As, 51.80%	31	10.36	1.14	1.11	9.25	9.22	40.62	40.28	50.5
	33	11.87	1.36	1.32	10.54	10.50	15.62	15.47	56.6
CdTe Cd, 46.84% Te, 53.16%	48	26.71	3.73	3.53	23.17	22.98	113.20	110.75	83.6
	52	31.81	4.61	4.34	27.47	27.20	59.32	57.85	87.3

The fluorescence yield increases with the atomic number

The mean free path of the fluorescence photons is in the same order of magnitude as the pixel pitch for high-Z materials

Implications: degradation of the energy measurement, blur the image



Signal induction

Induced charge on detector electrodes

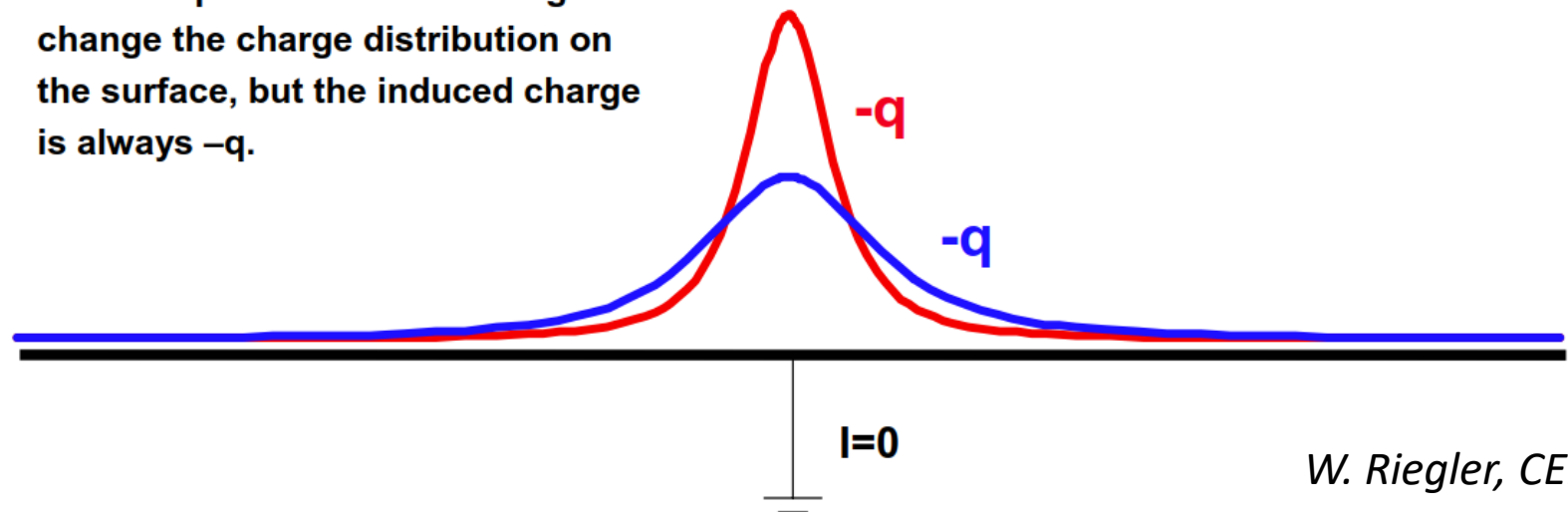
- Signals on detector electrodes arise from motion of charge carriers
- Induced current is derived from laws of electrostatics

A point charge in presence of an infinite grounded metal plane will **induce** a total charge of $-q$.

● q

● q

Different positions of the charge will change the charge distribution on the surface, but the induced charge is always $-q$.



Induced charge on detector electrodes

- Signals on detector electrodes arise from motion of charge carriers
- Induced current is derived from laws of electrostatics

In case the strips are segmented, the induced charge on each strip will change when the charge q is moving.

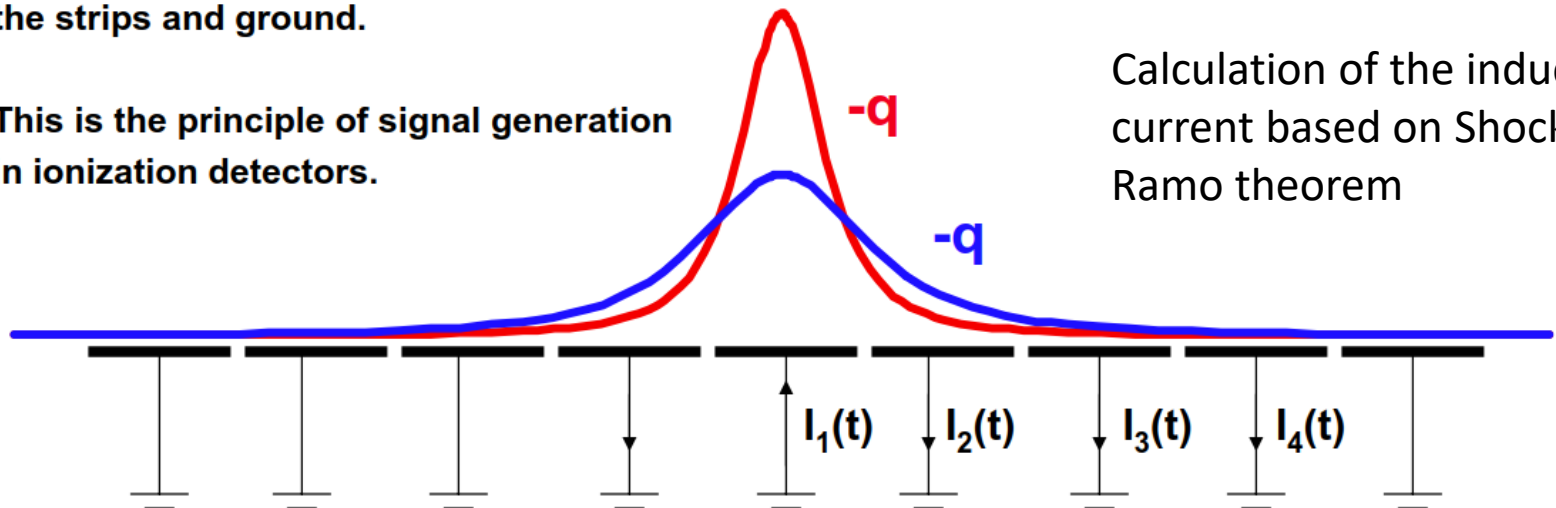
The **movement** of the charge therefore **induces currents** that flow between the strips and ground.

This is the principle of signal generation in ionization detectors.

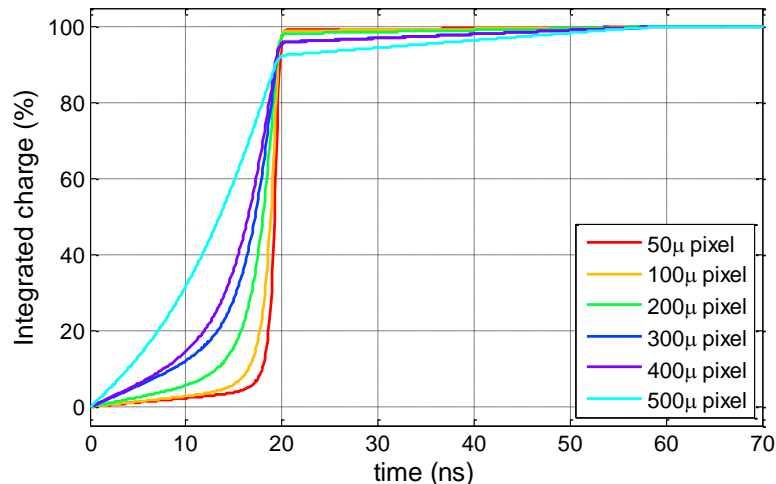
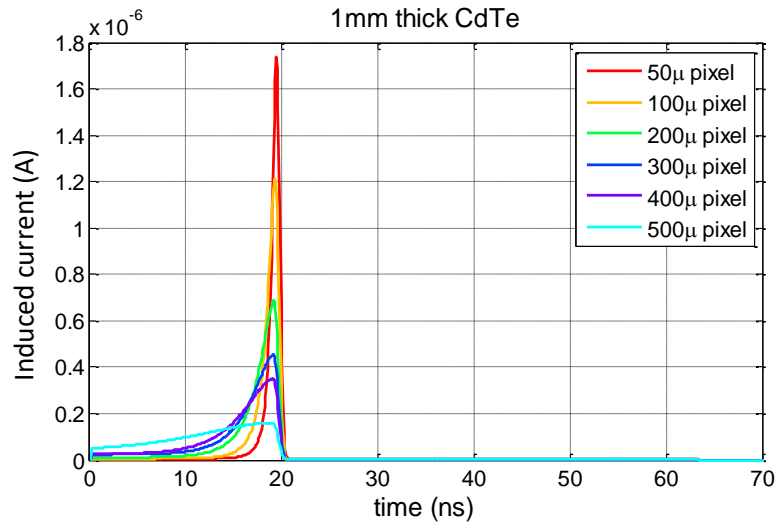
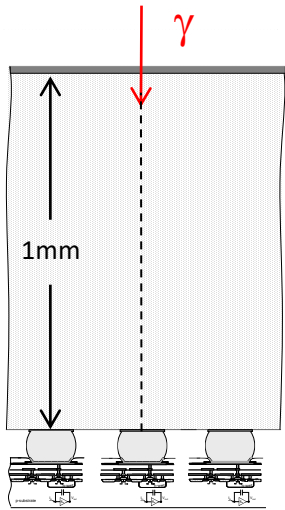


$$i(t) = \frac{dQ}{dt}$$

Calculation of the induced current based on Shockley-Ramo theorem



Signal induction in the pixel electrodes



Signal shape depends on detector geometry

Consequence of Shockley-Ramo theorem: The small pixel effect

It is the motion close to the pixel surface that contributes most strongly to the induced charge. The carrier that drifts towards the pixel electrodes will contribute to most of the charge induced on the pixel electrode.

- 1mm CdTe
- 60keV photon
- 600V sensor bias
- Energy deposition at $z=240\mu\text{m}$
- (No charge trapping, charge sharing included in simulation)

Message: The geometry of the sensor (pitch/thickness) determines the shape of the induced current pulse (and puts a lower limit on the electronics integration time)

Information from the incoming beam

- The number of particles deposited during a given exposure time
- The energy deposited by an individual particle
- The time of arrival of the particle
- The incoming type of particle, based on the shape of the cluster of pixels responding to a single charge deposition event
- The angle of incidence of the incoming charged particle based on the difference in the induced signal time in the pixels

60 deg

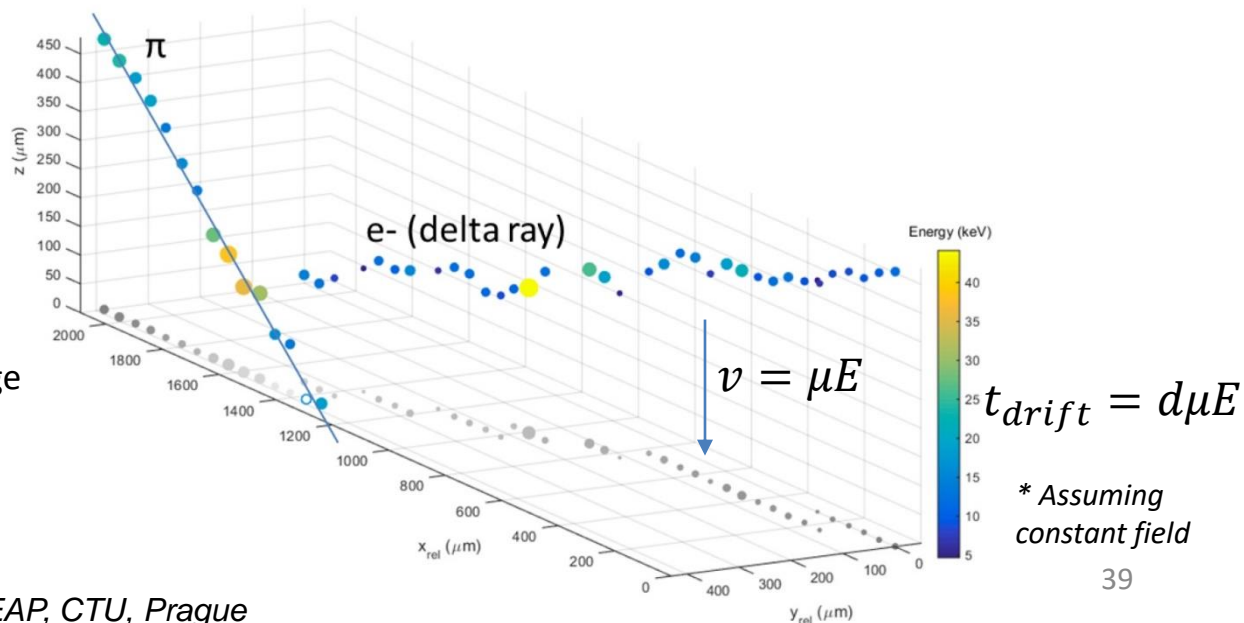
p+ in n Si sensor, Timepix3

500 μ m thick

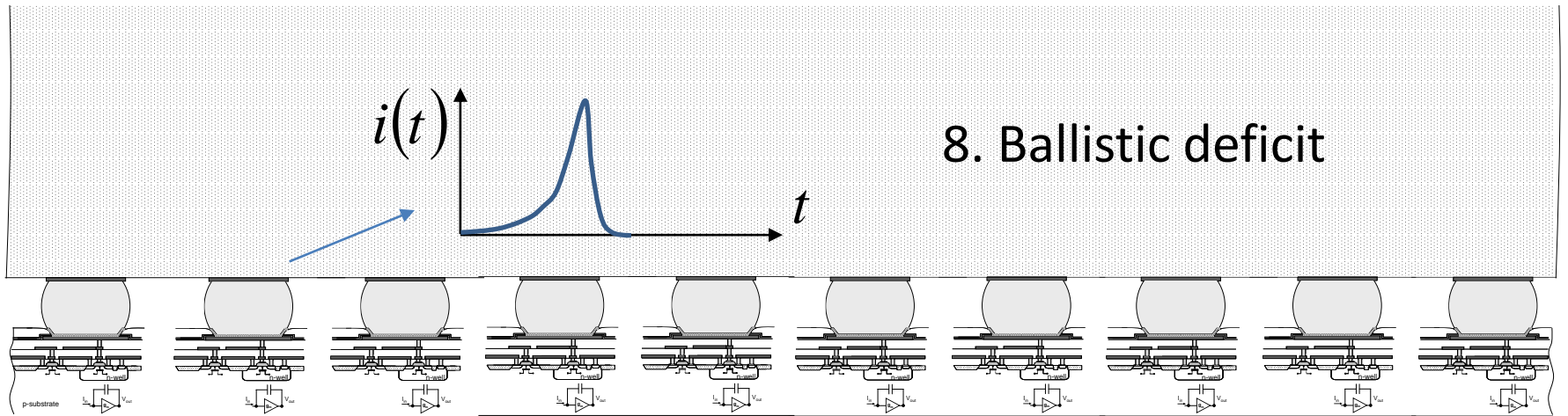
$V_{\text{bias}} = 130\text{V}$

Colour (and diameter) indicate charge

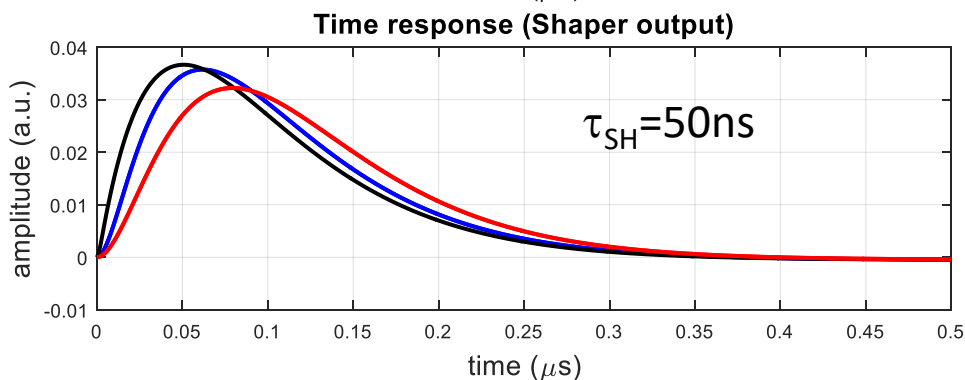
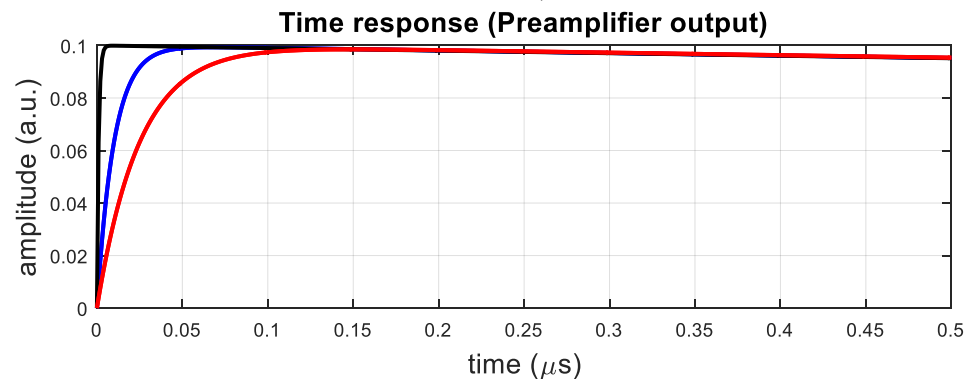
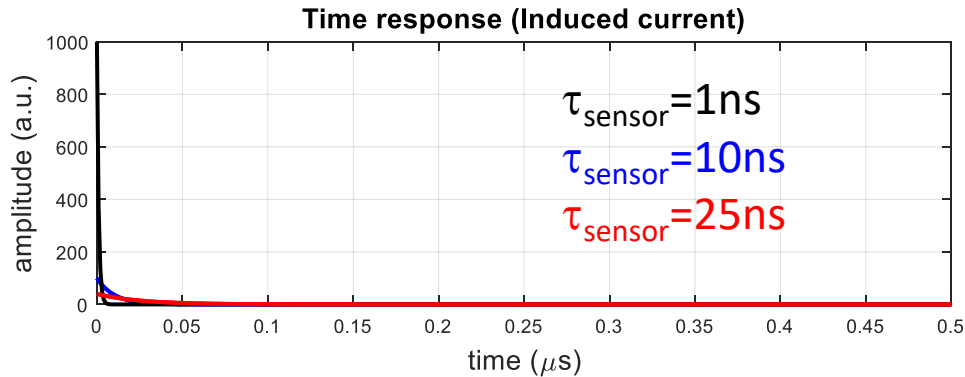
Measured z resolution $\sim 50\mu\text{m}$







Ballistic deficit



Ballistic deficit refers to the loss of signal amplitude at the shaper output due to an incomplete integration of the sensor signal by the readout electronics

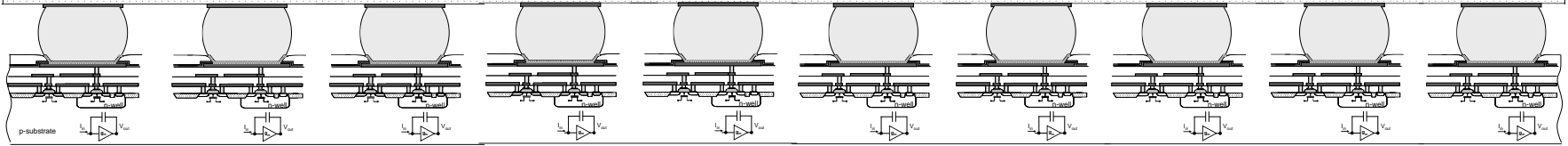
$$I_d = \frac{Q_{in}}{\tau_{\text{sensor}}} e^{-\frac{t}{\tau_{\text{sensor}}}}$$

$$H_{\text{CSA}}(s) = \frac{R_F}{1 + R_F C_F s}$$

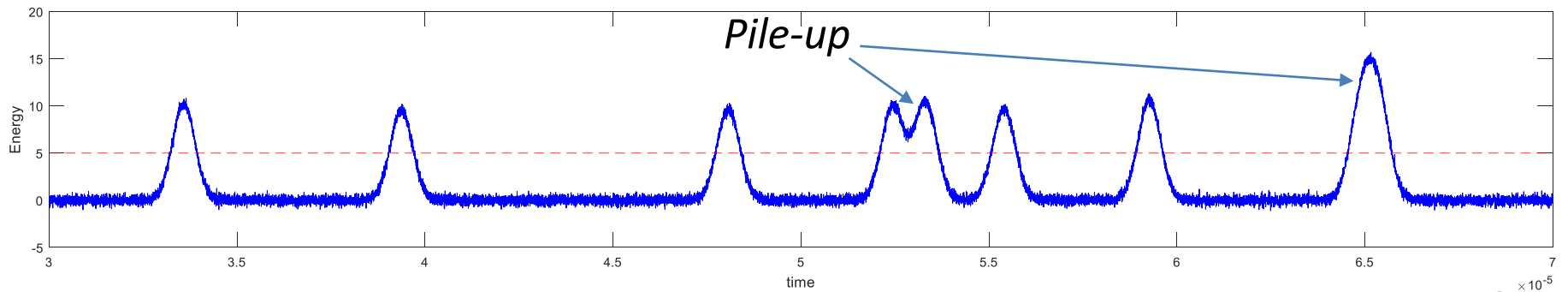
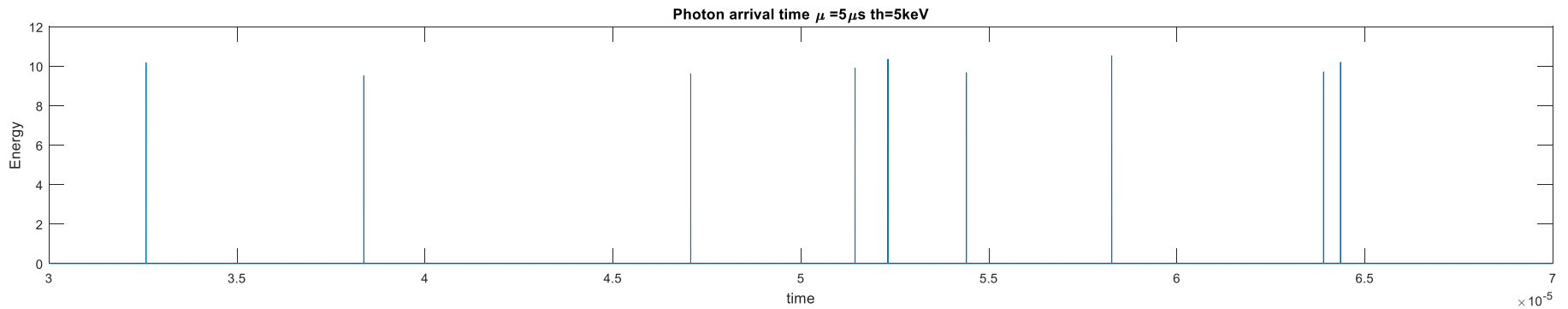
$$H_{\text{SHAPER}}(s) = \frac{s \tau_{\text{SH}}}{(1 + \tau_{\text{SH}} s)^2}$$

Mathematical model (other effects like charge sharing are not included).

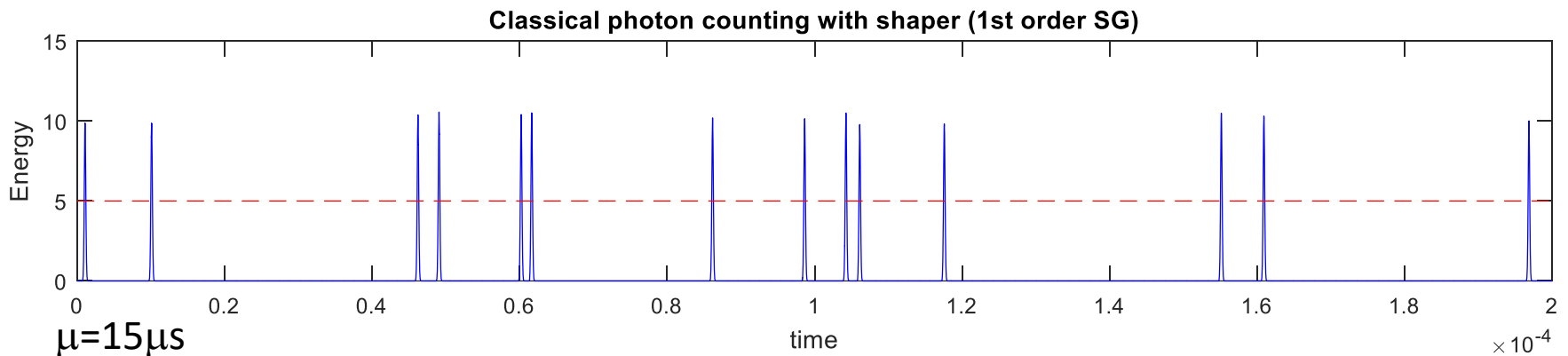
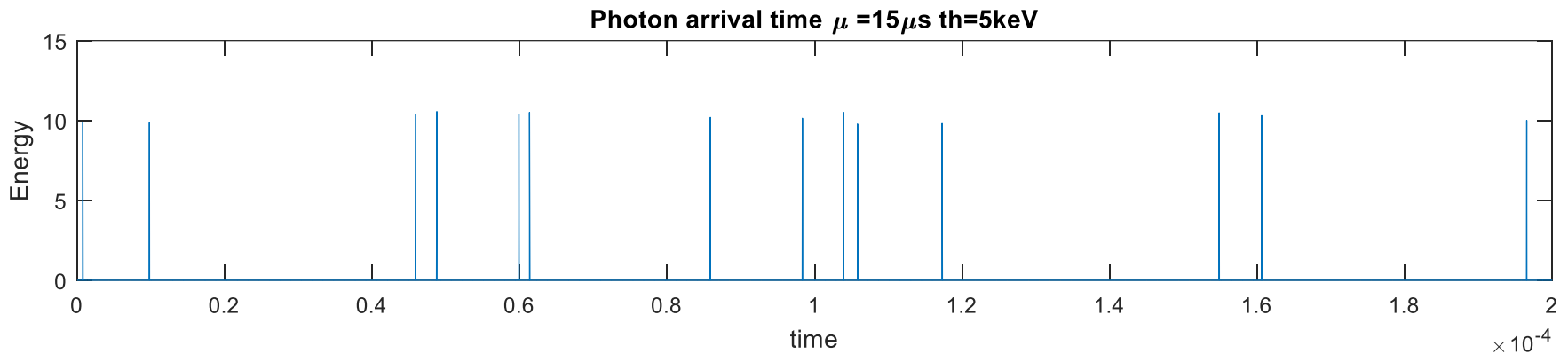
10. Pulse pile-up



Channel *i*



Pulse pile-up



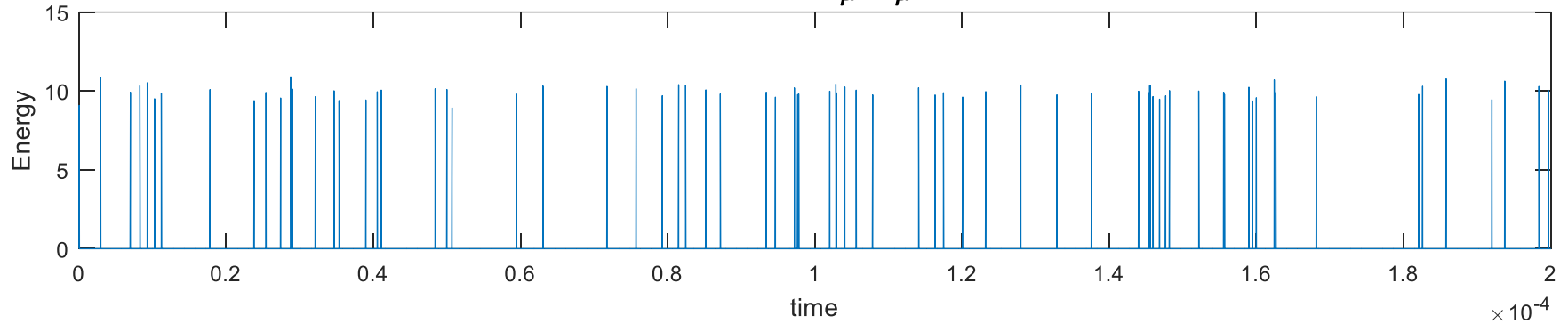
Gaussian shaper ($\sigma=100\text{ns}$), $\tau\sim 300\text{ns}$ (@Threshold=2.5keV)

$\tau/\mu=0.02$

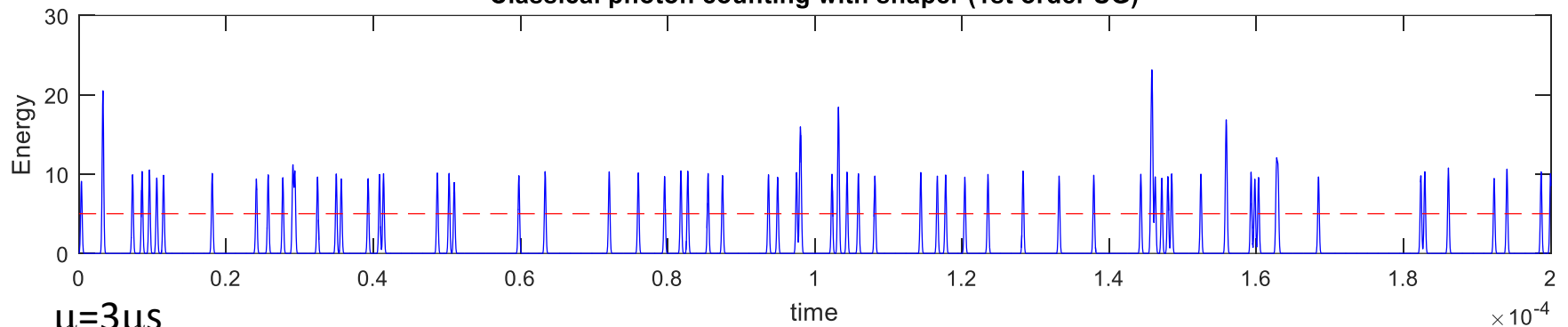
- Pile-up is the overlap in the processing chain, of the signals due to two consecutive photons
- The mean time between consecutive photons (μ) follows exponential probability density function

Pulse pile-up

Photon arrival time $\mu = 3\mu\text{s}$ $\text{th} = 5\text{keV}$



Classical photon counting with shaper (1st order SG)

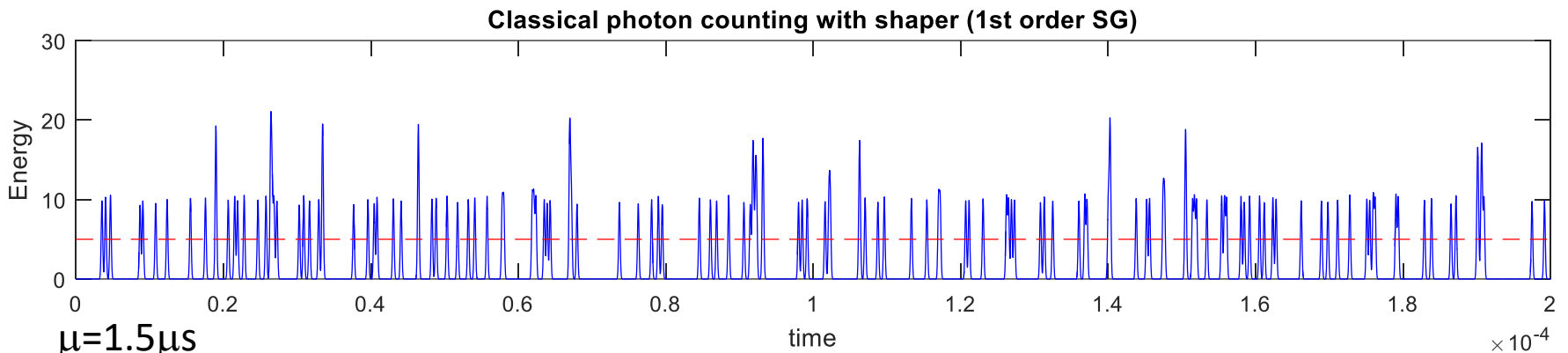
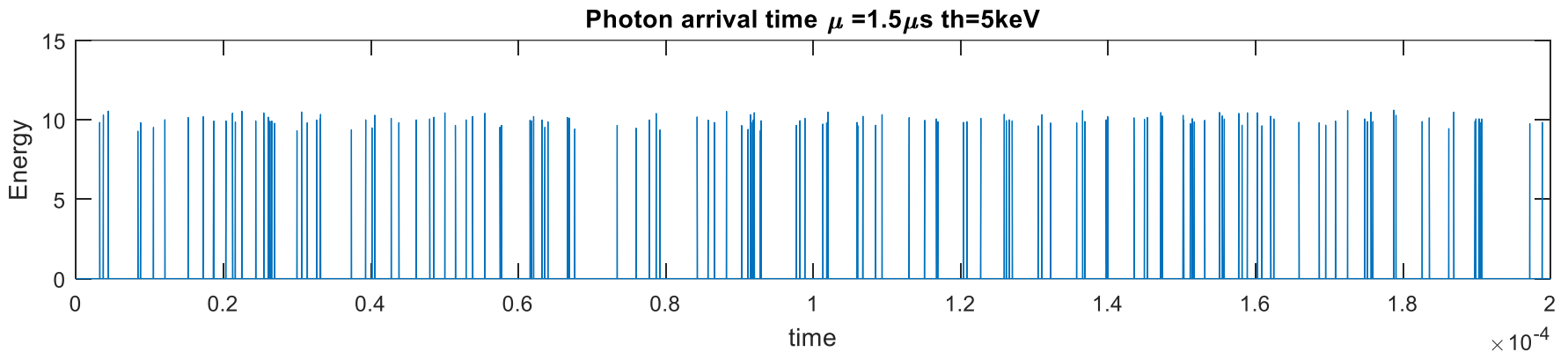


$\mu = 3\mu\text{s}$

Gaussian shaper ($\sigma = 100\text{ns}$), $\tau \sim 300\text{ns}$ (@Threshold = 2.5 keV)

$\tau/\mu = 0.1$

Pulse pile-up



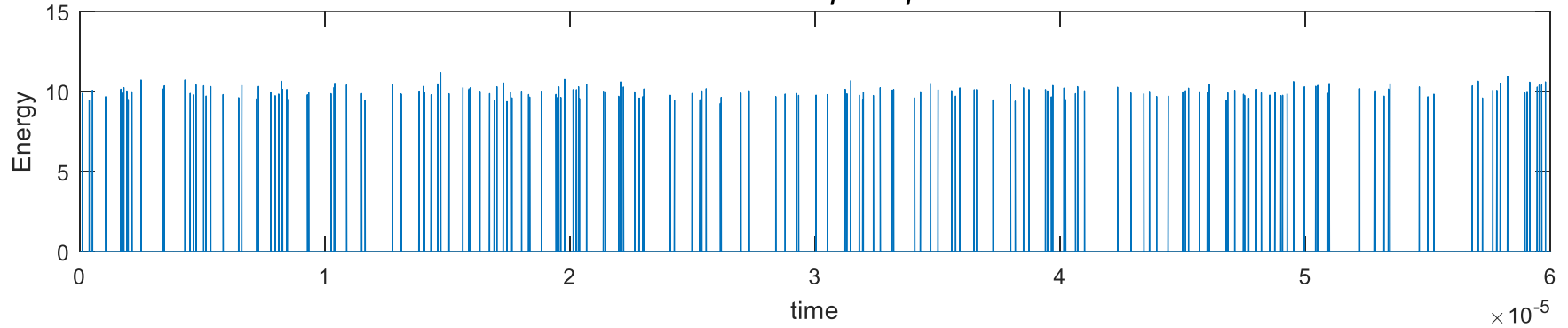
Gaussian shaper ($\sigma=100\text{ns}$), $\tau\sim 300\text{ns}$ (@Threshold=2.5keV)

$\tau/\mu=0.2$

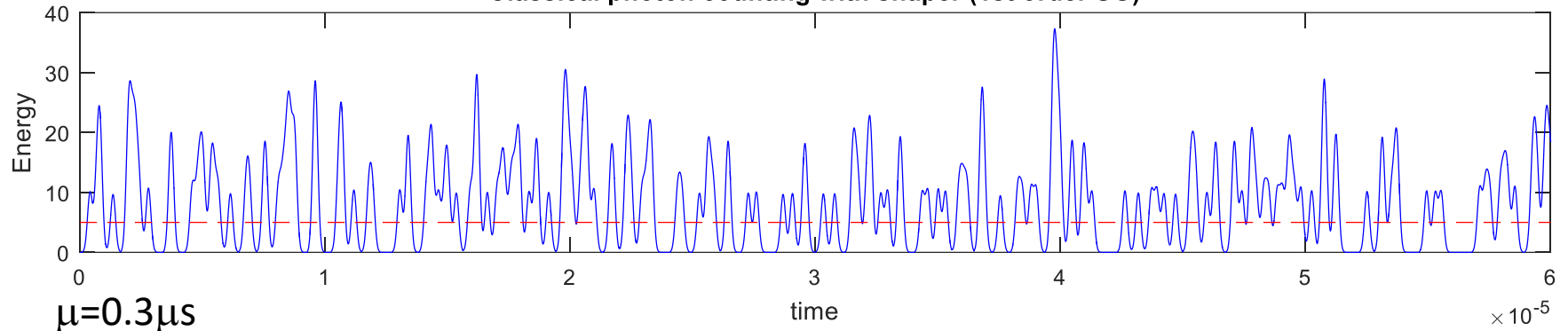
The impact of pulse pile up is on an incorrect number of recorded photons and also a distortion in the measured energy spectrum

Pulse pile-up

Photon arrival time $\mu = 0.3\mu\text{s}$ th=5keV



Classical photon counting with shaper (1st order SG)

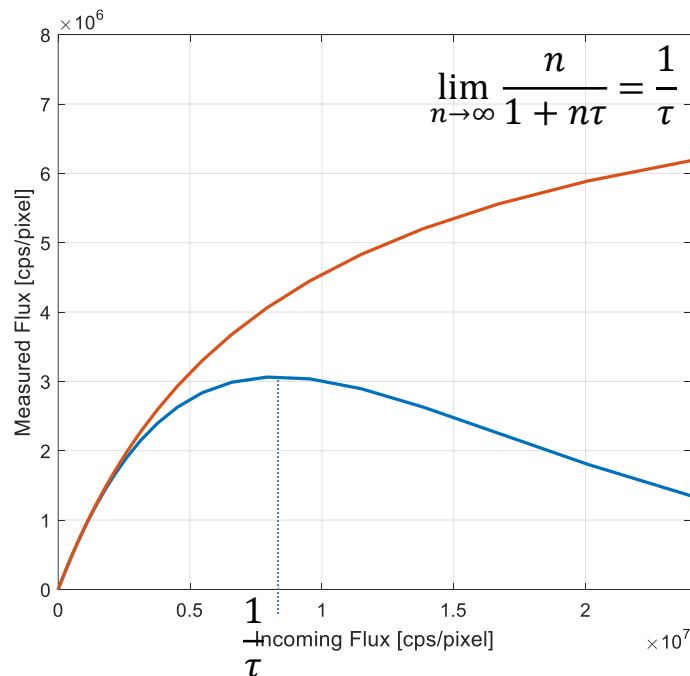
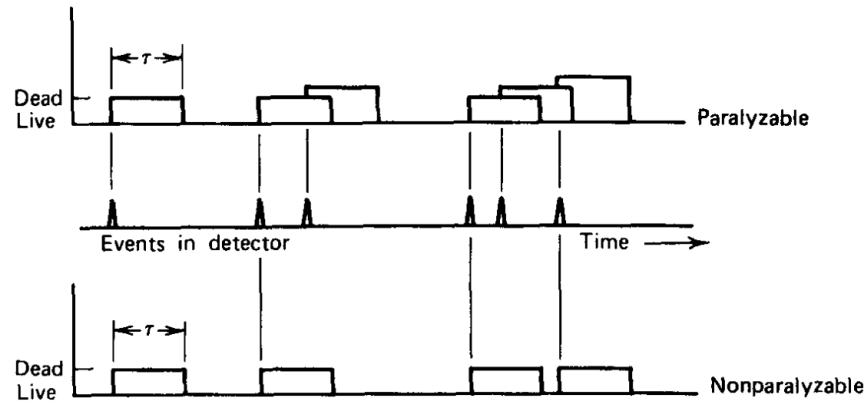


$\mu = 0.3\mu\text{s}$

Gaussian shaper ($\sigma = 100\text{ns}$), $\tau \sim 300\text{ns}$ (@Threshold=2.5keV)

$\tau/\mu = 1$

Dead time models



m : recorded rate
 n : true rate
 τ : pulse width

Non-paralyzable model:

$$m = \frac{n}{1 + n\tau}$$

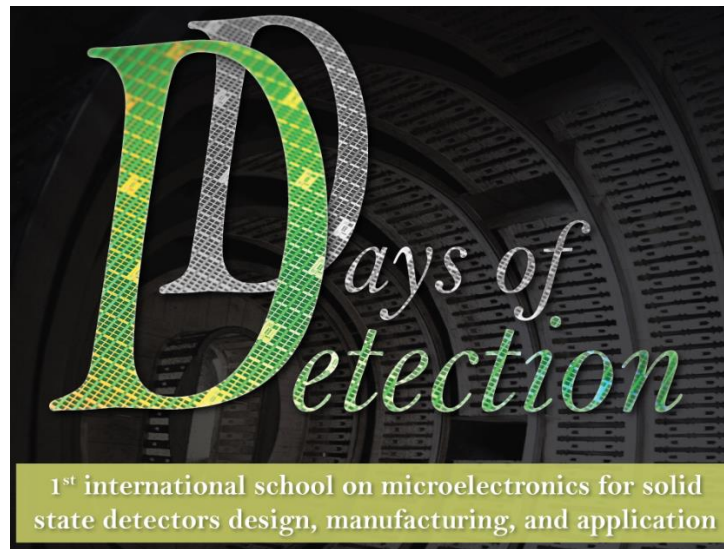
Paralyzable model:

$$m = ne^{-n\tau}$$

These models represent an idealized system behaviour. Real counting systems will often display a behavior that is intermediate between these extremes. Assumptions: 1. events arrive following Poisson statistics with average true interaction rate n , 2. Signals are rectangle-like shaped of duration τ .

Summary and conclusions

- We reviewed hybrid pixel detector systems (with emphasis on X-ray detection)
- We classified them in terms of
 - X-ray conversion
 - Signal processing
 - Detector geometry
- The ideal detector system
- The limiting factors in real systems



Part 1: Introduction to hybrid pixel detectors

Classification of technologies, limitations of hybrid pixel detectors

Part 2: Introduction to signal processing

Thanks to D. Gascón (ICCUB), A. Rivetti (INFN), J. Kaplon (CERN), P. O'Connor (BNL)

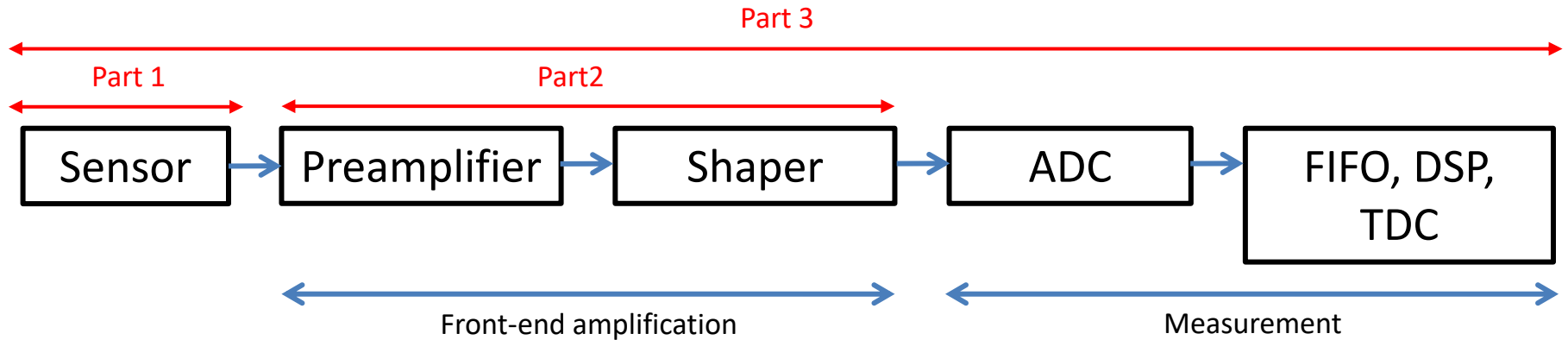
Part 3: Review of ASICs

Rafael Ballabriga Suñé

rafael.ballabriga@cern.ch

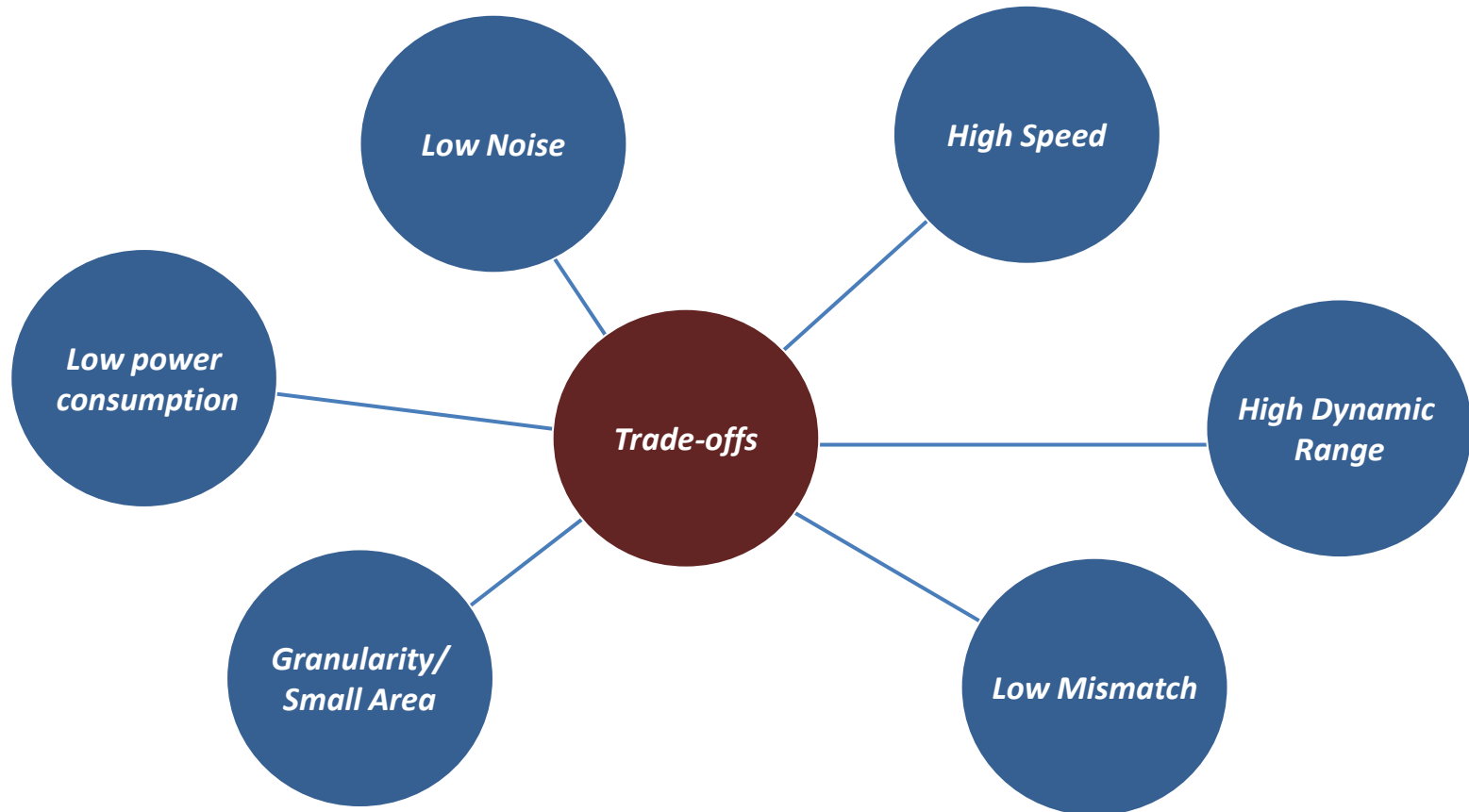
CERN Microelectronics Section

Signal chain for readout electronics



- The sensor converts the energy (or part of it) of an incoming particle into an electrical signal and delivers a small signal (fC)
- The front-end amplifier and shaper
 - amplifies and shapes the signal (optimizing the signal to noise ratio and ability to deal with flux)
 - ensures an efficient signal transfer in presence of parasitic elements between adjacent channels (ensuring low cross talk).
- The stages following the front-end amplifier extract the information from the signal about the incoming quanta in a quantized domain
 - Energy (ADC)
 - Time of arrival (TDC)
 - Number of particles above threshold
 - Location, particle type
- In modern detectors, this is done in systems containing thousands of channels (low power)

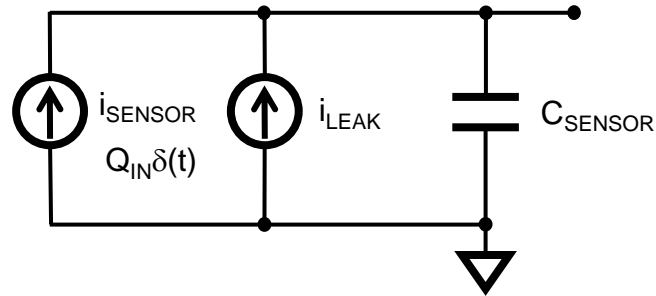
Requirements for readout electronics



Reliability, Radiation hardness, Low material, Low Cost

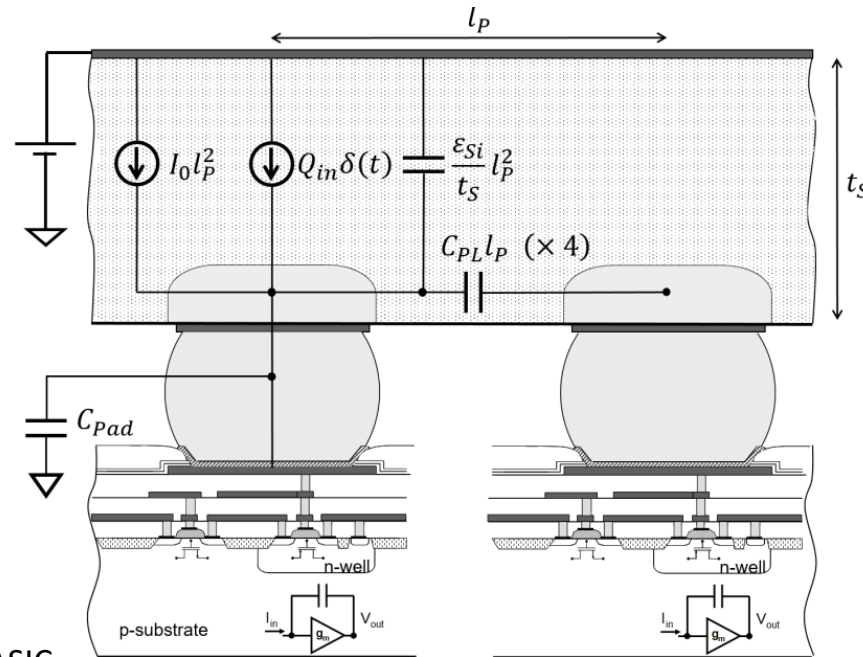
Sensor geometry modeling

The (simplified) detector model



- **Signal:**
 - Radiation event creates charges in the detector volume
 - i_{SENSOR} represents the currents induced in the sensing electrodes by the charge carriers moving in the detector volume
 - It is usually modeled as a $\delta(t)$, which is convenient because it allows to study the front-end electronics impulse response
 - The model is adequate if the impulse response of the electronics is long compared to the signal delivered by the sensor
 - The polarity of the source has to be accounted for
 - Q_{IN} depends on the interaction of the particle with the sensor material (For photons in Si: $Q_{\text{in}} = E_{\gamma} / \epsilon$, for MIPS 60-80e⁻ / h⁺ / μm (Presentation E. Heijne, L. Pancheri))
- **Leakage (semiconductor detectors)**
 - e⁻/h⁺ pairs thermally generated in the depletion region and swept by the electric field
 - The discrete nature of carriers crossing a junction intrinsically implies some fluctuations in their number (*shot noise*)
- **Capacitance: determines the system performance**
 - Monolithic Active Pixel Sensors (~1fF), Hybrid Pixel Detectors (10s of fF), Strips Detectors (~pF), PMT (10s of pF), SiPMs (pF-nF)
- Interconnect parasitics and accurate models for the sensor signal required especially for precise timing measurements.

Example 1: The detector model for a hybrid pixel detector



C_0 Parasitic Capacitances in ASIC
 ~20fF (Medipix3/Timepix2)
 ~80fF (Timepix4 (RDL))

Interpixel side wall capacitance (~1pF/cm)*

$$C_D = C_0 + C_1 l_p + C_2 l_p^2 = C_{PAD} + 4C_{PL} l_p + \frac{\epsilon_{Si}}{t_s} l_p^2$$

C_D Detector Capacitance

l_p Pixel pitch

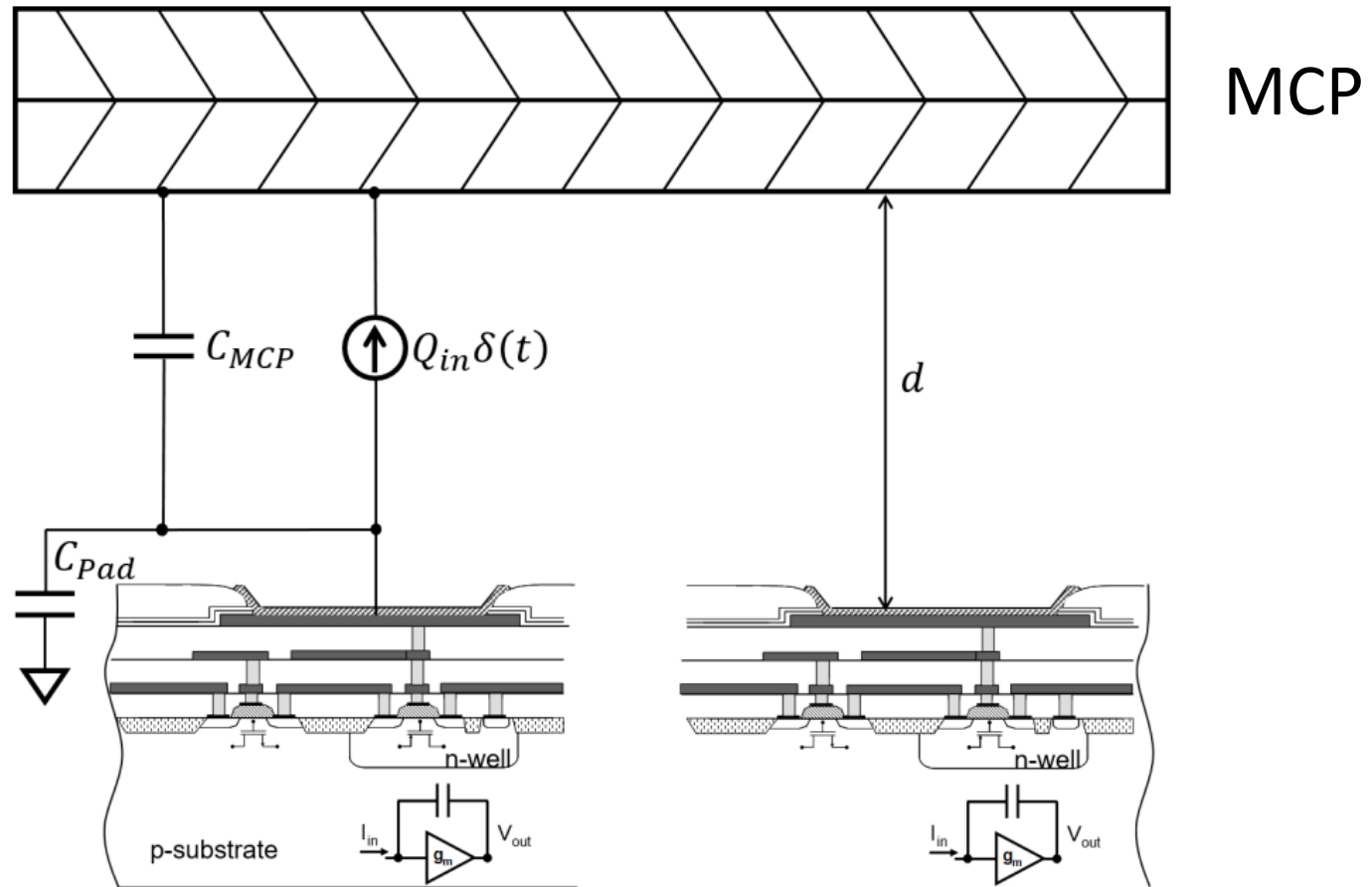
Pixel to back side electrode capacitance

Sensor thickness

R. Ballabriga et al. "The Timepix4 Analog Front-end Design: Lessons learnt on Fundamental Limits to Noise and Time Resolution in Highly Segmented Hybrid Pixel Detectors" <https://doi.org/10.1016/j.nima.2022.167489>

* G. Gorfine et al., "Capacitance of silicon pixels", Nucl. Instrum. Methods Phys. Res. A 460 (2) (2001) 336–351.

Example 2: The detector model



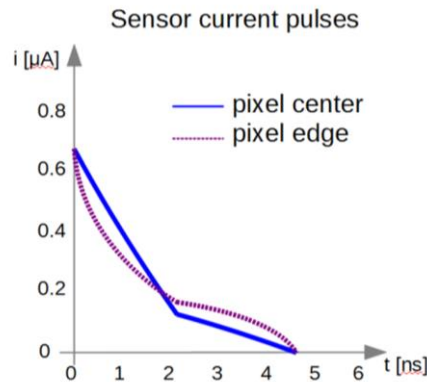
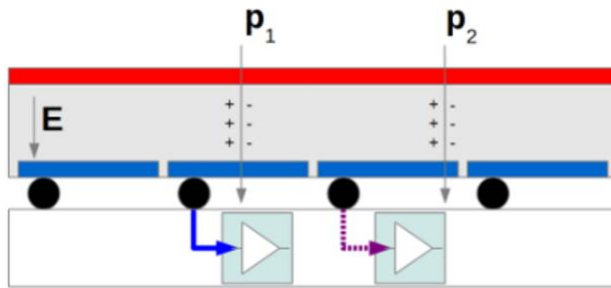
The model can be adapted to other sensor geometries

Example 3: Importance of the details in high performance measurements: timing for high energy charged particle detection

The $\delta(t)$ model is convenient and widely used if the impulse response of the electronics is long compared to the signal delivered by the sensor.

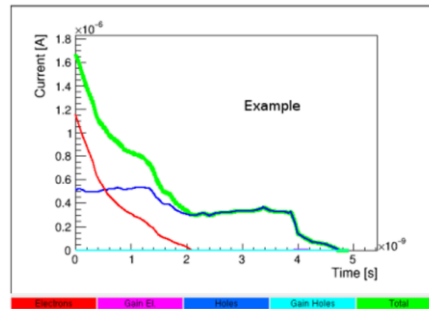
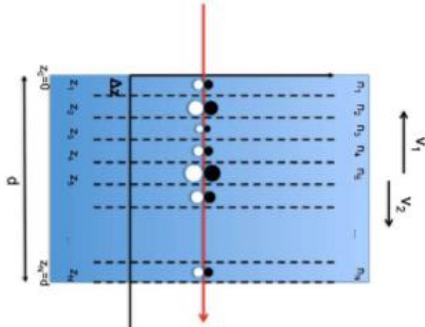
In precise timing applications with fast readout electronics, accuracy in the models is essential to capture some effects that can degrade the measured time resolution

Variations in the induced current



The preamplifier output waveform changes its shape depending on the position of the interaction. This leads to a contribution that can't be corrected for in leading edge discriminator systems

Charge straggling*



Fluctuations in the number of electron/hole pairs created along the path of the particle introduce fluctuations on the shape of the induced signal.

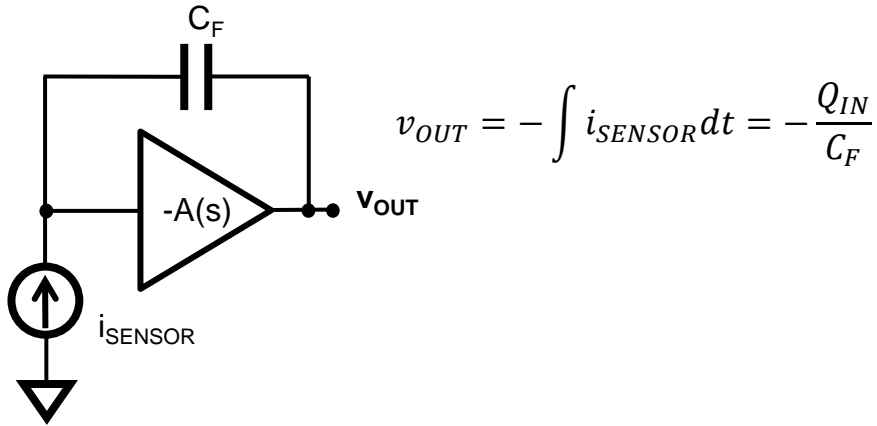
* H. Bichsel, Straggling in thin silicon detectors, *Rev. Mod. Phys.* 60 (1988) 663–699. doi:10.1103/RevModPhys.60.663.

Example: TDCpix time resolution was measured 71ps rms (laser at the center of the pixel generating 2.4fC signal at surface). Test beam with MIPs showed a time resolution of 115ps rms

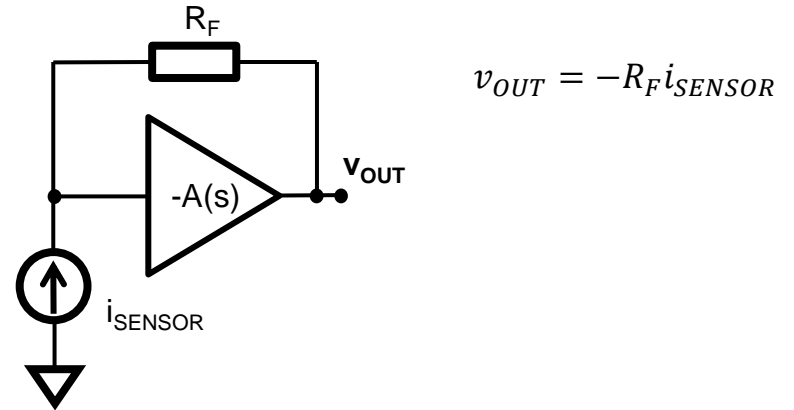
Preamplifier topologies

Preamplifier topologies

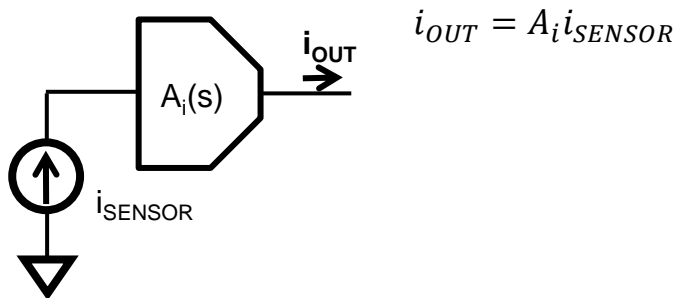
CHARGE SENSITIVE AMPLIFIER



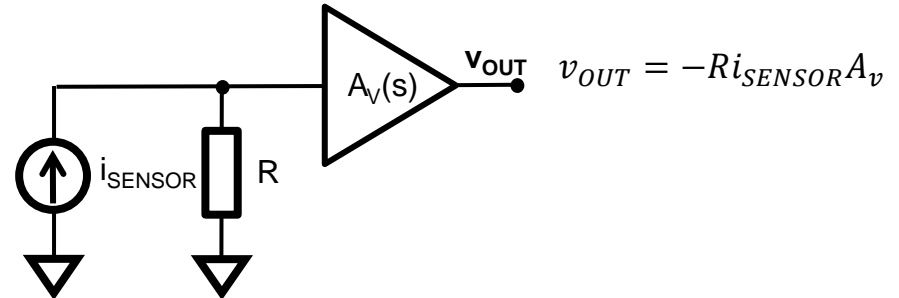
TRANSIMPEDANCE AMPLIFIER



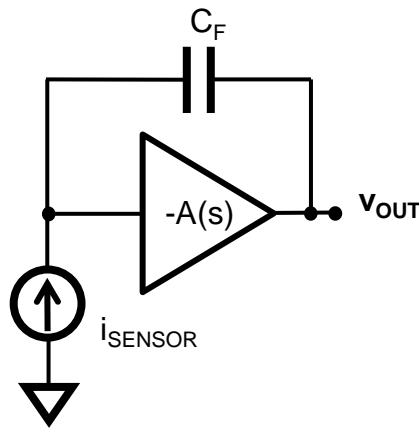
CURRENT BUFFER



VOLTAGE AMPLIFIER



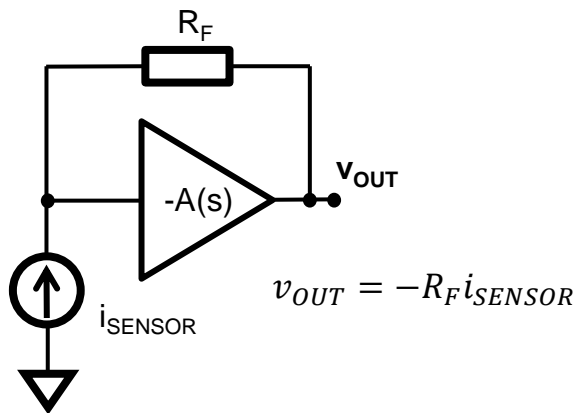
Charge sensitive amplifier



$$v_{OUT} = - \int i_{SENSOR} dt = - \frac{Q_{IN}}{C_F}$$

- Capacitive feedback around the amplifier (current integral)
- A resistor (R_F , usually very large) in parallel with the capacitor is required to discharge it and to fix the DC operating point at the preamplifier input
- Long tail in the signal at v_{out} ($\tau_F = C_F R_F$) might limit the count rate for the application
- Excellent noise performance
- Ideal to readout sensors without intrinsic amplification
- $\tau_F > \tau_{sensor}$ (time constant of the signal delivered by the sensor)

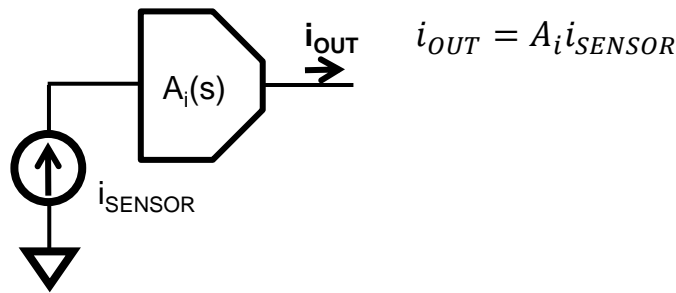
Transimpedance amplifier



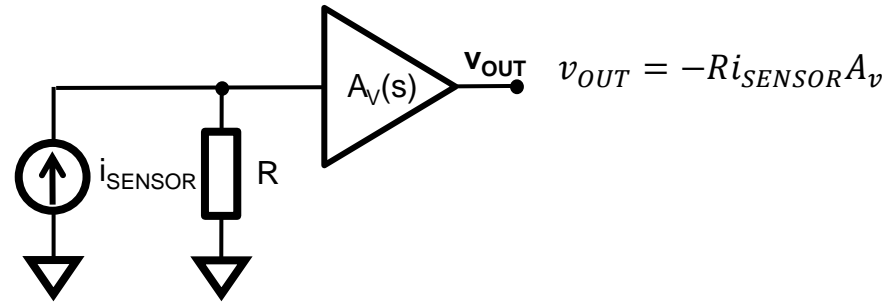
- Resistive feedback around the amplifier
- It preserves the shape of the signal delivered by the sensor
- A capacitor (C_F) in parallel with the resistor is required for stability
- Shorter tail in the signal at v_{out} ($\tau_F = C_F R_F$) makes this more adequate for high count rate applications
- $\tau_F < \tau_{\text{sensor}}$ (time constant of the signal delivered by the sensor)
- In practice, TIAs are used for fast front end electronics in which band pass filters following the input stage are tuned to high frequencies. For such applications, TIAs will offer lower input impedance and consequently lower crosstalk signals than CSAs.

Current buffer / voltage buffer

CURRENT BUFFER



VOLTAGE AMPLIFIER



- Typically used for the readout of detectors with intrinsic amplification (e.g. SiPMs) for precise timing
- In these applications the CSA is not optimal due to bandwidth limitations. Frequency associated with rising time (where typically $C_F < C_{SENSOR}$):

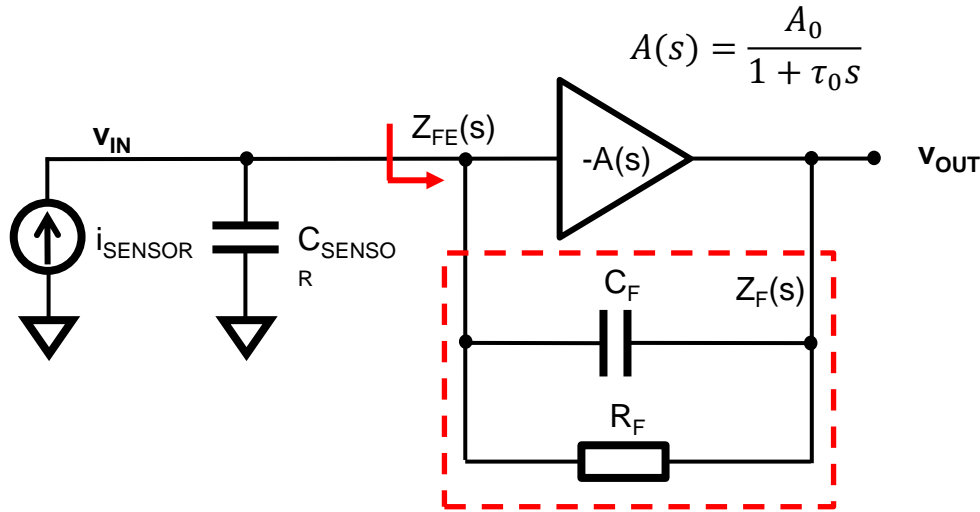
$$f_C = GBWP \frac{C_F}{C_F + C_{SENSOR}}$$

- The current buffer is more advantageous due to noise shaping effects and to the lower input impedance*.

*F. Ciciriello, F. Corsi, F. Licciulli, C. Marzocca and G. Matarrese, "Time performance of voltage-mode vs current-mode readouts for SiPM's," 2015 6th International Workshop on Advances in Sensors and Interfaces (IWASI), Gallipoli, Italy, 2015, pp. 249-253, doi: 10.1109/IWASI.2015.7184979.

The CSA/TIA

General case



$$\frac{v_{\text{OUT}}}{i_{\text{SENSOR}}}(s) \cong Z_F(s) \quad (1)$$

$$Z_{\text{FE}}(s) \cong \frac{Z_F(s)}{A(s)} \quad (2)$$

In the general case, the feedback impedance is the combination of a capacitor and a resistor

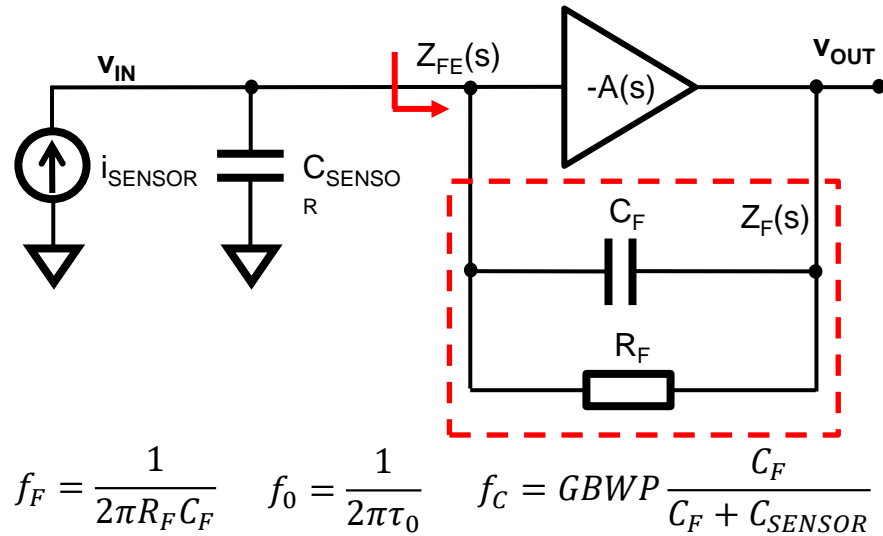
The real amplifier has finite gain bandwidth product.

The feedback impedance defines the transfer function $v_{\text{OUT}}/i_{\text{SENSOR}}$ (1)

The feedback lowers the input impedance to minimize the voltage swing at the input node (2):

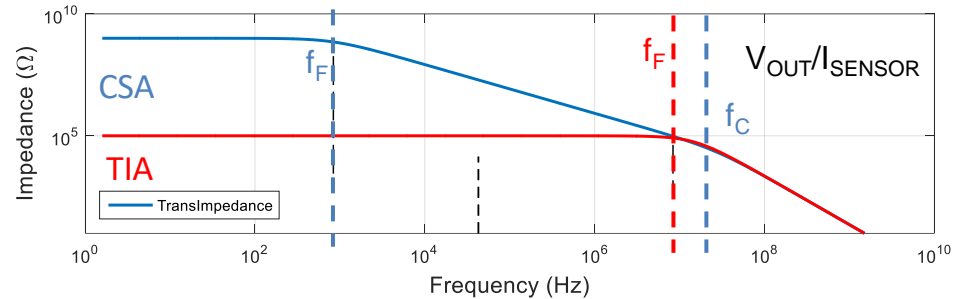
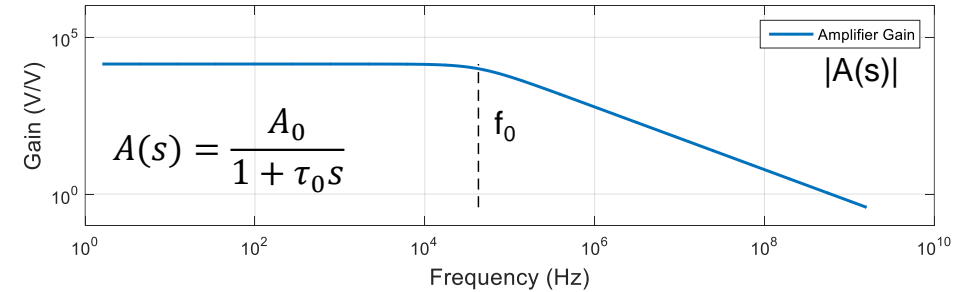
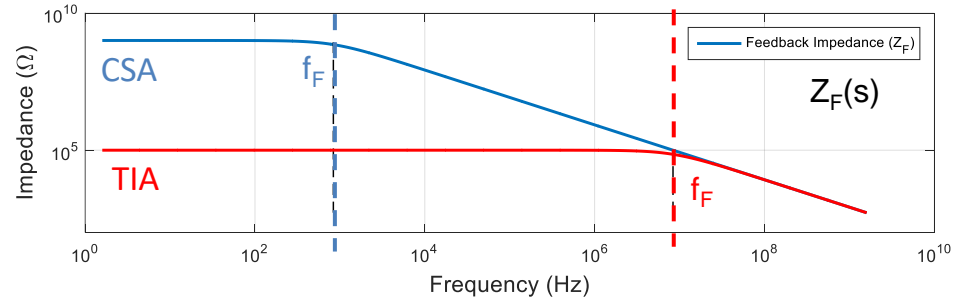
- Avoid destabilizing sensor
- Minimize crosstalk in multielectrode systems
- Reduce sensitivity of the output signal to the sensor capacitance
- Improve speed

General case



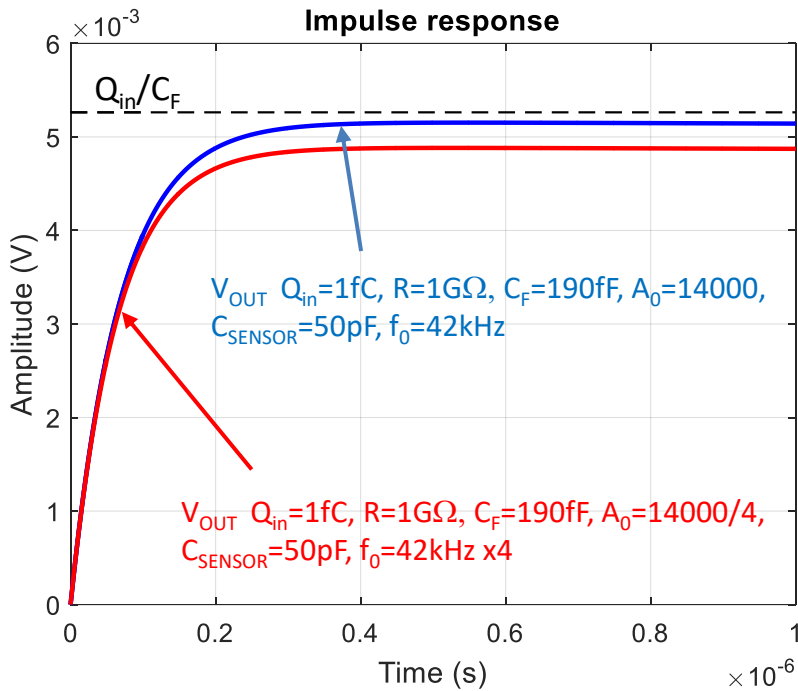
$$\frac{v_{OUT}}{i_{SENSOR}}(s) \cong Z_F(s)$$

$$Z_{FE}(s) \cong \frac{Z_F(s)}{A(s)}$$



CSA configuration: $C_F=190\text{fF}$, $R_F=1\text{G}\Omega$
 TIA configuration: $C_F=190\text{fF}$, $R_F=100\text{k}\Omega$
 Amplifier: $A_0=14000$ (83dB), $f_0=42.8\text{kHz}$, $GBWP=600\text{MHz}$

Time expressions (CSA)



Same GBWP for the two amplifiers but different gain

Increasing the open loop gain allows decreasing C_{FB} and increase the charge gain. This is important from the perspective of optimizing the system's noise-power. High gain is also important for low PSRR.

Transfer function when $R_F \rightarrow \infty$

$$\frac{v_{OUT}}{i_{IN}}(s) = \frac{1}{\left(C_F + \frac{C_{SENSOR}}{A_0}\right)s \left(1 + \frac{\tau_0}{1 + A_0 \frac{C_F}{C_{SENSOR}}}\right)s}$$

Impulse response $i_{IN} = Q_{IN} \delta(t)$

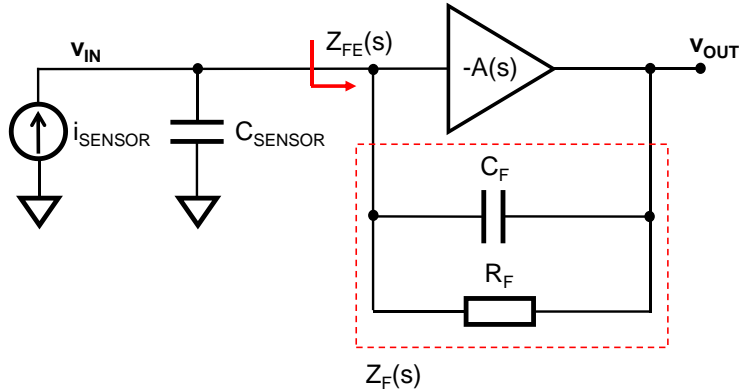
$$v_{OUT}(t) = \frac{Q_{IN}}{\left(C_F + \frac{C_{SENSOR}}{A_0}\right)} \left(1 - e^{-t/\tau}\right)$$

Importance of driving up the gain and the bandwidth of the amplifier in order to obtain a fast response of the amplitude independently of the capacitive load of the sensor (C_{SENSOR}).

By design:

$$C_F A_0 \gg C_{SENSOR}$$

Input impedance



CSA configuration: $C_F=190\text{fF}$, $R_F=1\text{G}\Omega$

TIA configuration: $C_F=190\text{fF}$, $R_F=100\text{k}\Omega$

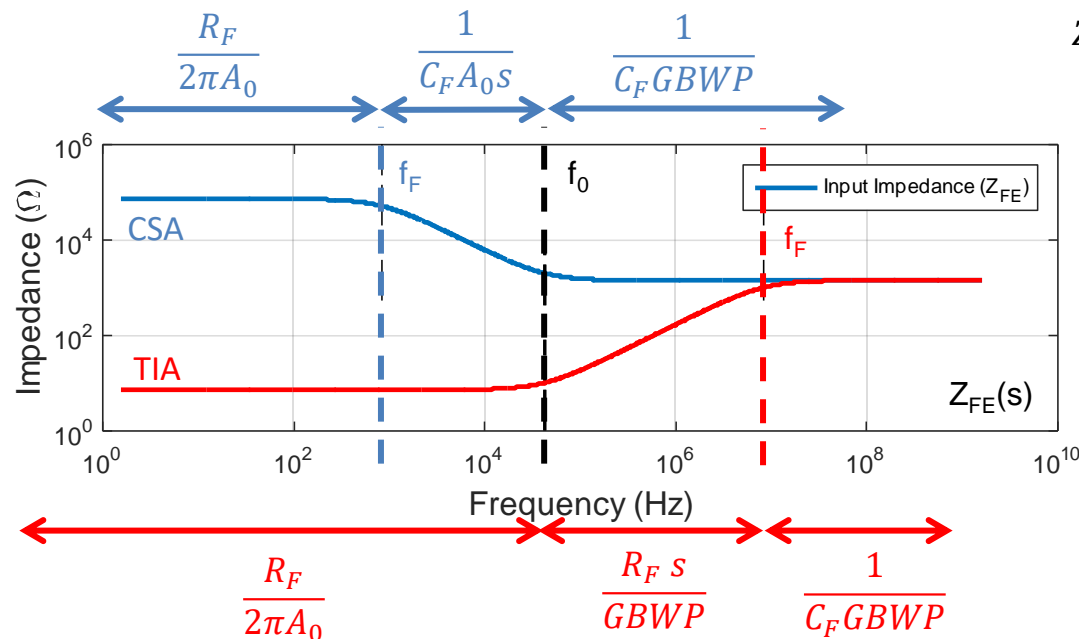
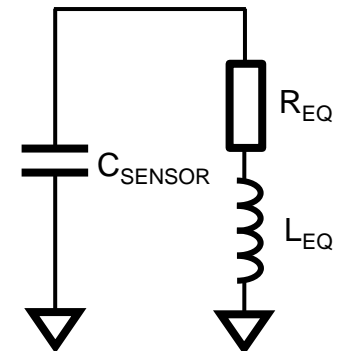
Amplifier: $A_0=14000$ (83dB) $f_0=42.8\text{kHz}$

$$Z_{FE} = \frac{Z_F(s)}{A(s) + 1} \cong \frac{Z_F(s)}{A(s)} = \frac{R_F}{(1 + R_F C_F s)} \frac{(1 + \tau_0 s)}{A_0}$$

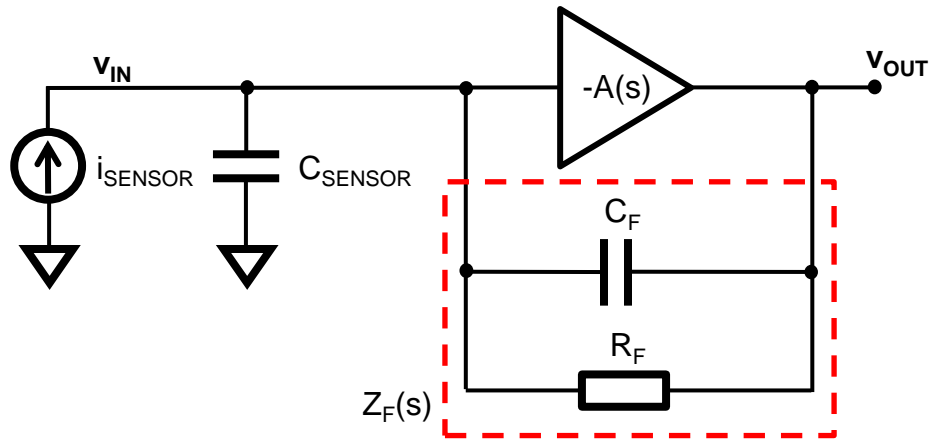
$$f_F = \frac{1}{2\pi R_F C_F}$$

$$f_0 = \frac{1}{2\pi \tau_0}$$

Inductive behaviour for the transimpedance configuration



Stability



- The expression for $v_{\text{OUT}}/i_{\text{SENSOR}}$ is that of a second order system
- In the case of a transimpedance amplifier we can calculate the minimum value for C_F required for stability

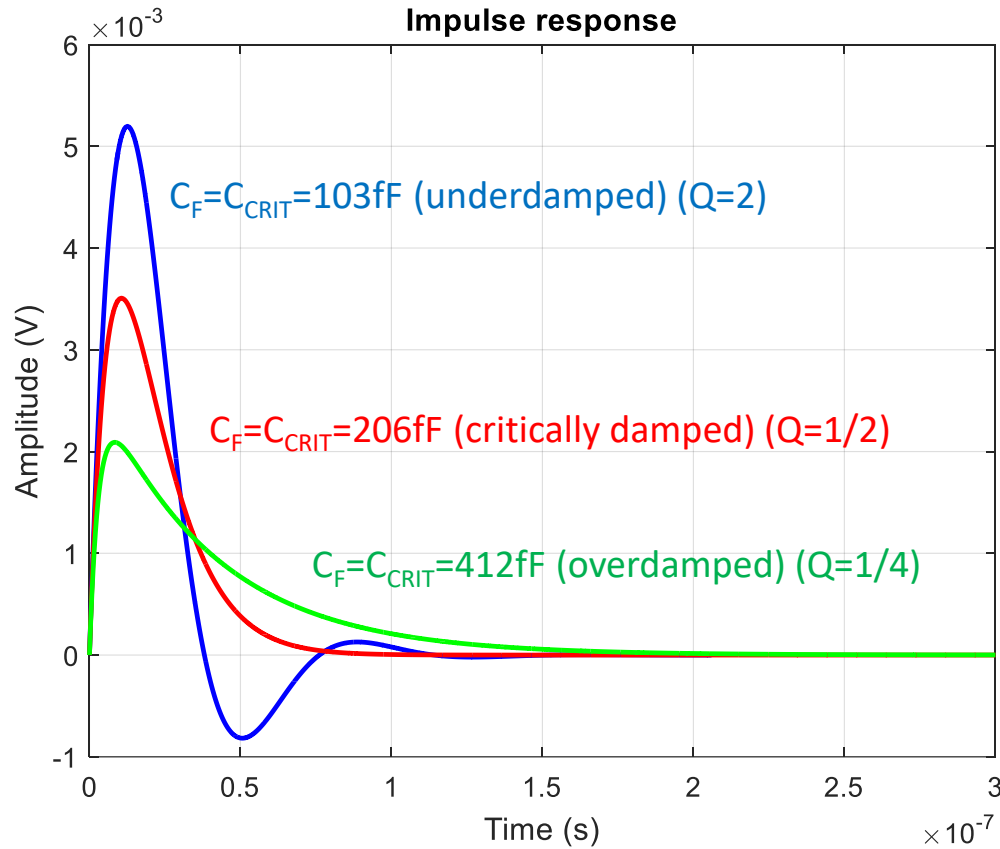
$$C_F = \frac{1}{Q} \sqrt{\frac{C_{\text{SENSOR}}}{\text{GBWP} \cdot R_F}} \quad \text{GBWP} = \frac{A_0}{\tau_0}$$

- $Q < 1/2$ (Overdamped system)
- $Q = 1/2$ (Critically damped system)
- $Q > 1/2$ (Underdamped system)

$$C_F > 2 \sqrt{\frac{C_{\text{SENSOR}}}{\text{GBWP} \cdot R_F}}$$

- For overdamped system
- High GBWP amplifiers are easier to compensate
- Trade off stability-closed loop bandwidth

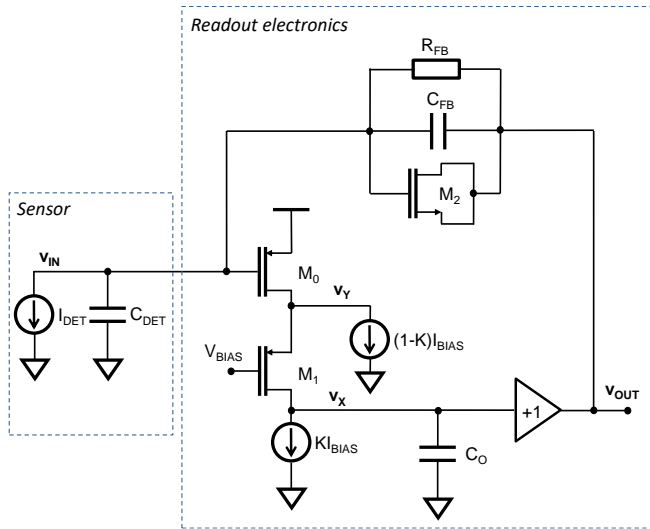
Stability



TIA configuration: $C_F = 120 \text{ fF}$, $R_F = 100 \text{ k}\Omega$
Amplifier: $A_0 = 14000$ (83dB) $f_0 = 42.8 \text{ kHz}$
 $Q_{in} = 1 \text{ fC}$

Preamplifier configurations: Examples

Hybrid Pixel Detector:

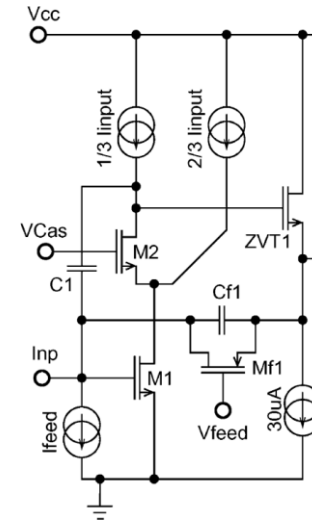


R. Ballabriga et al. "The Timepix4 Analog Front-end Design: Lessons learnt on Fundamental Limits to Noise and Time Resolution in Highly Segmented Hybrid Pixel Detectors"
<https://doi.org/10.1016/j.nima.2022.167489>

CSA configuration: $C_F \sim 3\text{fF}$, $R_F \sim 80\text{M}\Omega$ (tunable)
 Amplifier: $A_0 = 1000$ (60dB), GBWP=1GHz
 $C_{\text{SENSOR}} = 25\text{fF}$ (Nominal)

(R_F is simplified in this schematic)

Strip Detector:



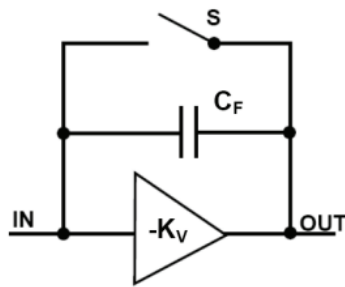
J. Kaplon and W. Dabrowski "Fast CMOS Binary Front End for Silicon Strip Detectors at LHC Experiments" IEEE TRANSACTIONS ON NUCLEAR SCIENCE, VOL. 52, NO. 6, DECEMBER 2005

TIA configuration: $C_F = 190\text{fF}$, $R_F \sim 120\text{k}\Omega$
 Amplifier: $A_0 = 14000$ (83dB), $f_0 = 42.8\text{kHz}$, GBWP=600MHz
 $C_{\text{SENSOR}} = 20\text{pF}$ (Nominal)
 $\tau_F = 22\text{ns}$

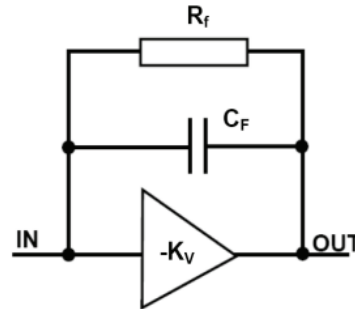
Single ended common source (cascode) configuration

M_2 MOS: M. Manghisoni, D. Comotti, L. Gaioni, L. Ratti, V. Re, "Dynamic compression of the signal in a charge sensitive amplifier: From concept to design", IEEE Trans. Nucl. Sci. 62 (5) (2015) 2318–2326

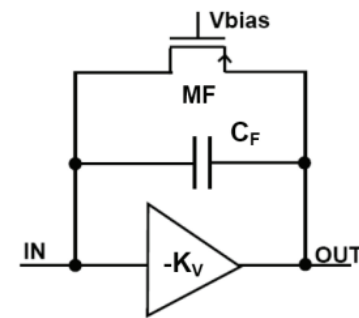
Reset configurations in CSAs



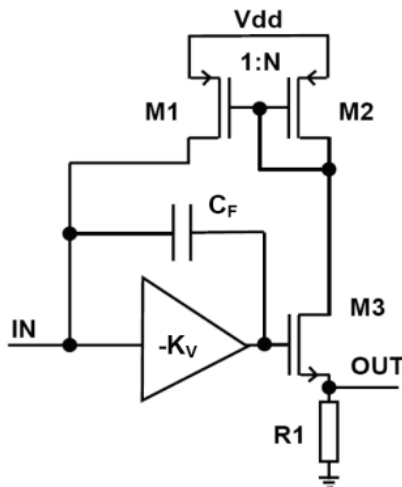
Switch Reset (charge injection to preamplifier input)



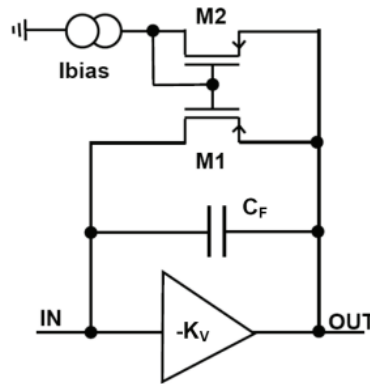
Continuous Reset: Resistor (high value for R difficult to implement in CMOS)



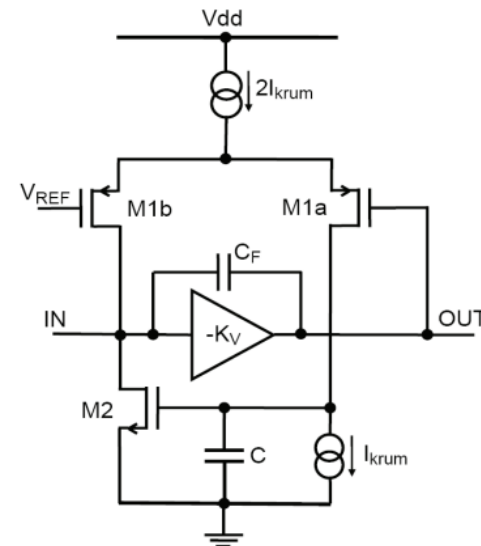
Continuous Reset: MOS transistor
Compact solution, Non-linearity



Current conveyor discharge



Current mirror (constant current discharge)



Differential stage, ($R_{eq} = 1/g_{m1}$ (small signal),
 $I_{dis} = I_{KRUM}$ (large signal, leakage current compensation, Krummenacher)

Noise

Basic introduction

Types of noise

Noise in the MOS transistor

Noise in a cascade of amplifiers

Noise (basic introduction)

- Noise is a random process (its value cannot be predicted at any time)
- Statistical model allows us to predict its long term r.m.s. value (its randomness) and its average power
- Average power delivered by a periodic signal to a load resistance

$$P_{av} = \frac{1}{T} \int_{-T/2}^{+T/2} \frac{v^2(t)}{R} dt \quad [Watts]$$

- The average power for a random signal is given by

$$P_{av} = \lim_{T \rightarrow \infty} \frac{1}{T} \int_{-T/2}^{+T/2} x^2(t) dt \quad [V^2]$$

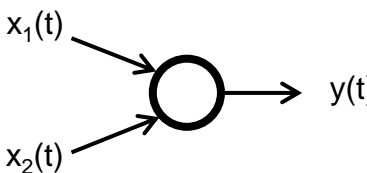
- We can also define the rms value as $\text{sqrt}(P_{av})$
- The power spectral density ($S_x(f)$) shows how much power the signal carries at each frequency. $S_x(f)$ is the average power carried by $x(t)$ in a 1Hz bandwidth around frequency f

$$P_{av} = \int_{-\infty}^{\infty} S_x(f) df \quad [V^2]$$

$$r. m. s. = \sqrt{P_{av}} \quad [V r. m. s.]$$

Noise (basic introduction)

- The average noise power of the sum of two separate sources is:



A block diagram showing a summing junction represented by a circle with two input arrows labeled $x_1(t)$ and $x_2(t)$ entering from the left, and one output arrow labeled $y(t)$ exiting to the right.

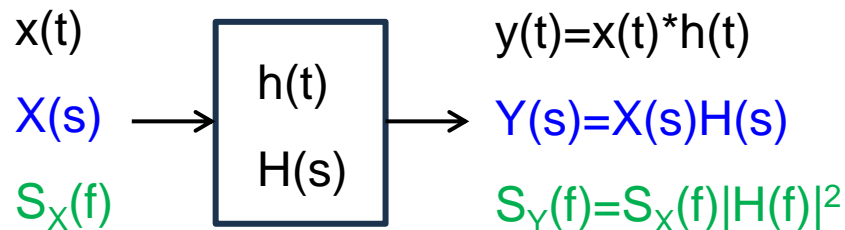
$$P_{avy} = P_{avx1} + P_{avx2} + \lim_{T \rightarrow \infty} \frac{1}{T} \int_{-T/2}^{+T/2} 2x_1(t)x_2(t) dt \quad [V^2]$$

Correlation factor

The third term indicates how similar the two waveforms are (equals zero if the two sources are uncorrelated)

- If a signal (noise) with power spectral density $S_X(f)$ is applied to a linear time-invariant system with transfer function $H(f)$, then the output spectrum $S_Y(f)$ is given by

$$S_Y(f) = S_X(f)|H(f)|^2$$

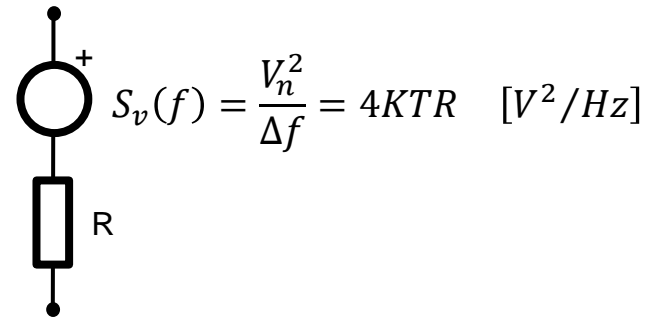


The noise (in the frequency domain) is shaped by the filter

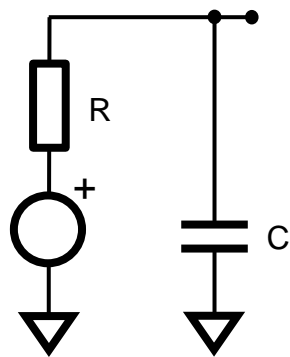
Types of noise

Thermal noise

- Results from random thermal motion of carriers in a conductor. The thermal noise of a resistor can be modelled by a series voltage source with one sided spectral density:



- We can consider thermal noise is white (in reality it decreases at high frequencies $\sim 10\text{THz}$ at room temperature or $\sim 10\text{GHz}$ at 4K)



$$S_v(f) = \frac{V_n^2}{\Delta f} = 4KTR \quad [V^2/Hz]$$

$$P_{n,out} = \frac{KT}{C} [V^2]$$

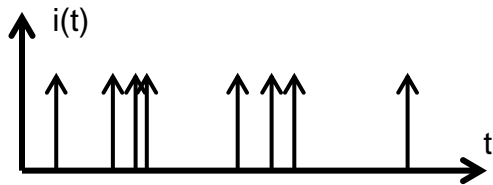
$$v_{rms} = \sqrt{\frac{KT}{C}} [V \text{ r. m. s.}]$$

The noise is independent of R
Larger values of R, the associated noise per unit bandwidth increases but the overall bandwidth of the circuit decreases.

Sound: "shhhhhh"

Shot noise

- Occurs when there exist distinctive transitions of charge carriers happening (for example carriers crossing a potential barrier p-n junction)

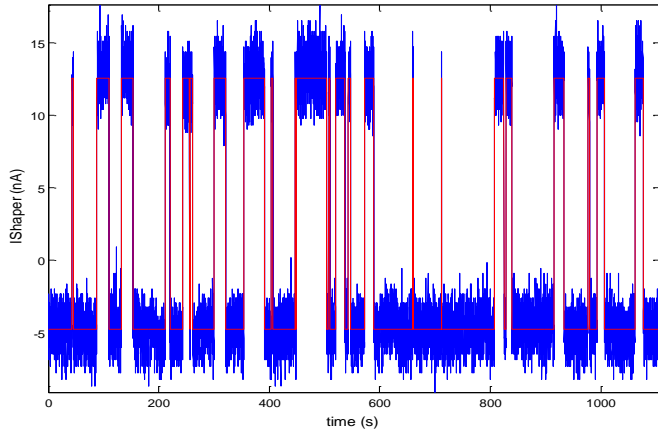


$$S_i(f) = \frac{i_{sh}^2}{\Delta f} = 2qI \quad [I^2/Hz]$$

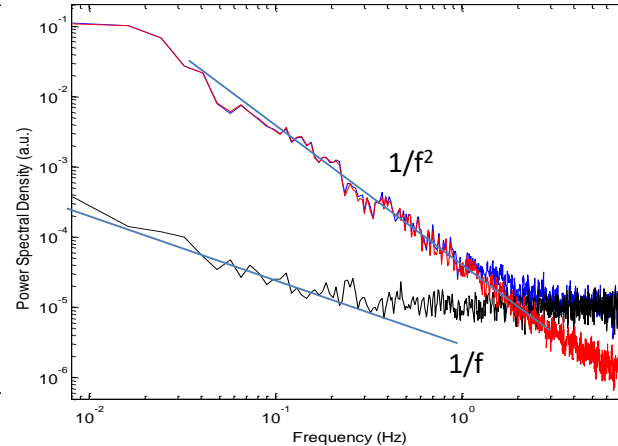
- We consider it white although the shape of the power spectral density is determined by the shape of the current that is generated in every distinctive event
- Sound: "rain hitting the ground"*

Pop corn noise, Burst Noise, Random Telegraph Noise

AC component of Shaper I - time trace



Power Spectral Density of Shaper Current



$$R_{XX}(\tau) = \lim_{T \rightarrow \infty} \frac{1}{T} \int_{-\frac{T}{2}}^{+\frac{T}{2}} x(t)x(t + \tau) dt$$

$$S_X(f) = F\{R_{XX}(\tau)\}$$

- Can be determined by the behaviour of a single trap site in the semiconductor. It is the basis for the discussion on flicker noise
- Autocorrelation function (cusp shape), Lorentzian ($1/f^2$) Power Spectral Density due to a single trap:

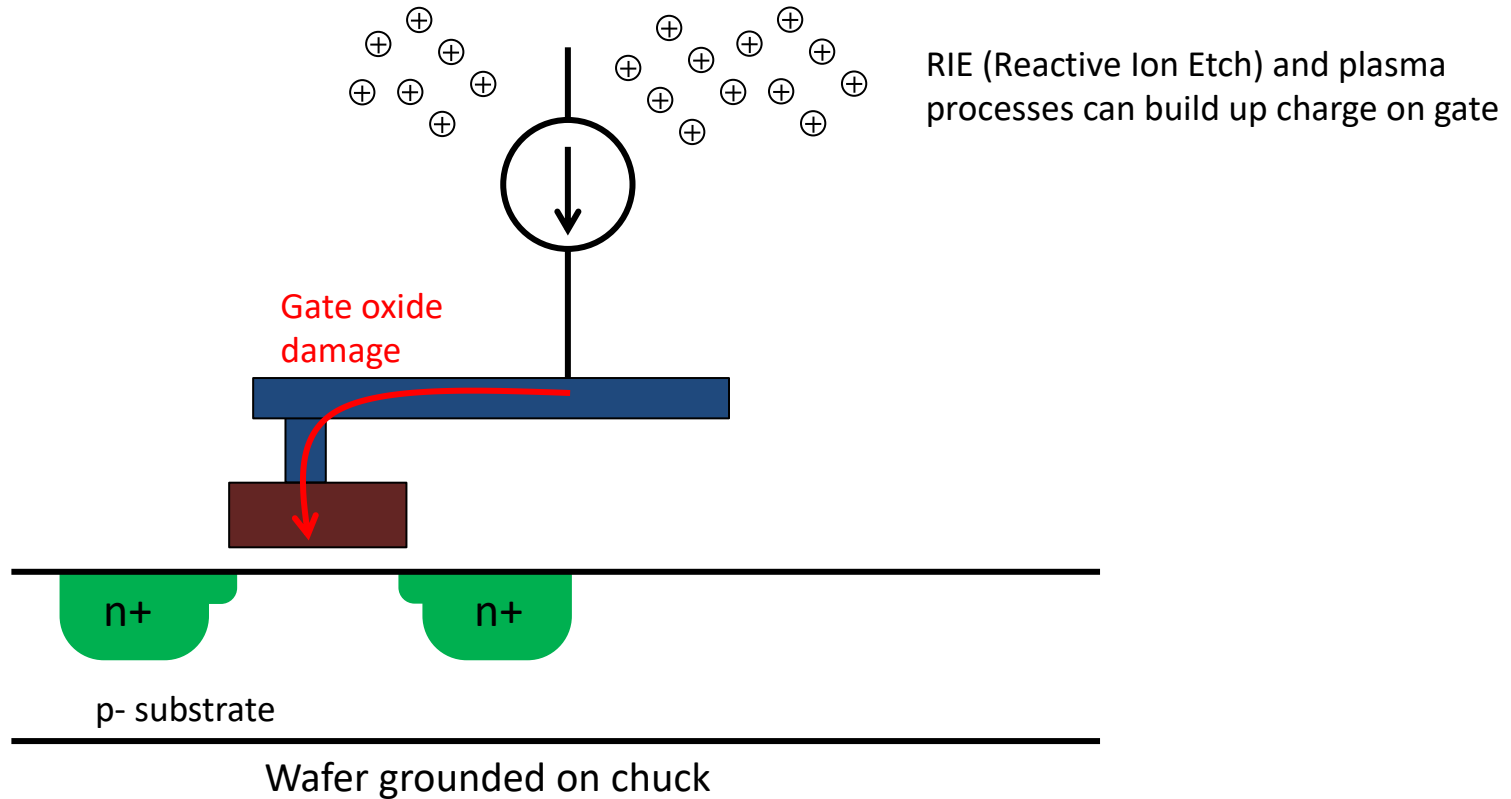
$$R_{XX}(\tau) = R_{XX}(0)e^{-|\tau|/\tau_t} \quad S_i(f) = \frac{c_t \tau_t}{1 + (2\pi f)^2 \tau_t^2}$$

- *Sound: "Old audio systems, clicking sound (gold impurities in bipolars)"*

We saw it due to the switching behaviour of post breakdown conduction in thin oxide SiO₂ films

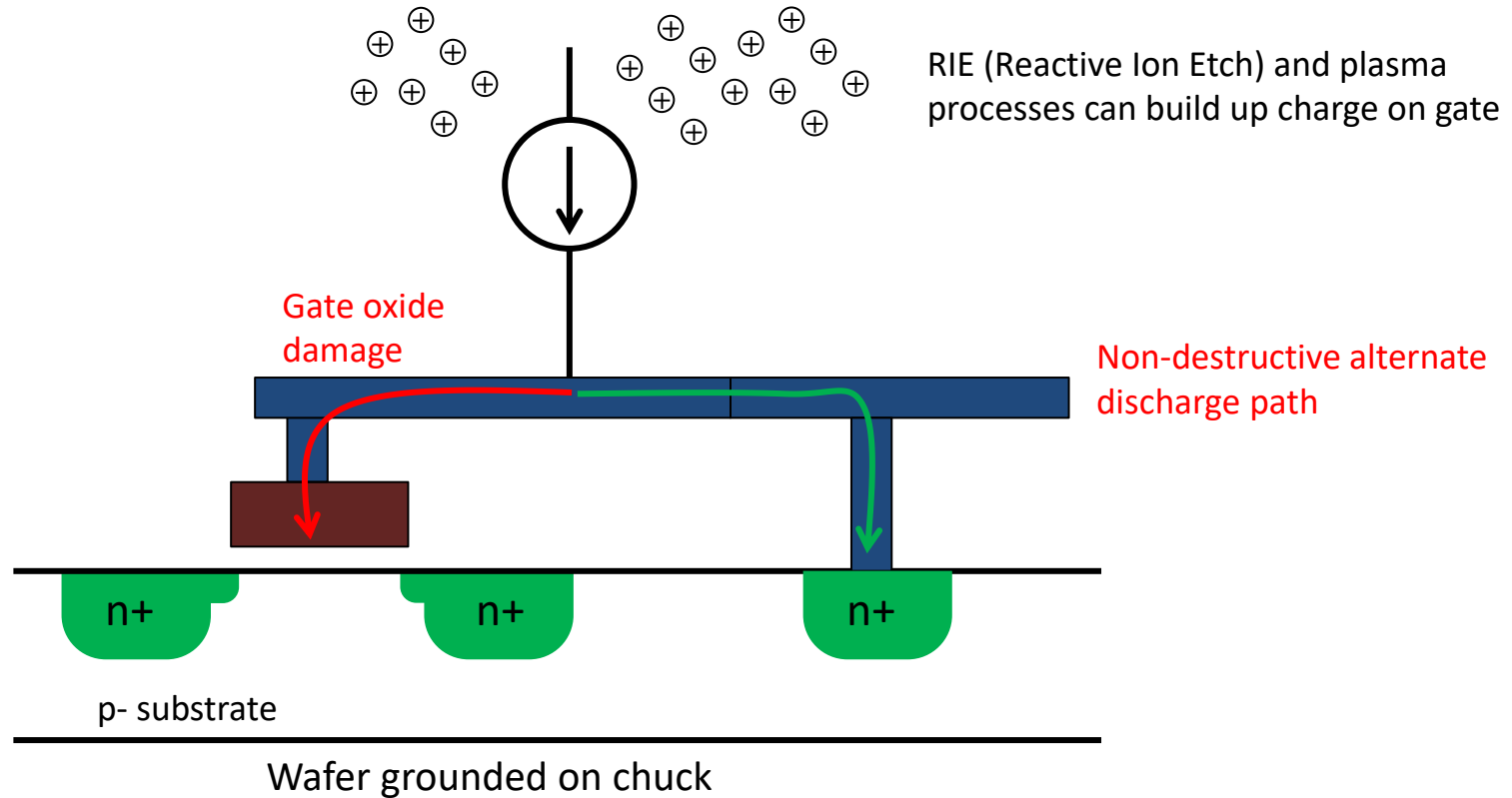
Can also be observed in very small transistors due to the percolation nature of the I_{DS} and the impact on this current from a single charge trap

Antenna effects



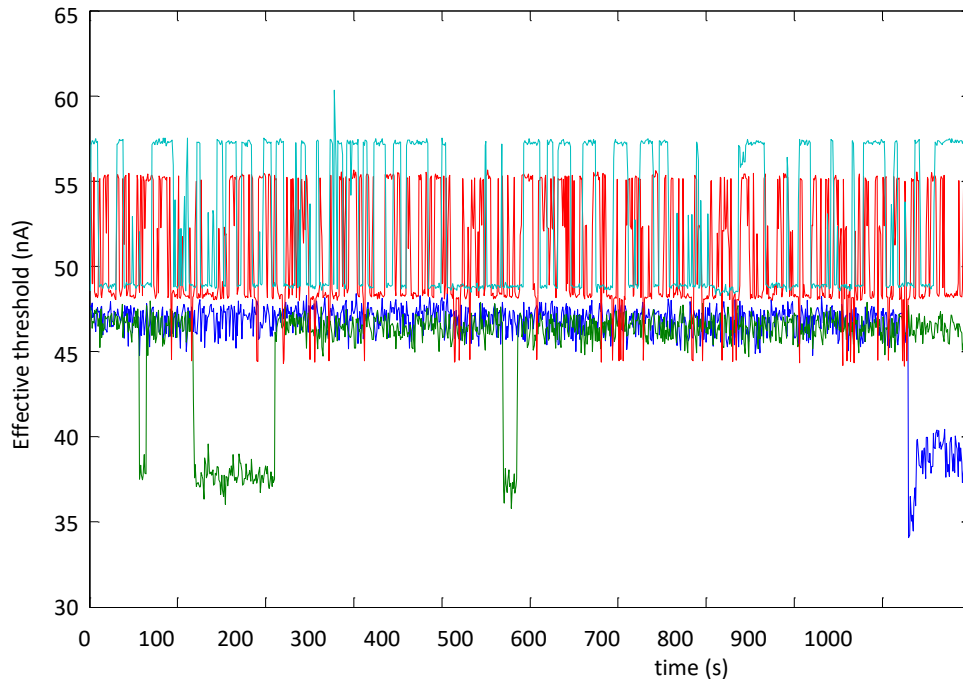
“The thin oxide degradation in the plasma environment would appear as a random effect due to the fact that it would influence differently every transistor”^a

Antenna effects



- Charge build up → Oxide breakdown → Reliability degradation
- Effects: increased gate leakage current and V_T and transconductance shift
- A diode to substrate is an effective way to prevent charge build up across the gate dielectric. At wafer processing temperatures, the diode is sufficiently conductive to prevent any charge build up. At normal circuit operation temperatures the diode is in low leakage, low capacitance reverse state.
- “Recommended that all gates be tied down to a diode at M1” .

Pop corn noise, Burst Noise, Random Telegraph Noise

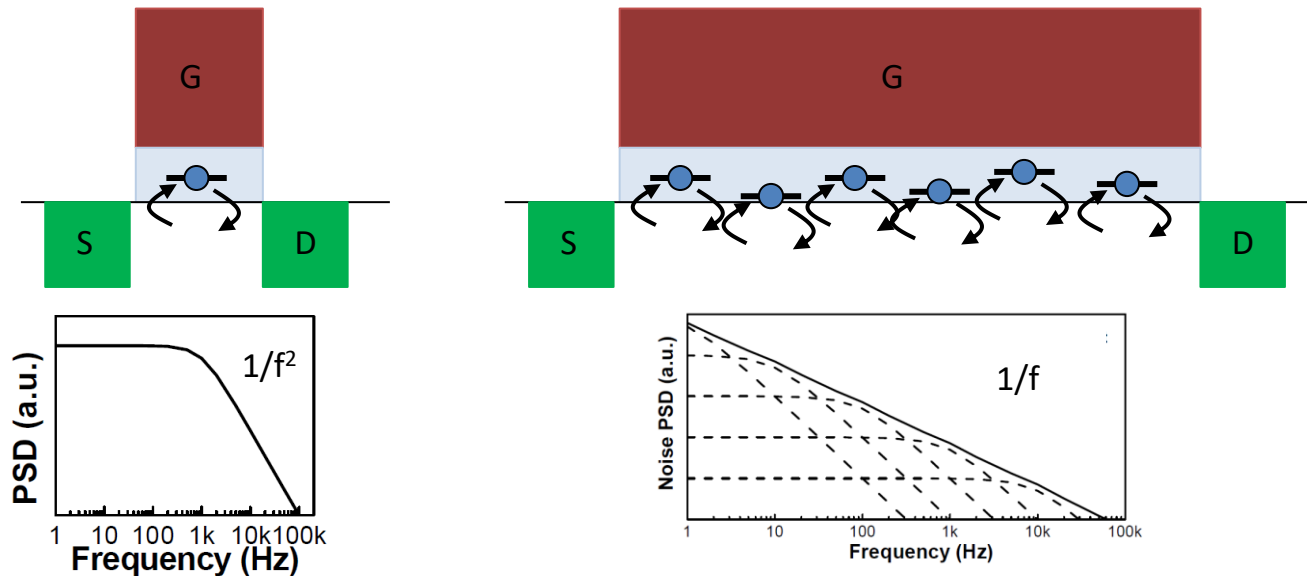


- We measured RTS on individual pixels
- 2 hour measurement RTS on less than 1% of the pixels showing RTS
- Different frequencies (changes between states from tens of second to hours)

Take home message: “If you want to keep a good integrity of the thin oxide of your transistors (and have a good matching and prevent gate leakage current) put a (minimum size) tie down diode at the gate connected to the poly with M1.”

Flicker noise

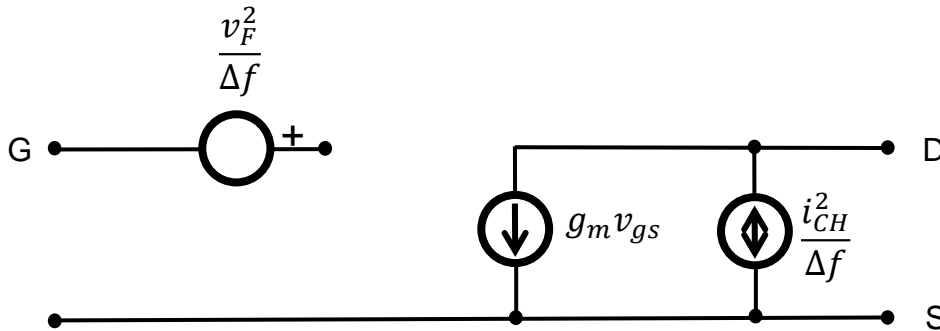
- $1/f$ noise is related to the random distribution of time constants of charge traps (e.g. in interfaces or in dislocations of the crystal structure)
- Interface traps “capture” and “release” charge
- In the case of the transistor, the larger the gate area, the more these fluctuations are averaged out
- Large number of traps uniformly distributed with independent τ_t values means that their superposition approximates a $1/f$ behaviour



Noise in the MOS transistor

MOS transistor noise (simplified)

- MOS transistors exhibit thermal noise generated in the channel and 1/f noise (other noise sources are neglected here)



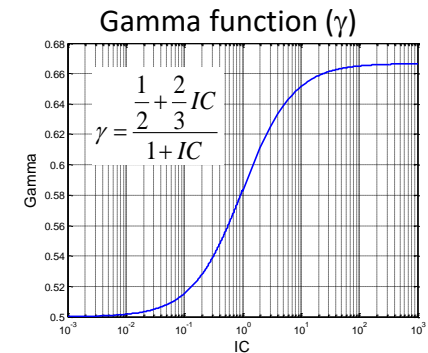
Thermal noise from the channel and flicker noise expressions (referred to the gate terminal) :

$$\frac{v_{CH}^2}{\Delta f} + \frac{v_F^2}{\Delta f} = 4KTn\gamma \frac{1}{g_m} + \frac{K_a}{C_{ox}WLf^\alpha}$$

$$\frac{i_{CH}^2}{\Delta f} = 4KTn\gamma\alpha_w g_{d0}$$

α_w is the noise excess factor (1.09 NMOS, 1.04 PMOS in 65nm CMOS)*

g_{d0} is the drain-source conductance when $V_{DS}=0$, the same as R_{ON}^{-1} . For long channel devices (i.e. non velocity saturation) $g_{ds0}=g_m$



Variability of Low Frequency Noise and Mismatch in Enclosed-Gate and Standard nMOSFETs

Matthias Bucher¹, Aristeidis Nikolaou¹, Nikolaos Mavredakis¹, Nikolaos Makris¹,
Mathieu Coustans², Jérôme Lolivier³, Predrag Habas³, Alexandre Acovic³, and René Meyer³

¹School of Electrical and Computer Engineering, Technical University of Crete, 73100 Chania, Greece

²Ecole Polytechnique Fédérale de Lausanne (EPFL), 1015 Lausanne, Switzerland

³EM Microelectronic-Marin SA, 2074 Marin-Epagnier, Switzerland

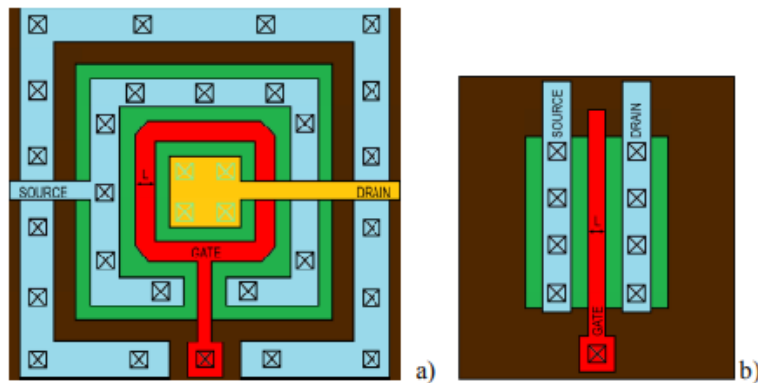


Fig. 1. Layout of enclosed gate transistors with drain at the center, and outer poly-edge cut a), and layout of standard transistor b).

IV. CONCLUSIONS

Enclosed gate nMOS transistors show reduced low frequency noise levels compared to standard-layout devices of the same technology, reduced by a factor of 2 to 3 in weak-moderate inversion. Furthermore, the EG nMOS devices show also a reduced standard deviation of LFN. Another advantage is the suppression of gate voltage mismatch degradation in weak inversion. These improvements are all attributed to the absence of the STI-edge effect in the enclosed-gate transistor structures. The 50 measured devices show a typical $1/f$ noise behavior at higher gate voltages, while RTN components appear at gate voltages around moderate and weak inversion. The statistical LFN model [17], [18] can cover both gate- and drain-voltage bias-dependence of average noise and its standard deviation, similarly for enclosed-gate as well as standard-layout transistors.

ELT transistors are effective in minimizing flicker noise

In the early 90's E. Heijne suggested the use of special gate all around design techniques to make radiation hard components in standard commercial CMOS processes.

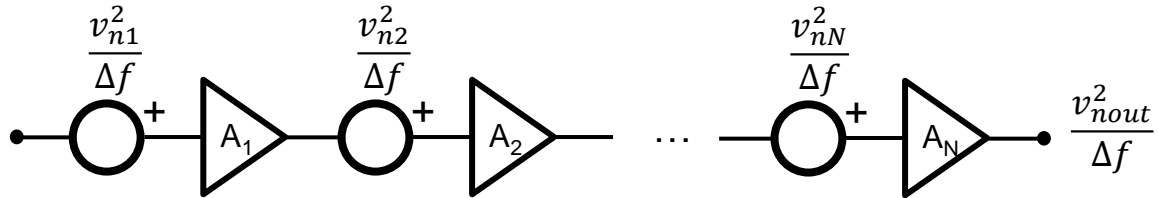
A. Marchioro was key to getting access to the $0.25\mu\text{m}$ CMOS process and led the development of a digital library which was radiation tolerant.

Thesis: G. Anelli «Conception et caractérisation de circuits intégrés résistants aux radiations pour les détecteurs de particules du LHC en technologies CMOS submicroniques profondes»

Noise in a cascade of amplifiers

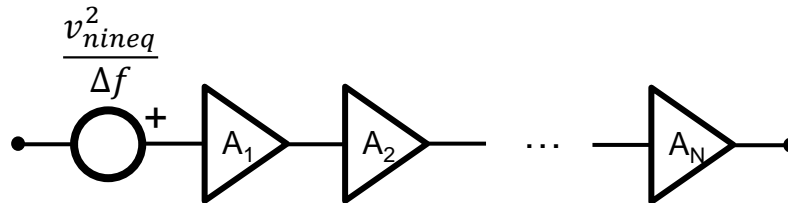
Noise in a cascade of amplifiers

Output noise:



$$\frac{v_{nout}^2}{\Delta f} = \frac{v_{n1}^2}{\Delta f} A_1^2 A_2^2 \dots A_N^2 + \frac{v_{n2}^2}{\Delta f} A_2^2 \dots A_N^2 + \dots + \frac{v_{nN}^2}{\Delta f} A_N^2$$

Input referred noise:



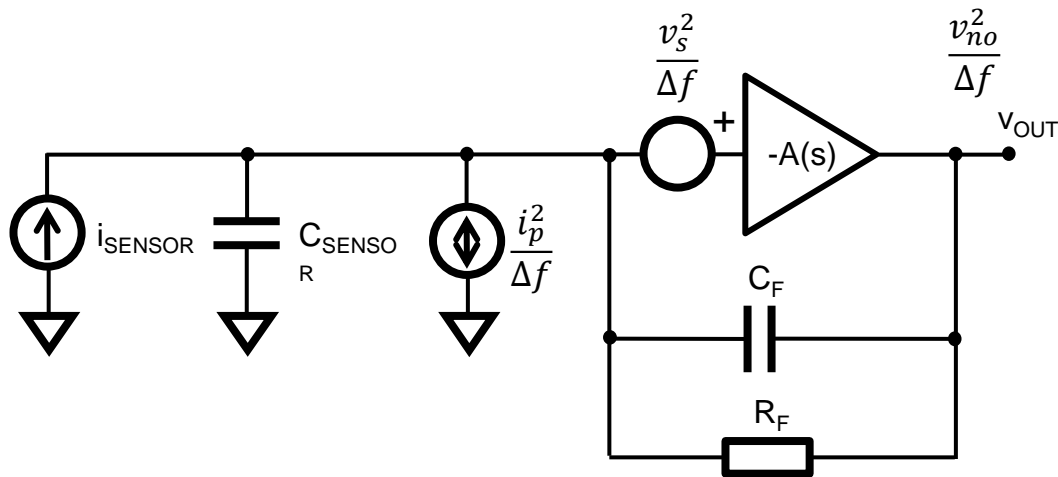
The most important noise source in a cascade of amplifiers is the one from the input stage

$$\frac{v_{n1}^2}{\Delta f} = \frac{v_{n1}^2}{\Delta f} + \frac{v_{n2}^2}{\Delta f} \frac{1}{A_1^2} + \dots + \frac{v_{nN}^2}{\Delta f} \frac{1}{A_1^2 A_2^2 \dots A_{N-1}^2}$$

Most of the noise in a typical readout electronics chain for the readout of semiconductor detectors comes from the input transistor.

Transfer of noise sources to the output of the CSA

Transfer of noise sources to the output of the CSA



The power spectral density at the output is “coloured”

$$\frac{v_{no}^2}{\Delta f} = \frac{v_s^2}{\Delta f} \frac{C_{\text{SENSOR}}^2}{C_F^2} + \frac{i_p^2}{\Delta f} \frac{1}{C_F^2 (2\pi f)^2}$$

Series component:

$$\frac{v_s^2}{\Delta f} = \frac{v_{\text{CH}}^2}{\Delta f} + \frac{v_F^2}{\Delta f} = 4KTn\gamma \frac{1}{g_m} + \frac{K_a}{C_{\text{ox}}WLf^\alpha}$$

Parallel component:

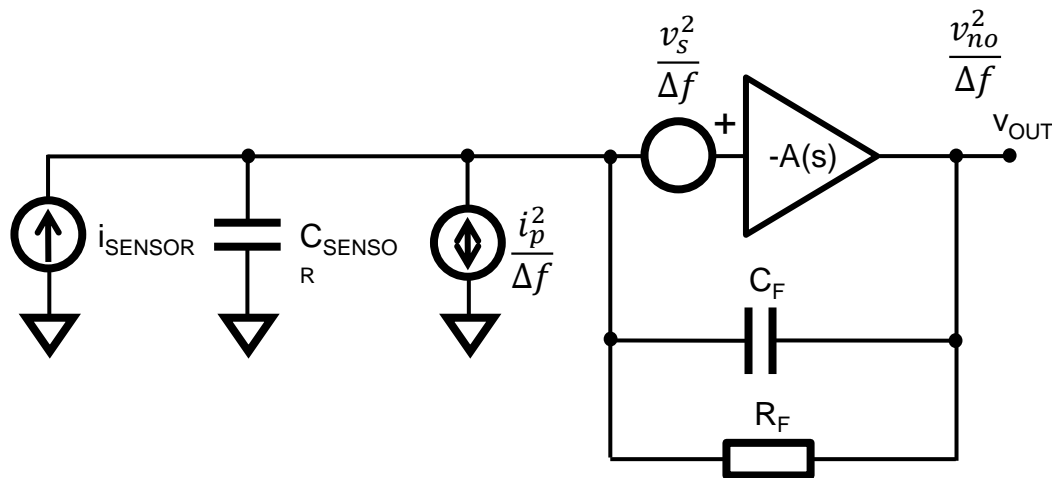
$$\frac{i_p^2}{\Delta f} = \frac{i_{\text{leak}}^2}{\Delta f} + \frac{i_{\text{RF}}^2}{\Delta f} = 2qI_{\text{LEAK}} + 4KT \frac{1}{R_F}$$

Noise mechanisms arising from (1) the preamplifier’s transistors (thermal, flicker), (2) the feedback resistor (thermal) and (3) the sensor (shot) can be represented in the circuit domain by two equivalent noise generators placed at the input in “series” and “parallel”.

The series noise generator usually has two components, thermal noise with a white spectral density and flicker noise (more generally $1/f^\alpha$) due to interface effects and is strongly process dependent.

The parallel noise generator includes the thermal noise from R_F and the shot noise from the sensor.

Transfer of noise sources to the output of the CSA



The power spectral density at the output is "coloured"

$$\frac{v_{no}^2}{\Delta f} = \frac{v_s^2}{\Delta f} \frac{C_{SENSOR}^2}{C_F^2} + \frac{i_p^2}{\Delta f} \frac{1}{C_F^2 (2\pi f)^2}$$

Series component:

$$\frac{v_s^2}{\Delta f} = \frac{v_{CH}^2}{\Delta f} + \frac{v_F^2}{\Delta f} = 4KTn\gamma \frac{1}{g_m} + \frac{K_a}{C_{ox}WLf^\alpha}$$

Parallel component:

$$\frac{i_p^2}{\Delta f} = \frac{i_{leak}^2}{\Delta f} + \frac{i_{RF}^2}{\Delta f} = 2qI_{LEAK} + 4KT \frac{1}{R_F}$$

Value for which the thermal noise from the resistor (R_F) is equal to the shot noise from the detector leakage current

$$2qI_{LEAK} = 4KT \frac{1}{R_F} \quad R_F = \frac{4KT}{2qI_{LEAK}} \cong \frac{50mV}{I_{LEAK}}$$

e.g. If $I_{LEAK}=1nA$ then $R_F > 50M\Omega$

$$ENC_{CH} = \frac{\sqrt{v_{nout}^2}}{\frac{q}{C_F}} \frac{1}{q} \sqrt{KTn\gamma \frac{C_{SENSOR}C_F}{C_L}}$$

r.m.s. noise
amplitude to 1e

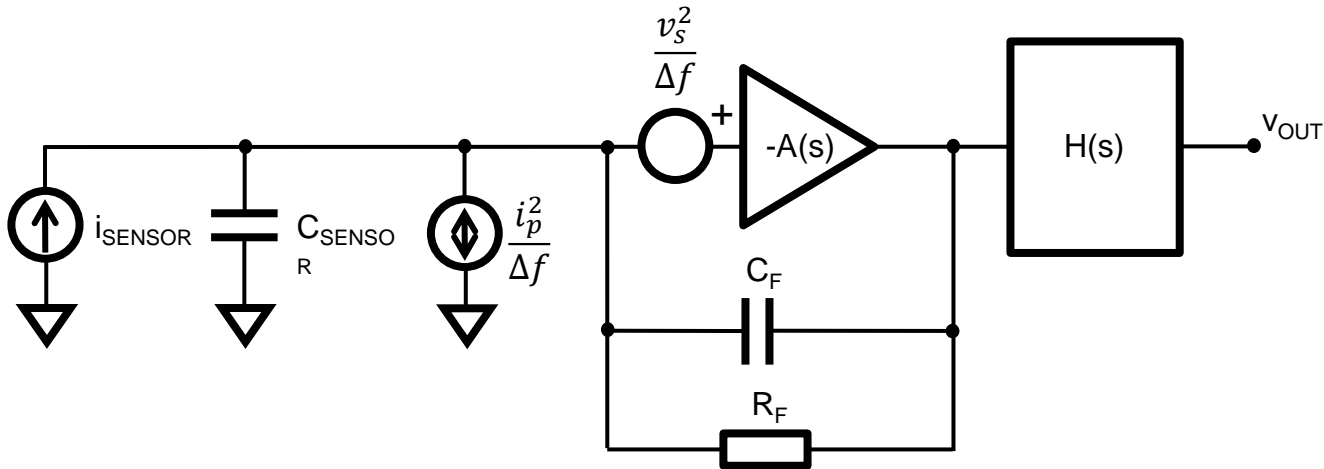
Equivalent Noise Charge (ENC) does not depend on g_m i.e. does not depend on power*

Full noise calculations can be found in A. Rivetti "CMOS Front-End Electronics for Radiation Sensors"

* X. Llopart et al 2019 JINST 14 C01024

Noise filtering

Noise filtering



Objectives of signal processing after preamplifier:

- Improve the Signal-to-Noise ratio
- Minimize pile-up by *shaping* the signal
- Minimize baseline fluctuations
- Add additional gain

Shaping implies manipulating the frequency component of the signal i.e. a shaper is a filter

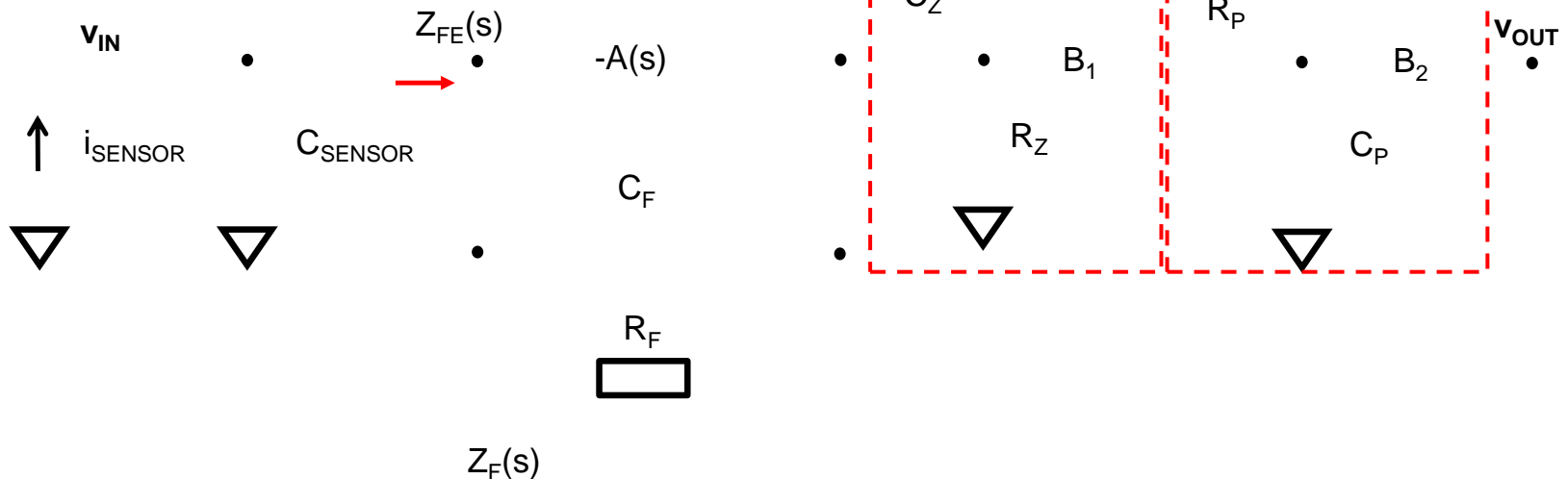
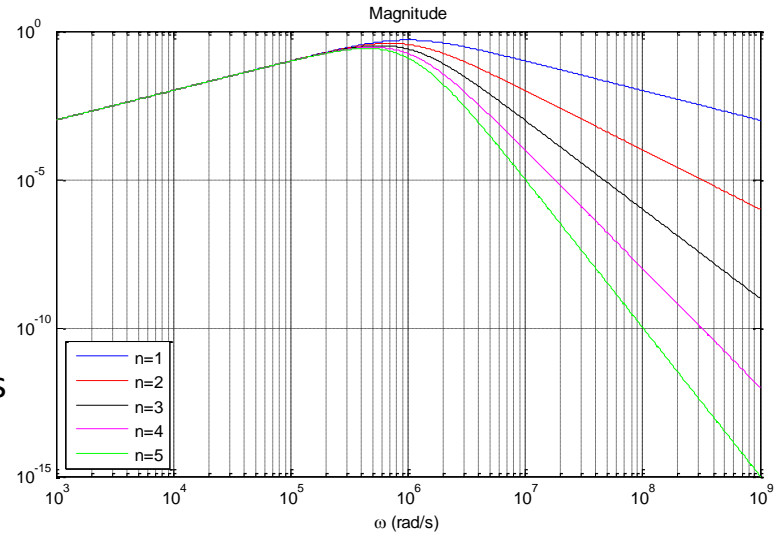
CR-RC shaper

The shaper

- CR-RCⁿ filters offer a good compromise between performance, power consumption and simplicity
- Unipolar semi gaussian shaper (CR-RCⁿ) consists of one differentiation of the signal followed by n integrations
- n is the order of the shaper
- If the differentiation and integration time constants are chosen to be the same the transfer function of the shaper is given by:

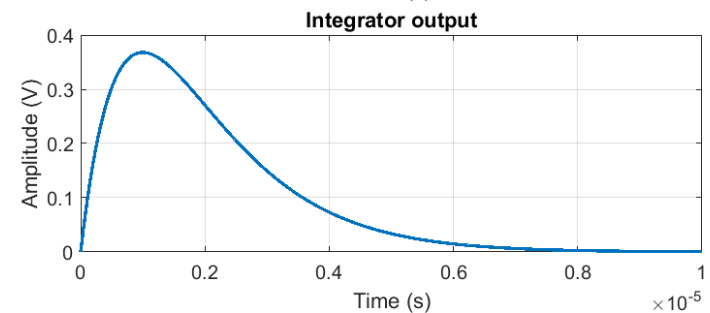
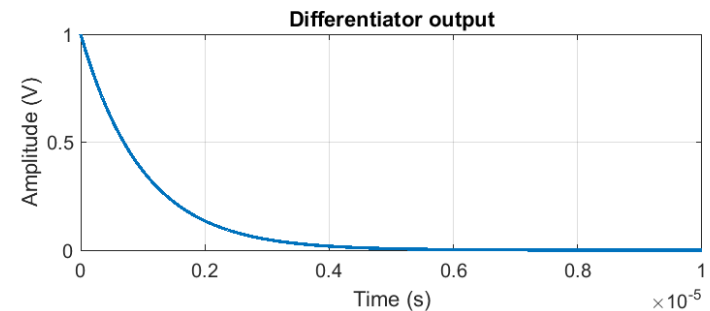
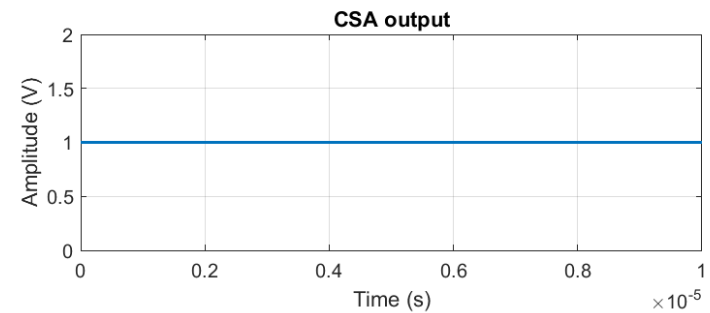
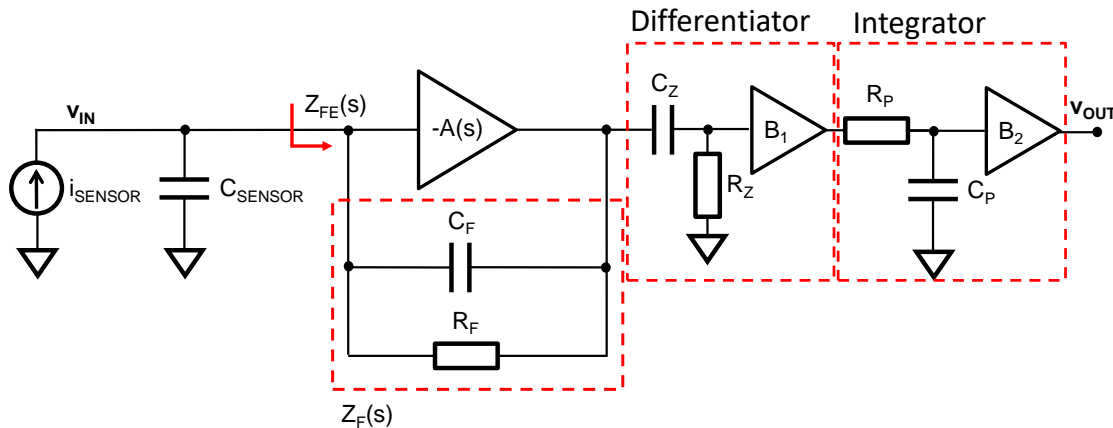
$$H(s) = \left(\frac{s\tau}{1+s\tau} \right) \left(\frac{1}{1+s\tau} \right)^n$$

Differentiator Integrator



The shaper

- In the time domain the high pass filter removes low frequency part of the signal creating a waveform that goes to the baseline before the next pulse arrives.
- Following the high pass filter, a low pass filter smooths the signal



The shaper

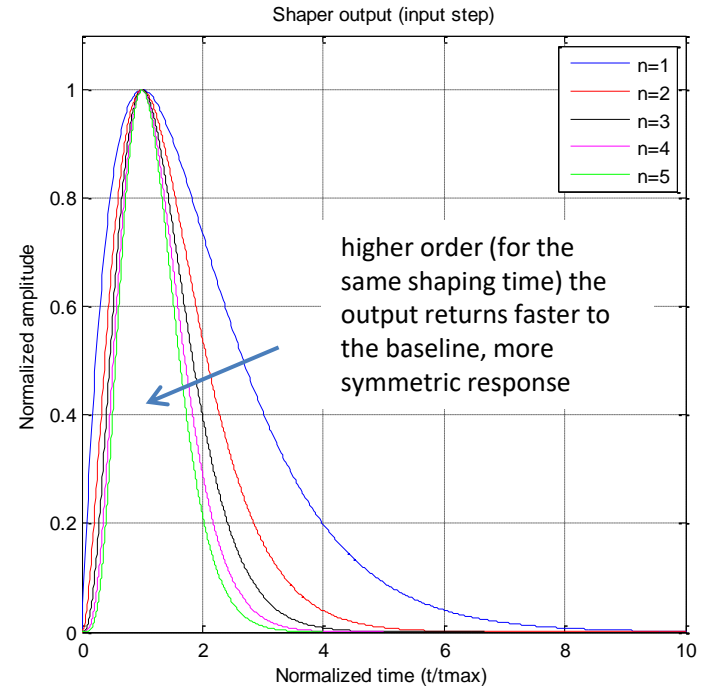
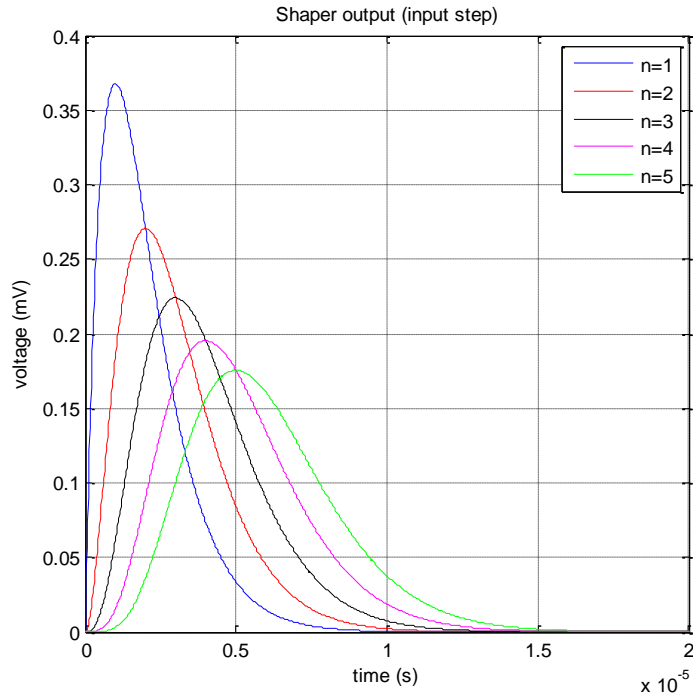
- In the time domain the response to a step function is:

$$v_{out}(t) = \frac{1}{n!} \left(\frac{t}{\tau} \right)^n \exp\left(-\frac{t}{\tau} \right)$$

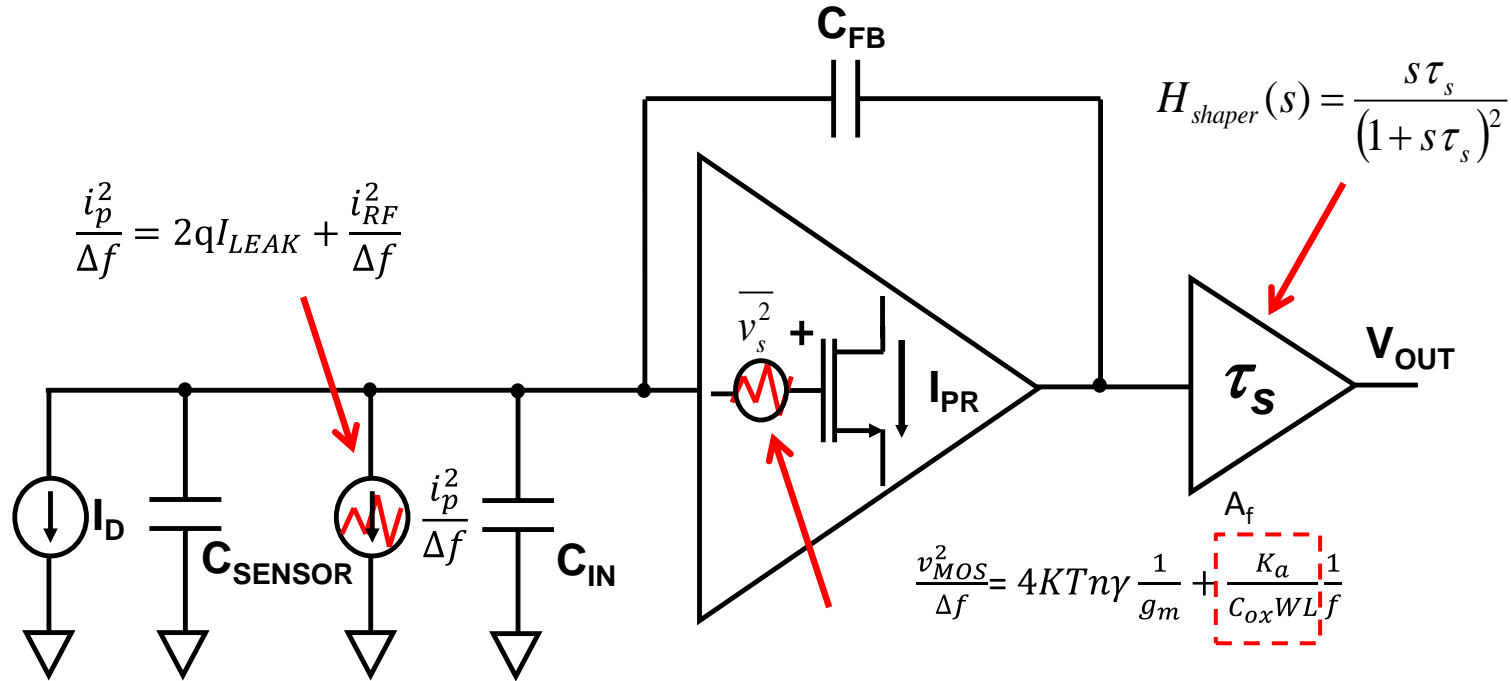
- The peaking time is at $t = n\tau$

- And the amplitude of the signal is

$$v_{out_max}(t) = \frac{n^n}{n! e^n}$$



Noise equation of the system:



Series thermal Series flicker Parallel

$$ENC^2 = (C_{SENSOR} + C_{IN})^2 \left[\frac{v_{MOS}^2}{\Delta f} \frac{1}{\tau_s} a_s + A_f 2\pi a_f \right] + \frac{i_p^2}{\Delta f} \tau_s a_p$$

Sensor capacitance → C_{SENSOR}
 Input transistor capacitance → C_{IN}
 Shaping time (τ_s) → τ_s
 Shaper parameters (a_s, a_f, a_p) → a_s, a_f, a_p

Noise equation of the system:

$$ENC^2 = (C_{SENSOR} + C_{IN})^2 \left[\frac{v_{MOS}^2}{\Delta f} \frac{1}{\tau_s} a_s + A_f 2\pi a_f \right] + \frac{i_p^2}{\Delta f} \tau_s a_p$$

Series thermal

Series flicker

Parallel

Sensor capacitance

Input transistor capacitance

Shaping time (τ_s)

Shaper parameters (a_s, a_f, a_p)

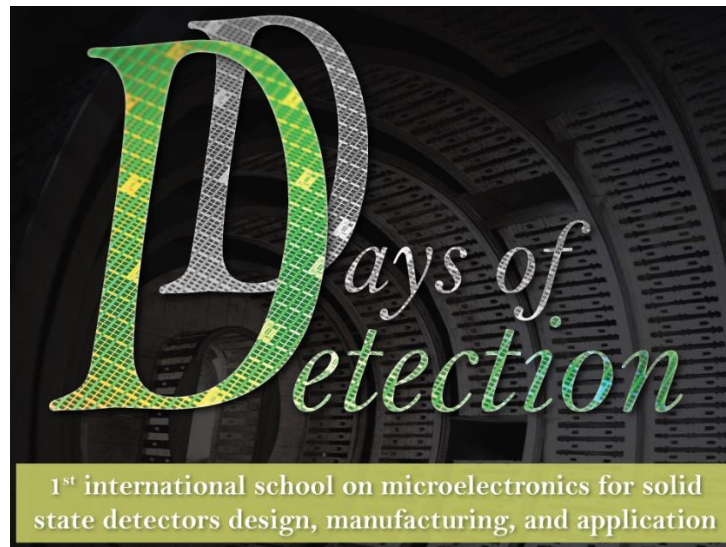
In most designs, the dominant noise source is the input transistor

Increasing the width of the input transistor (if biased in s.i.) increases both its g_m and the input capacitance. Usually an optimum of ENC exists w.r.t. input transistor width.

Note as well that a minimum exists w.r.t. the shaping time. For small values, the thermal noise dominates, for high values of τ_s the parallel noise dominates.

In a system in which the peaking time can be optimized, the flicker noise imposes the achievable noise performance. The flicker can be improved increasing the area and choosing the right transistor type (PMOS instead of NMOS).

In front-ends optimized for low power, and speed the channel thermal is the dominant contribution.



Part 1: Introduction to hybrid pixel detectors

Classification of technologies, limitations of hybrid pixel detectors

Part 2: Introduction to signal processing

Part 3: Review of ASICs

Rafael Ballabriga Suñé

rafael.ballabriga@cern.ch

CERN Microelectronics Section

Outline

- Review of ASICs
- Digitization methods
- Techniques for increasing the count rate
- Techniques for allowing spectroscopic information at fine pixel pitch
- Towards large area detectors
- Summary and conclusions

Review of ASICs (full picture)

Photon Counting Detectors for X-Ray Imaging With Emphasis on CT

R. Ballabriga^{ID}, J. Alozy, F. N. Bandi, M. Campbell^{ID}, *Member, IEEE*, N. Egidos, J. M. Fernandez-Tenllado, E. H. M. Heijne, *Life Fellow, IEEE*, I. Kremastiotis^{ID}, X. Llopart, B. J. Madsen, D. Pennicard, V. Sriskaran^{ID}, and L. Tlustos

- *Tables (included for completeness)*
- *Tables report published material*
- *Reported measurement values not taken as absolute values for comparison but should be used to identify trends and performance envelopes*

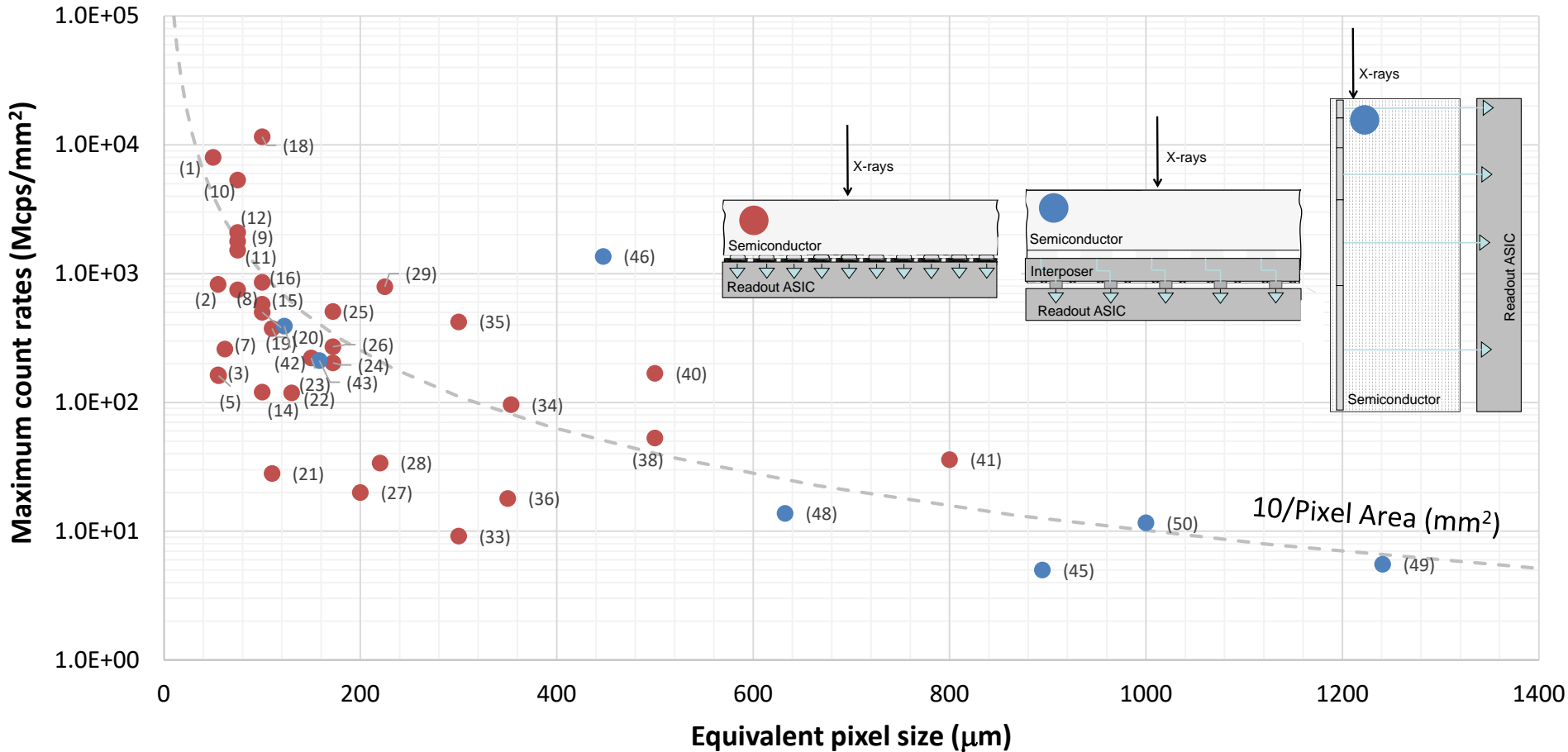
Name	Matrix	Channel size (μm^2)	Energy thresholds	Peaking time (ns)	Buttable sides	Tech. node	Specific information	Ref.
<i>FRIC (AGH) (1)</i>	64 x 64	50 x 50	2	10	1	40 nm	Prototype chip, 2x16 bit counters, 1.05V supply voltage. 2 modes of operation: 1. High Speed and 2. High Gain	[70]
<i>Medipix3 (2),(3)</i>	256 x 256	55 x 55	2	120	3	130 nm	Fine Pitch mode (55 μm); (1) Single Pixel Mode (SPM), (2) Charge Sharing Correction Mode (CSM); ASIC is compatible with Through Silicon Vias technology (TSVs)	[71],[52]
<i>Timepix3 (4)</i>	256 x 256	55 x 55	10 bits	30	3	130 nm	Data push mode; event-by-event energy and time measurement; Charge Sharing Correction possible off-chip	[72]
<i>Pixirad Pixie II (5)</i>	512 x 476	52 x 60	2	300	2	180 nm	Hexagonal pixels, equivalent pixel pitch of 55.6 μm	[73]
<i>Samsung PC (6)</i>	128 x 128	60 x 60	3	NS	0	130 nm	On-pixel successive approximation Analog to Digital Converter (ADC)	[74]
<i>Pixirad Pixie III (7)</i>	512 x 402	62 x 62	2	125	2	160 nm	Large area ASIC (31.7x25mm ²), Charge Sharing Correction algorithm	[75]
<i>Eiger (8)</i>	256 x 256	75 x 75	1	30	3	250 nm	Radiation hard electronics design	[68],[76]
<i>PXD23K (AGH) (9)</i>	128 x 184	75 x 75	2	48	3	130 nm		[77]
<i>IBEX (Dectris) (10),(11)</i>	256 x 256	75 x 75	2	NS	3	110 nm	Radiation hard electronics design; (10) Instant Retrigger technology, (11) Paralyzable operation	[64]
<i>UFXC32K (12)</i>	128 x 256	75 x 75	2	40	3	130 nm		[78]
<i>LNPIX (13)</i>	128 x 176	75 x 75	2	100	3	130 nm	Designed mainly for synchrotron applications; 2x14 bit counters/pixel up to 70k frames per second (2 bit/pixel)	[79]
<i>X-Counter PC (14)</i>	256 x 256	100 x 100	2	NS	3	NS	Charge Sharing Correction algorithm	[80], [81]
<i>PXD18K (AGH) (15)</i>	96 x 192	100 x 100	2	30	3	180 nm		[82]
<i>FPDR90 (AGH) (16)</i>	40 x 32	100 x 100	2	28	3	90 nm	Prototype ASIC	[83]
<i>AGH_Fermilab (17)</i>	18 x 24	100 x 100	2	48	0	40 nm	Prototype ASIC, Charge Sharing Correction algorithm	[84]
<i>PXF40 (18)</i>	18 x 24	100 x 100	1	8	0	40 nm	Prototype ASIC	[85]
<i>Tsinghua PC (19)</i>	32 x 32	100 x 100	2	100	3	180 nm		[86]
<i>Medipix3 (20),(21)</i>	128 x 128	110 x 110	8	120	3	130 nm	Spectroscopic mode (110 μm pixels); (20) Single Pixel mode, (21) Charge Sharing Correction Algorithm; Compatible with TSVs	[71],[52]
<i>XPAD3 (22)</i>	80 x 120	130 x 130	2	150	3	250 nm		[87], [88]
<i>HEPS-BPIX (23)</i>	104 x 72	150 x 150	1	20	3	130 nm	ASIC mainly designed for synchrotron applications	[89], [90]
<i>Pilatus 2 (24)</i>	60 x 97	172 x 172	1	110	3	250 nm	Radiation hard electronics design	[91][92]
<i>Pilatus 3 (25),(26)</i>	60 x 97	172 x 172	1	110	3	250 nm	Radiation hard design; (25) Instant retrigger technology, (26) paralyzable model	[65]
<i>Telesystems (27)</i>	40 x 40	200 x 200	4	300-500	3	250 nm		[93]
<i>Dosepix (28)</i>	16 x 16	220 x 220	16	300	3	130 nm	On pixel energy binning with 16 programmable digital thresholds	[94]
<i>Actina (CEA Siemens) (29)</i>	64 x 64	225 x 225	2	20	3	NS	ASIC used in pre-clinical prototype systems. Supports pile-up trigger method.	[95][36][69]
<i>Hexitec (30)</i>	80 x 80	250 x 250	14 bits	2000	3	350 nm	Digitization of pulse amplitude off-chip with 14 bit ADC; ASIC compatible with TSVs	[56]
<i>MC1 (Siemens) (31)</i>	32 x 32	250 x 250	4	NS	4	NS	Chip can be tiled on 4 sides seamlessly. ASIC pixel layout is designed to match the geometry of the anticscatter grid	[37]
<i>D2R1 (32)</i>	16 x 16	300 x 300	13 bits	NS	2	180 nm	Triggered readout, Multi Correlated Double Sampling (MCDS)	[96]
<i>ERICA (33)</i>	8 x 20	330 x 330	6	100	3	250 nm	Digital Charge Sharing Correction Algorithm	[97]
<i>CIX 0.2 (34)</i>	8 x 8	500 x 250	1	NS	1	350 nm	Simultaneous charge integration and photon counting measurement	[98][99]
<i>Philips ChromAIX1 (35)</i>	16 x 16	300 x 300	4	20	2	180 nm		[29]
<i>Ajat-0.35 (PC) (36)</i>	32 x 64	350 x 350	1	1000	3	350 nm		[100],[101]
<i>Ajat-0.35 (ADC) (37)</i>	32 x 64	350 x 350	64	1000	3	350 nm	On-pixel ADC	[100],[101]
<i>DxRay-Interon (38)</i>	16 x 16	500 x 500	4	10	NS	NS		[102][103]
<i>Ajat-0.5 (39)</i>	44 x 22	500 x 500	2	1000-2000	3	350 nm		[104]
<i>Philips ChromAIX2 (40)</i>	22 x 32	500 x 500	5	10	3	180 nm		[30]
<i>CEA-MultiX (41)</i>	4 x 8	756 x 800	8 bits	NS	2	130 nm	On-pixel SAR ADC. Charge sharing, charge induction and pile-up correction	[105][106]

The indexes (in italics and inside curly brackets) in the table identify the chips in the following plots (they should not be confused with the references).

Name	Max input count rate (Mcps/pixel)	Max input count rate (Mcps/mm ²)	10% count rate deviation (Mcps/mm ²)	Dead time (ns)	Electronics noise (e ⁻ r.m.s.)	Energy resolution (FWHM)	Power/pix (μW)
<i>FRIC (AGH) (1)</i>	8.5	1520	888	50 (High Speed Mode)	90	0.71 keV @ 8 keV, Si (High Gain) 1.13 keV @ 8 keV, Si (High Speed)	12 (High Gain) 18 (High Speed)
<i>Medipix3 (SPM) (2)</i>	2.5	825	81.7	400	80	1.37 keV @ 10 keV, 300 um Si	7.5
<i>Medipix3 (CSM) (3)</i>	0.5	165	17.2	2020	174	2.03 keV @ 10 keV, 300 um Si	9.3
<i>Timepix3 (4)</i>	$1.3 \cdot 10^{-3}$	0.43	0.43	$76 \cdot 10^5$	62	4.07 keV @ 59.5 keV, 300 um Si	15.2
<i>Pixirad Pixie II (5)</i>	0.5	160	17.93	2000	50	1.73 keV @ 60 keV, CdTe	12.5
<i>Samsung PC (6)</i>	NS	NS	NS	NS	68	NS	4.6
<i>Pixirad Pixie III (7)</i>	1	260	28.88	1000	50 (SPM) 100 (CSM)	2 keV @ 20 keV, CdTe	34
<i>Eiger (8)</i>	4.2	750	82.88	238.1	121/160/185	NS	8.8
<i>PXD23K (AGH) (9)</i>	8.55	1520	168.66	117	90	NS	25
<i>IBEX (Dectris) (Instant retrigger) (10)</i>	30	5300	197.33	100	90	850 eV FWHM @ 8 keV (300 um Si)	8
<i>IBEX (Dectris) (paralyzable) (11)</i>	10	1800	186.67	100	90	850 eV FWHM @ 8 keV (300 um Si)	8
<i>UFXC32K (12)</i>	11.8	2100	220	85.03	123	NS	26
<i>LNPIX (13)</i>	NS	NS	NS	NS	60	NS	37
<i>X-Counter PC (14)</i>	1.2	120	13.32	833.33	NS	10 keV @ 60 keV, CdTe	NS
<i>PXD18K (AGH) (15)</i>	5.8	580	64.38	172.41	168	NS	23
<i>FPDR90 (AGH) (16)</i>	8.55	855	94.87	117	91	NS	42
<i>AGH_Fermilab (17)</i>	NS	NS	NS	NS	84 (SPM) 168 (CSM)	NS	34
<i>PXF40 (18)</i>	115	11600	1276.5	8.7	185	NS	105
<i>Tsinghua PC (19)</i>	5	500	52.5	200	< 100	NS	40
<i>Medipix3 (SPM) (20)</i>	4.55	375	21.8	220	80	1.43 keV @ 10 keV, Si	30
<i>Medipix3 (CSM) (21)</i>	0.34	28	4.31	2940	174	4.4 keV @ 60 keV, 2mm CdTe	37.2
<i>XPAD3 (22)</i>	2	118	12.43	500	127	2.3 keV @ 59.5 keV CdTe	40
<i>HEPS-BPIX (23)</i>	5	220	24.67	200	115	NS	36.6
<i>Pilatus 2 (24)</i>	6	203	22.51	166.67	123	1 keV @ 8 keV	20.2
<i>Pilatus 3 (instant retrigger) (25)</i>	15	507	30.02	125	123	1 keV @ 8 keV	20.2
<i>Pilatus 3 (paralyzable) (26)</i>	8	270	28.39	125	123	1 keV @ 8 keV	20.2
<i>Telesystems (27)</i>	0.8	20	2.22	1250	NS	4.88 keV @ 122 keV	94.4
<i>Dosepix (28)</i>	1.64	34	3.76	610	150	3.12 keV @ 35 keV	14.6
<i>Actina (CEA Siemens) (29)</i>	40	790	87.7	25	NS	NS	NS
<i>Hexitec (30)</i>	0.001	0.02	$1.8 \cdot 10^{-3}$	$1 \cdot 10^6$	NS	0.8 keV @ 60 keV	220
<i>MC1 (Siemens) (31)</i>	NS	NS	44.4	40	NS	5 keV FWHM @ 60 keV	< 125
<i>D2R1 (32)</i>	$40 \cdot 10^{-6}$	$0.44 \cdot 10^{-3}$	0.00	$25 \cdot 10^6$	30	584 eV FWHM @ 60 keV	315
<i>ERICA (33)</i>	1	9.2	1.02	1000	90	NS	150
<i>CIX 0.2 (34)</i>	12	96	10.08	83.33	330	NS	3200
<i>Philips ChromAIX1 (35)</i>	38	422	44.33	26.32	400	4.7 keV @ 60 keV	3000
<i>Ajat-0.35 (PC) (36)</i>	2.2	18	1.89	454.55	NS	4 keV @ 122 keV, CdTe	390.6
<i>Ajat-0.35 (ADC) (37)</i>	$4.88 \cdot 10^{-5}$	$4 \cdot 10^{-4}$	0.00	$20.5 \cdot 10^6$	NS	4 keV @ 122keV, CdTe	390.6
<i>DxRay-Interon (38)</i>	13.25	53	5.57	75.47	NS	7 keV @ 60 keV, CdTe	NS
<i>Ajat-0.5 (39)</i>	NS	NS	NS	NS	NS	4.7 keV @ 122 keV, CdTe	413.2
<i>Philips ChromAIX2 (40)</i>	42	168	17.64	23.81	260	4.8 keV FWHM @ 60 keV	NS
<i>CEA-MultiX (41)</i>	23	36	3.77	43.48	NS	8.5 keV @ 122 keV, CdTe	10000

Name	Channels	Sensor pixel (μm^2)	Energy thresholds	Peaking time (ns)	Tech. node	Specific information	Ref.
<i>Mythen II (42)</i>	128	50 x 300	1	NS	250 nm	Si strip readout chip, edge-on orientation, designed with radiation hard techniques	[107]
<i>Microdose Mammography (43)</i>	NS	50 x 500	2	NS	NS	Si strip readout chip, edge-on orientation	[108][109]
<i>Redlen module 330 (44)</i>	864	330 x 330	6	NS	NS	Module can be tiled seamlessly on 4 sides. Sensor connected to readout chip through interposer. The module contains 2 chips (i.e. 1728 pixels)	[110]
<i>IDEAS (45)</i>	64	2000 x 400	6	50	NS	Optimized for Cd(Zn)Te linear sensor array	[111][112]
<i>KTH_Lin_SPD (46)</i>	160	500 x 400	8	10-20-40-60	180 nm	Optimized for readout of 16-segment Si-strips oriented edge-on	[33][61][34]
<i>Redlen module 500 (47)</i>	864	500 x 500	6	NS	NS	Module can be tiled seamlessly on 4 sides. Sensor connected to readout chip through interposer. The module contains 2 chips (i.e. 1728 pixels)	[110]
<i>Hamamatsu (48)</i>	64	800 x 500	5	NS	NS	Optimized for Cd(Zn)Te linear sensor array	[113]
<i>BNL (49)</i>	64	2200 x 700	5	40-80-160-320	250 nm	Optimized for CdZnTe sensors, 9th order shaper	[114]
<i>GE-DxRay (50)</i>	128	1000 x 1000	2	30	250 nm	Connected to 2-D CdZnTe by means of interposer board, Clinical images taken with the GE lightSpeed VCT scanner	[103][17]

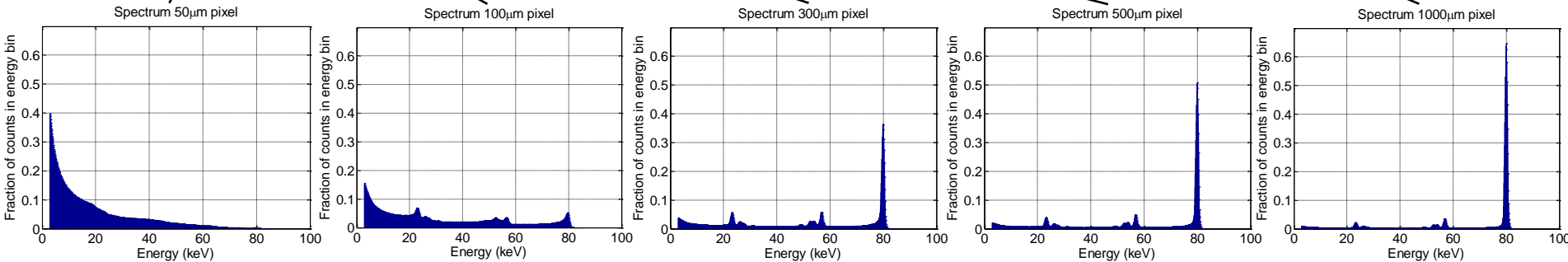
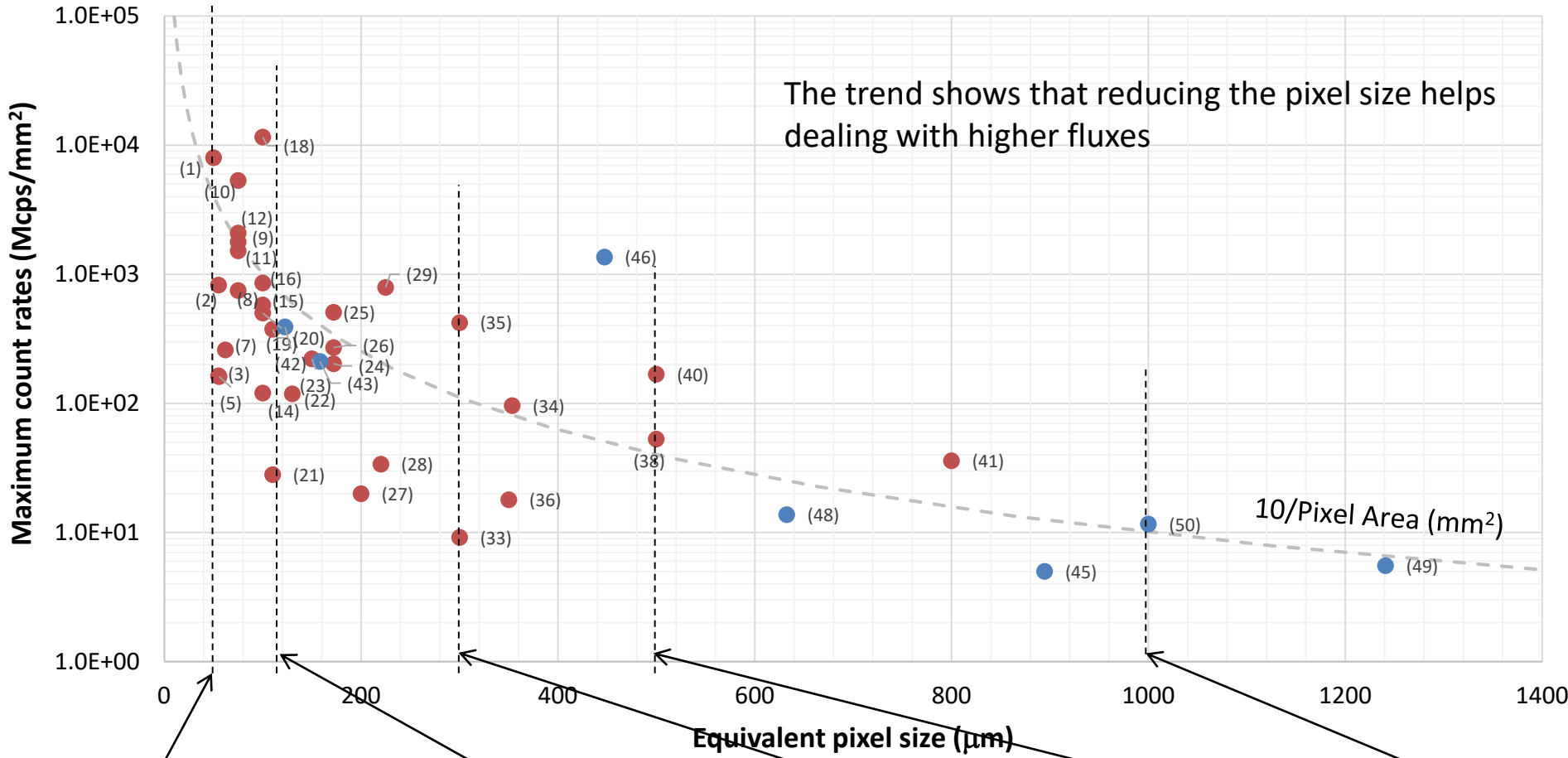
Name	Max count rate (Mcps/pixel)	Max count rate (Mcps/mm ²)	10% count rate deviation (Mcps/mm ²)	Dead time (ns)	Electronics noise (e ⁻ r.m.s.)	Energy resolution (FWHM)	Power/channel (μ W)
<i>Mythen II (42)</i>	5.88	392	41.18	170	151 + 55.6 e ⁻ /pF	NS	368.75
<i>Microdose Mammography (43)</i>	5.29	212	22.22	189	200 (without detector)	NS	NS
<i>Redlen module 330 (44)</i>	>50	> 500	120	12		~7 keV FWHM @ 60 keV, CZT	<2
<i>IDEAS (45)</i>	4	5	0.53	250	105 + 40 e ⁻ /pF	7 keV @ 60 keV, CdTe (10 pF Cin total)	4200
<i>KTH_Lin_SPD (46)</i>	272	1360	142.8	3.68	214 @ 5pF Cin (40 ns pk time)	1.09 keV @ 15 keV	80000
<i>Redlen module 500 (47)</i>	> 50	> 200	40	12	NS	~8 keV FWHM @ 60 keV, CZT	<2
<i>Hamamatsu (48)</i>	5.5	14	1.44	181.82	NS	12 keV @ 120 keV, CdTe	NS
<i>BNL (49)</i>	4	6	0.58	250	170 @ 2 pF Cin (40ns pk time)	5.5 keV @ 40 ns pk time / 2.15keV @ 320 ns pk time (4.6pF Cin)	4700
<i>GE-DxRay (50)</i>	11.6	12	1.22	86.21	NS	5.8keV @ 122keV, CdZnTe (5pF Cin total)	2100



The maximum count-rate corresponds to the input flux at which the output count-rate saturates (which corresponds, for the particular case of the paralyzable model, to the inverse of the dead time)

For ASICs implementing a non-paralyzable type of behaviour, the maximum count-rate corresponds to the input count-rate for which the measured count-rate reaches ~95% of the asymptotic maximum.

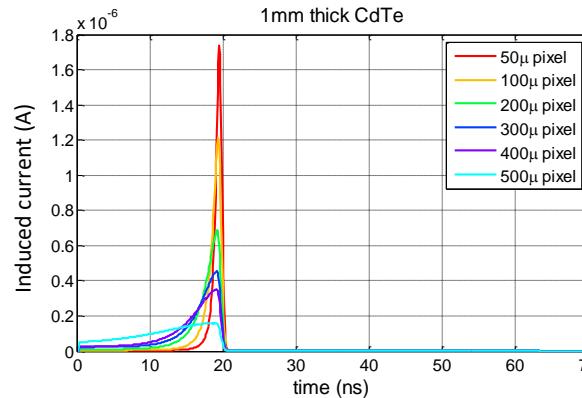
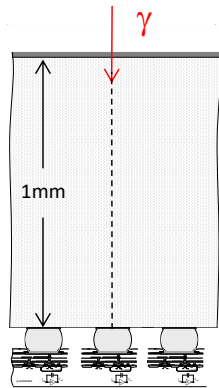
The trend shows that reducing the pixel size helps dealing with higher fluxes



Simulation 80keV photons, 2mm CdTe, -800V, 100e- r.m.s. noise (no threshold dispersion, no charge trapping)

In order to do spectroscopy at fine pitches a charge reconstruction and hit allocation architecture is required.

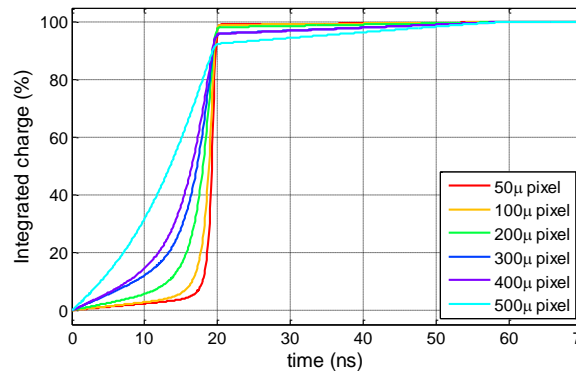
Reminder



Signal shape depends on detector geometry

We calculate the maximum count-rate for a given pixel size for a given charge integration time

- 1mm CdTe
- 60keV photon
- 600V sensor bias
- Energy deposition at $z=240\mu\text{m}$
- (No charge trapping, charge sharing included in simulation)



Pixel pitch

Time to integrate a given percentage of the charge

Pixel pitch	$t_{90\%}$	$t_{97.5\%}$
50 μm	2.4ns	13.5ns
300 μm	14.7ns	38.2ns

We assume $t_{x\%} = t_p$ and $\tau = 2t_p$

$$\frac{1}{\tau} \frac{1}{\text{pixel area}} \left[\text{Mcps} / \text{mm}^2 \right]$$

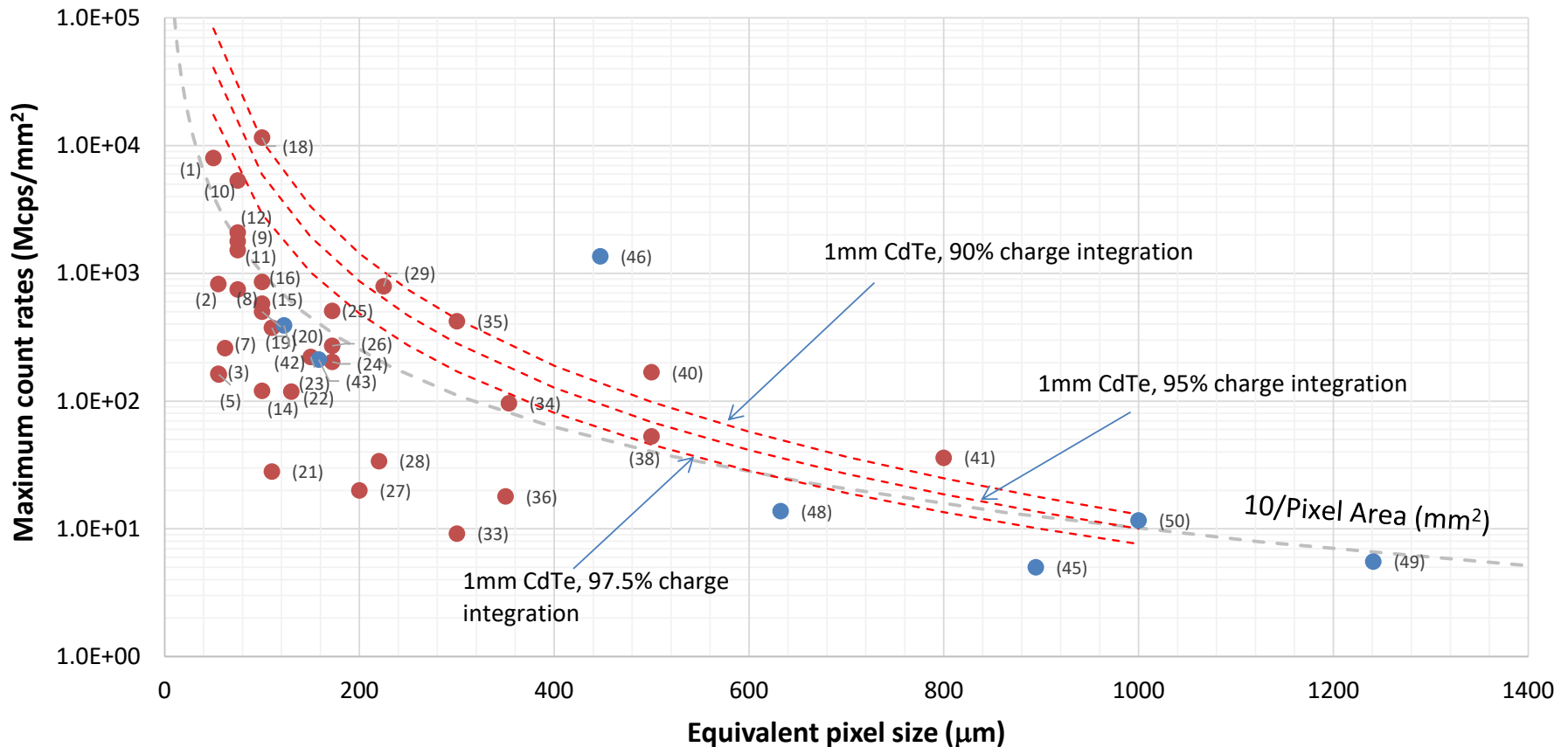
Message: The geometry of the sensor (pitch/thickness) determines the shape of the induced current pulse (and puts a lower limit on the electronics integration time)

46

We assume the maximum count rate as $\frac{1}{\tau} \frac{1}{\text{pixel area}} \left[\text{Mcps} / \text{mm}^2 \right]$

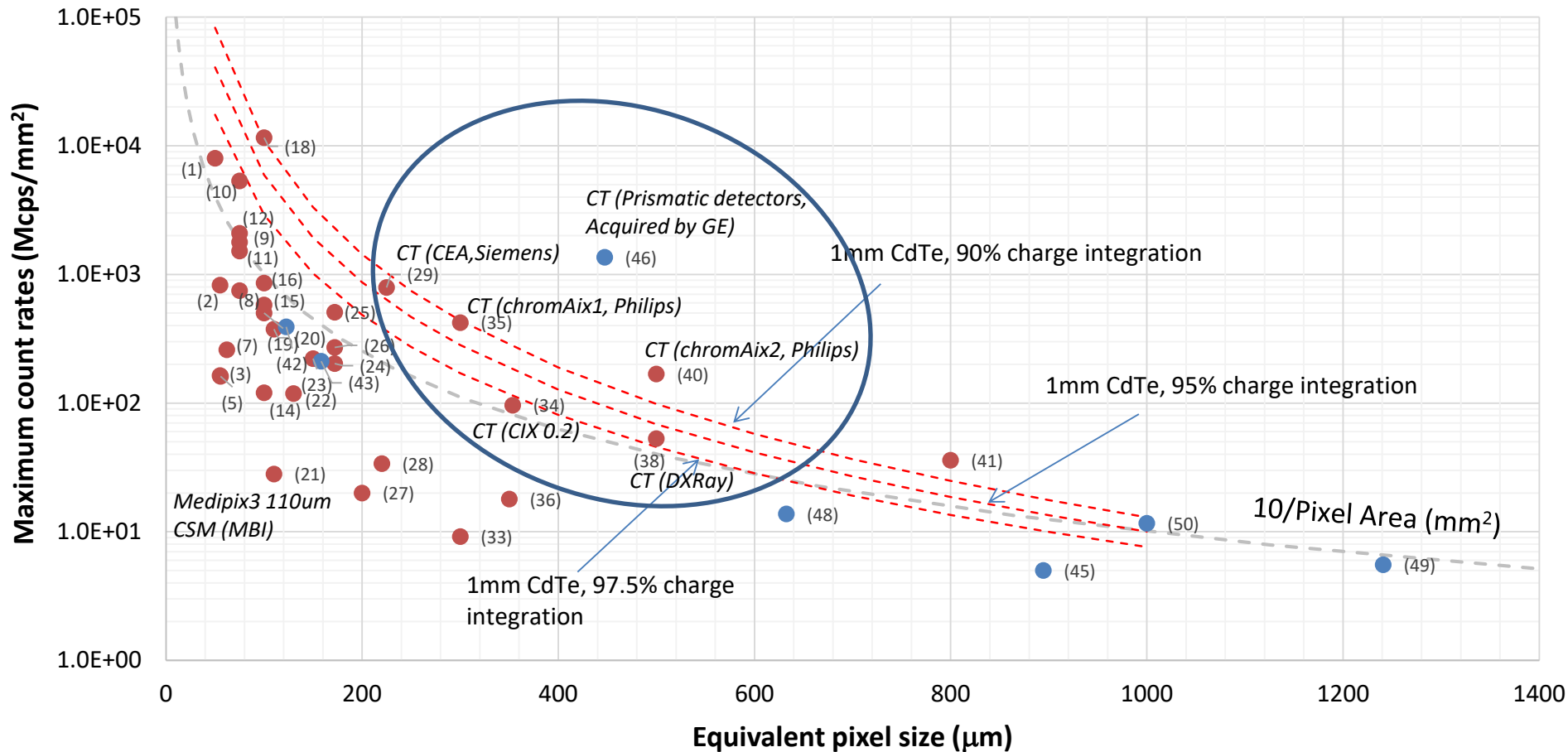
In which the dead time of the channel is chosen to ensure that a percentage of the charge will be integrated in the electronics

Maximum count rates (Mcps/mm²) vs pixel size (μm)



The red curves indicate the maximum count rate that we would achieve if we designed the electronics system to integrate 90%, 95% or 97.5% of the charge

Maximum count rates (Mcps/mm²) vs pixel size (μm)



Review of ASICs (details)

Digitization methods

Digitization methods

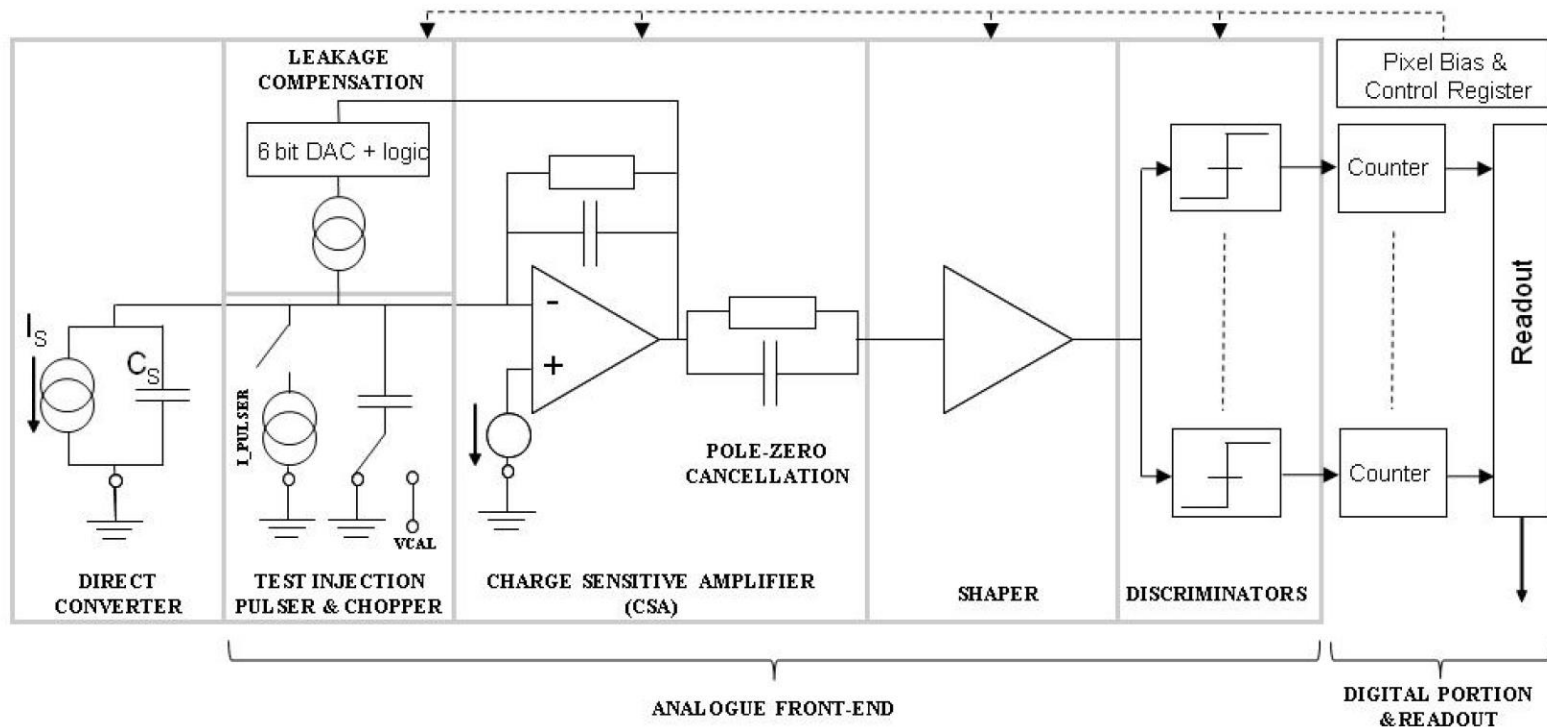
- On-pixel
 - Flash ADC (e.g. ChromAIX chips)
 - SAR ADC (e.g. CEA-Multix)
 - Ramp-compare ADC (e.g. Ajat-0.35)
 - Time-Over-Threshold (e.g. Timepix3, Dosepix)
- Other
 - Digitization off-pixel (e.g. Hexitec)

ChromAIX: A high-rate energy-resolving photon-counting ASIC for Spectral Computed Tomography

Roger Steadman, Christoph Herrmann, Oliver Mühlhens
Philips Research Europe, Weissshausstrasse 2, 52066 Aachen, Germany



- ChromAIX1 (published 2010)
 - 8x16 pixels (300 μ m pitch), 0.18 μ m CMOS
 - 4 energy thresholds, 20ns peaking time
 - Flash (parallel) ADC, applications for large bandwidth, high power consumption

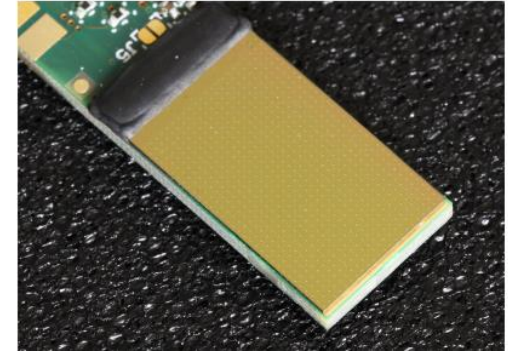




Contents lists available at ScienceDirect

Nuclear Instruments and Methods in Physics Research A

journal homepage: www.elsevier.com/locate/nima



ChromAIX2: A large area, high count-rate energy-resolving photon counting ASIC for a Spectral CT Prototype

Roger Steadman^{a,*}, Christoph Herrmann^a, Amir Livne^b

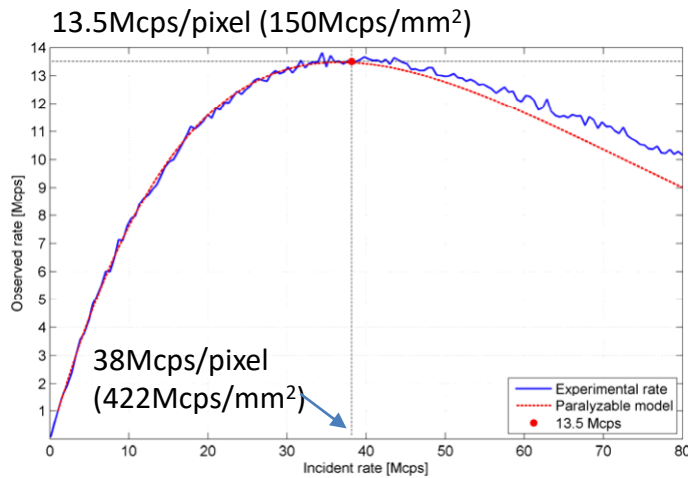
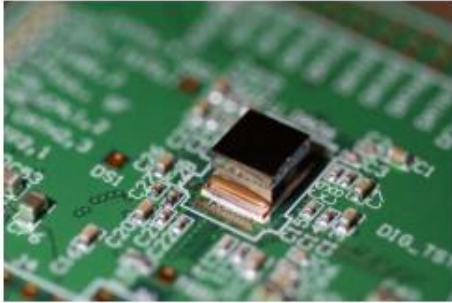
^a Philips Research Europe, High Tech Campus, 5656 AE Eindhoven, Netherlands

^b Philips Healthcare, 31004 Haifa, Israel

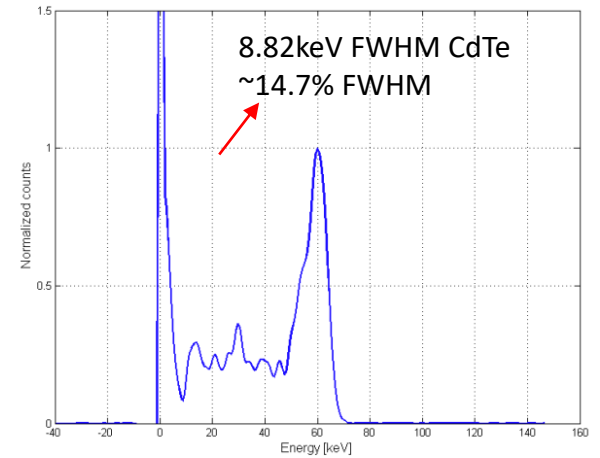


- ChromAIX2 (published 2017)
 - 22x32 pixels (500 μ m pitch), 0.18 μ m CMOS
 - 5 energy thresholds, ~10ns peaking time, ~23.5ns dead time @25keV Threshold

ChromAIX1 ASIC on evaluation PCB
 (2 side buttable design)
 8x16 pixels
 300 μ m pixel pitch

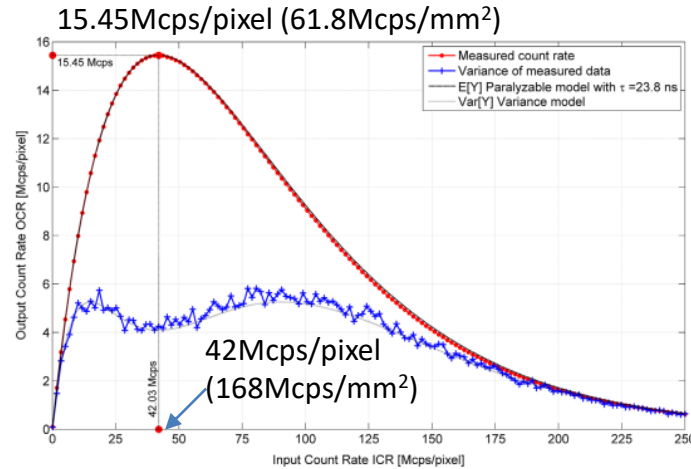
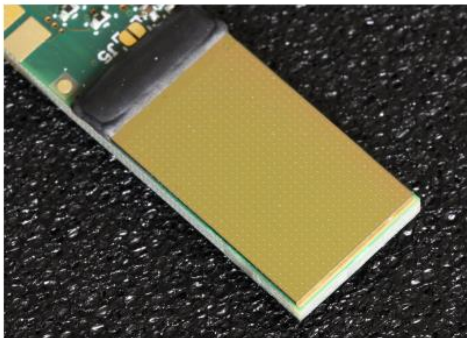


Measured count rate vs input count rate (Mcps/pixel)

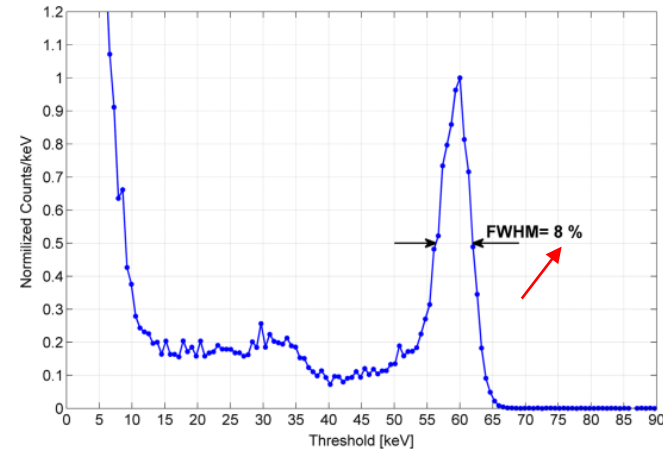


Spectrum measured with a ²⁴¹Am source (threshold scan)

ChromAIX2 ASIC on evaluation PCB
 (3 side buttable design)
 22x32 pixels
 500 μ m pixel pitch



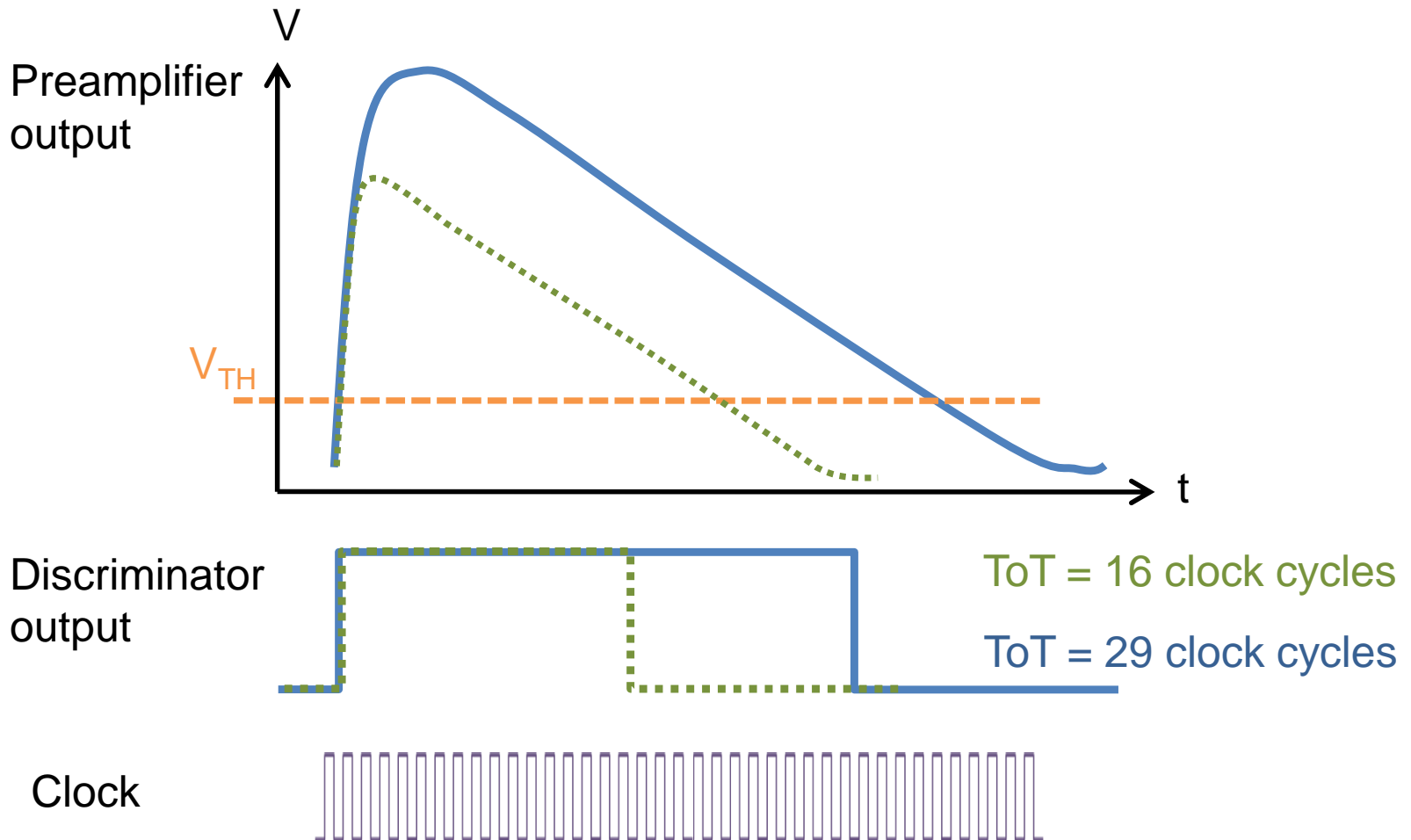
Measured count rate vs input count rate (Mcps/pixel)



Spectrum measured with a ²⁴¹Am source (threshold scan)

This example illustrates how the pixel size is related to (1) the ability to process high fluxes and (2) the spectral fidelity

Time-over-Threshold (ToT) digitization



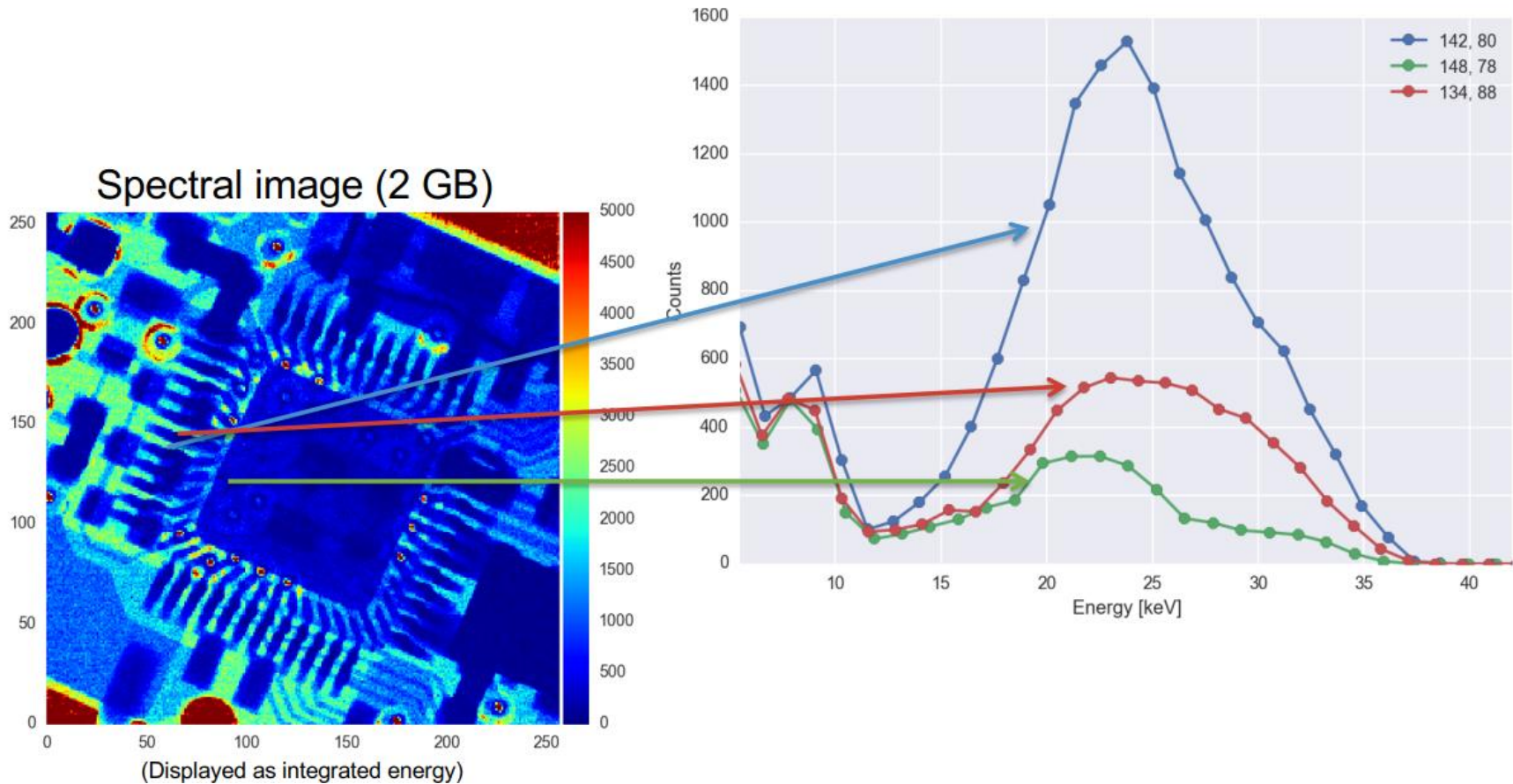
ToT digitization: Timepix3 chip

- Developed in the framework of the Medipix3 collaboration
- 256x256 pixel matrix, 55x55 μm^2 pixels
- CMOS 0.13 μm technology
- **Simultaneous measurement of Time and Energy per event with a data driven readout**
- **No frames but continuous data stream. Every event consists of**
 - **16 bits address**
 - **18 bits Time (1.56ns resolution)**
 - **10 bits Energy**
- Maximum hit rate of **0.4 10^6 hits/s/mm 2**
- Impact of charge diffusion/fluorescence can be compensated by offline processing, sub-pixel resolution possible

row	col	tot	toa[ns]	
103	110	21.88	399145.31	
115	154	33.88	1604.69	
75	152	7.81	3175.00	→ (75 151), 39.1 keV
75	151	24.06	3168.75	
85	126	25.94	6129.69	
109	108	5.25	25540.62	→ (108, 109), 41.2 keV
109	109	7.44	25535.94	
108	108	9.56	25532.81	
108	109	10.56	25532.81	
101	130	9.19	55710.94	
102	130	14.38	55707.81	
92	149	8.31	65276.56	
95	147	26.62	102270.31	
89	130	15.75	121687.50	
89	131	16.75	121687.50	

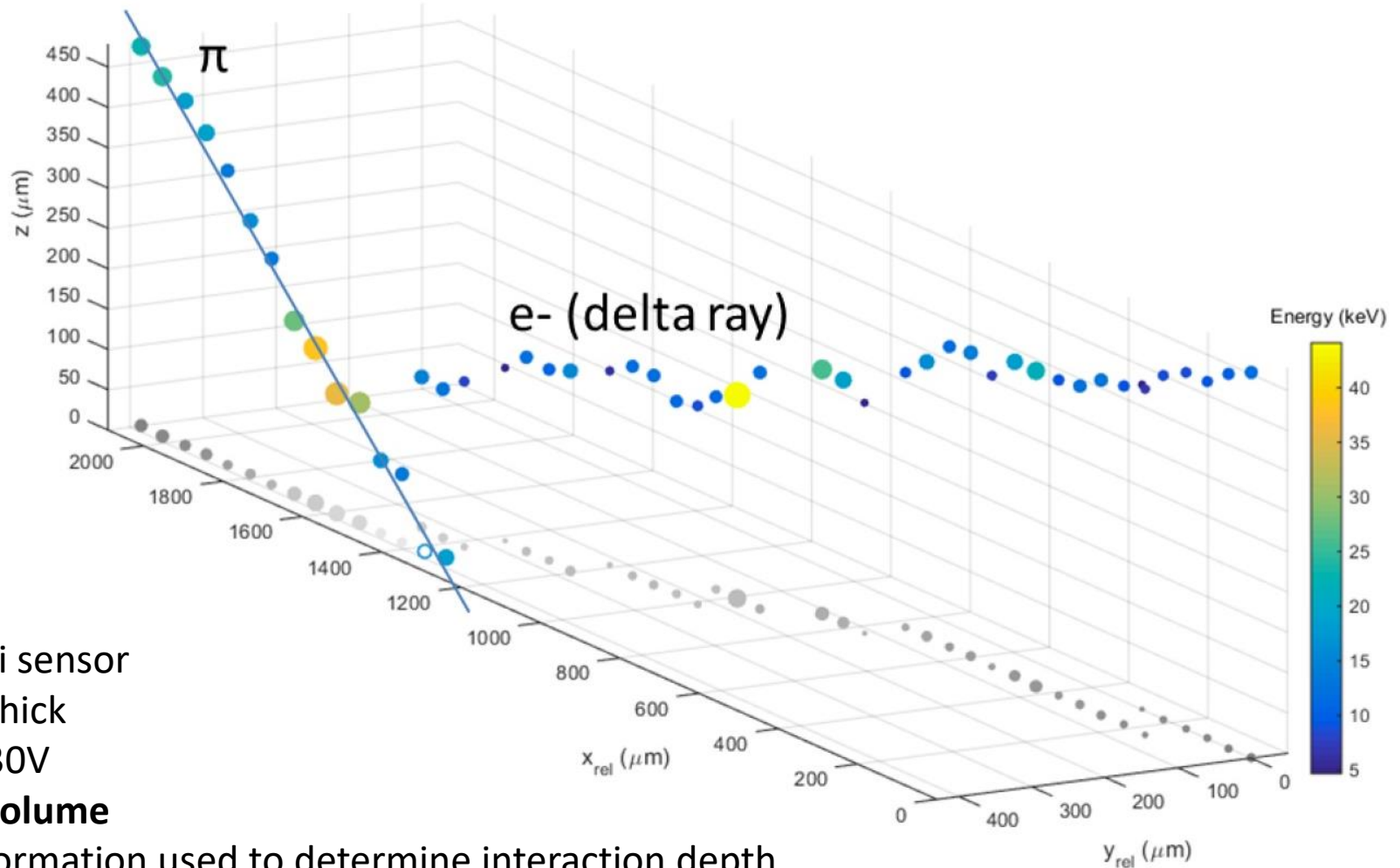
T. Poikela et al. "Timepix3: a 65K channel hybrid pixel readout chip with simultaneous ToA/ToT and sparse readout" JINST 9 C05013, 2014.

ToT digitization: Timepix3 chip



T. Poikela et al. "Timepix3: a 65K channel hybrid pixel readout chip with simultaneous ToA/ToT and sparse readout" JINST 9 C05013, 2014.

Test with 120GeV/c Pion Track



p^+ in n Si sensor

500 μm thick

$V_{\text{bias}} = 130\text{V}$

Sensor volume

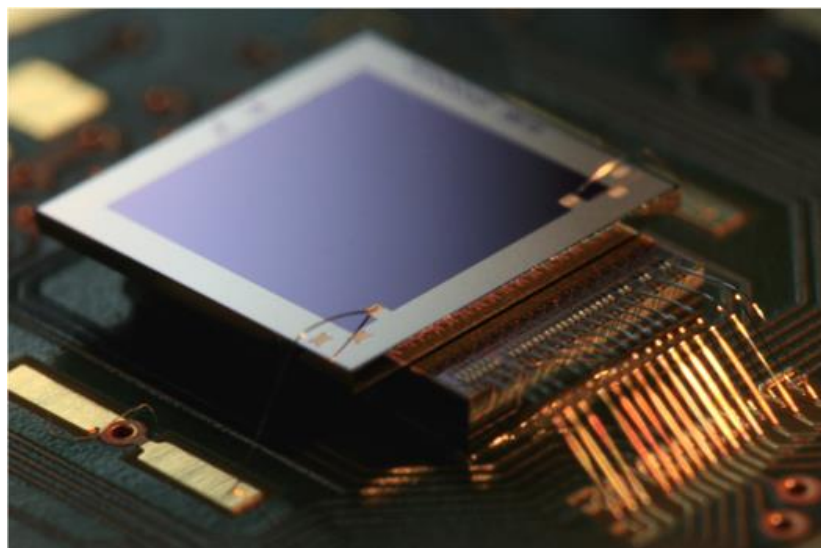
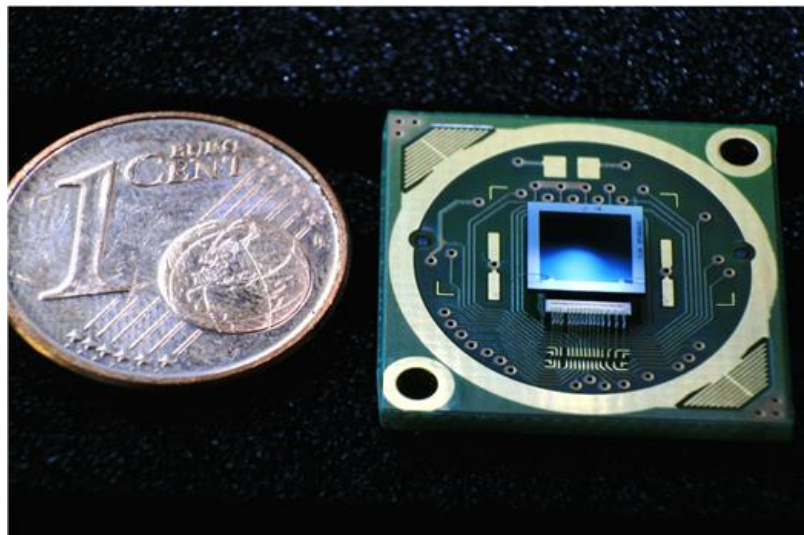
Time information used to determine interaction depth

Colour (and diameter) indicate energy deposited

Measured z resolution $\sim 50\mu\text{m}$

Slide courtesy of B. Bergmann, S. Pospisil, IEAP, CTU, Prague

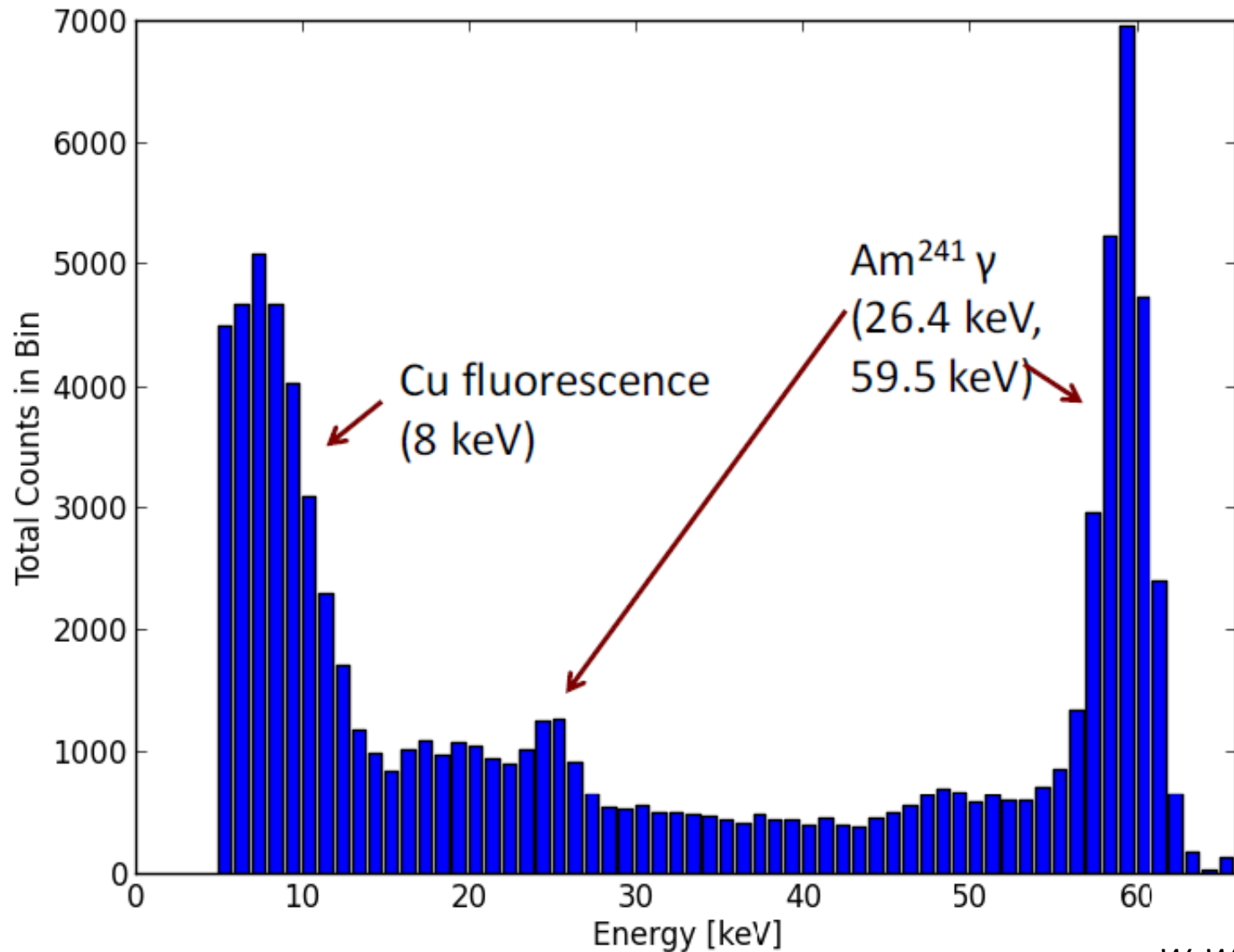
ToT digitization: Dosepix chip



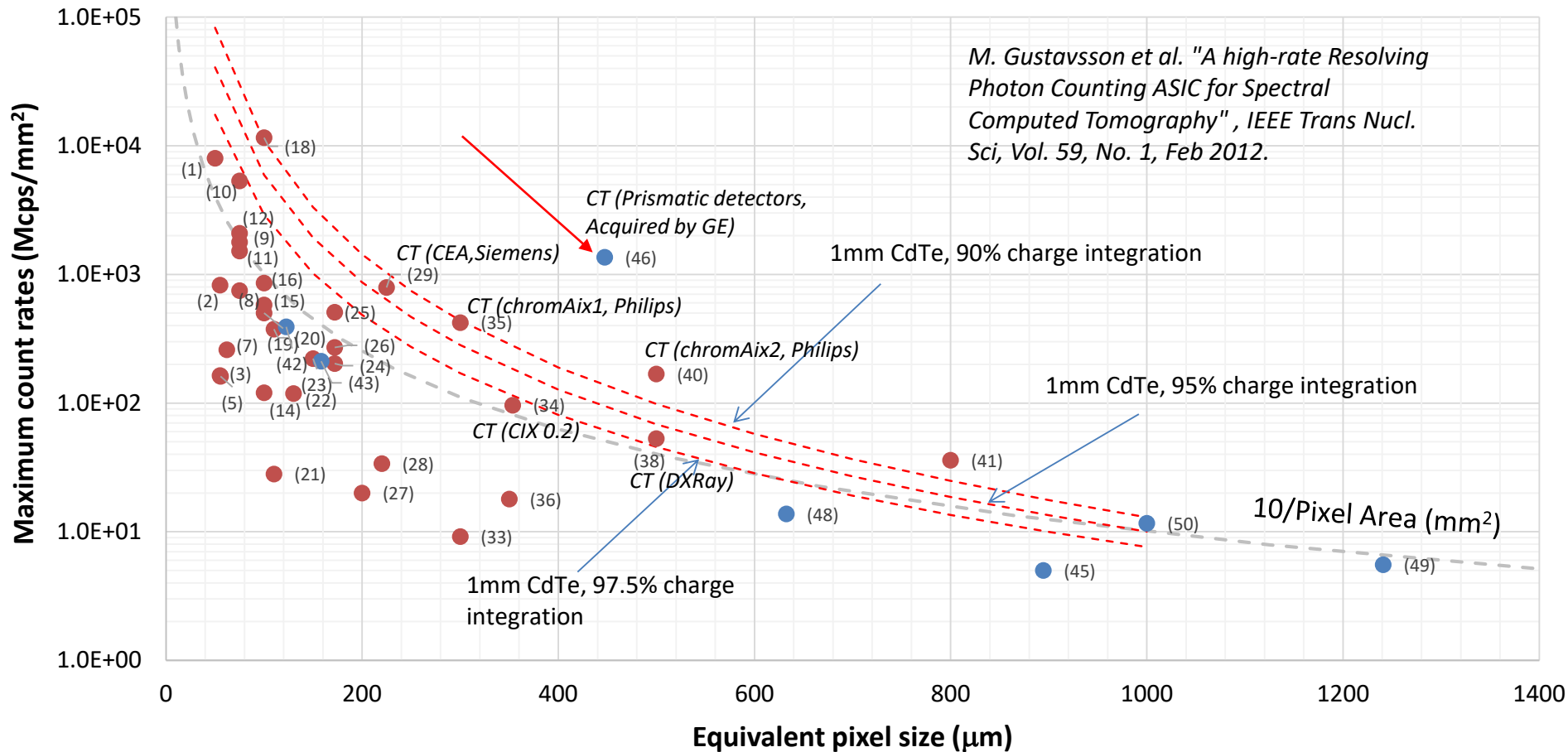
- Developed in a partnership between CERN, University of Erlangen and IBA dosimetry
- Main applications: dosimetry, X-ray tube diagnostics tool
- 16x16 pixel matrix, $220 \times 220 \mu\text{m}^2$ pixels
- CMOS $0.13 \mu\text{m}$ technology
- 1 global analog threshold
- Operation Modes:
 - Energy binning mode
 - 12 bit ToT measurement @100MHz
 - 16 digital thresholds (on each pixel) for event-by-event energy binning
 - 16x 16-bit energy bin registers
 - Photon counting mode (8 bits)
 - Integral ToT (24 bits)

ToT digitization: Dosepix chip

Spectrum of gamma emissions Am^{241} source, filtered to block alphas (1 frame of data)



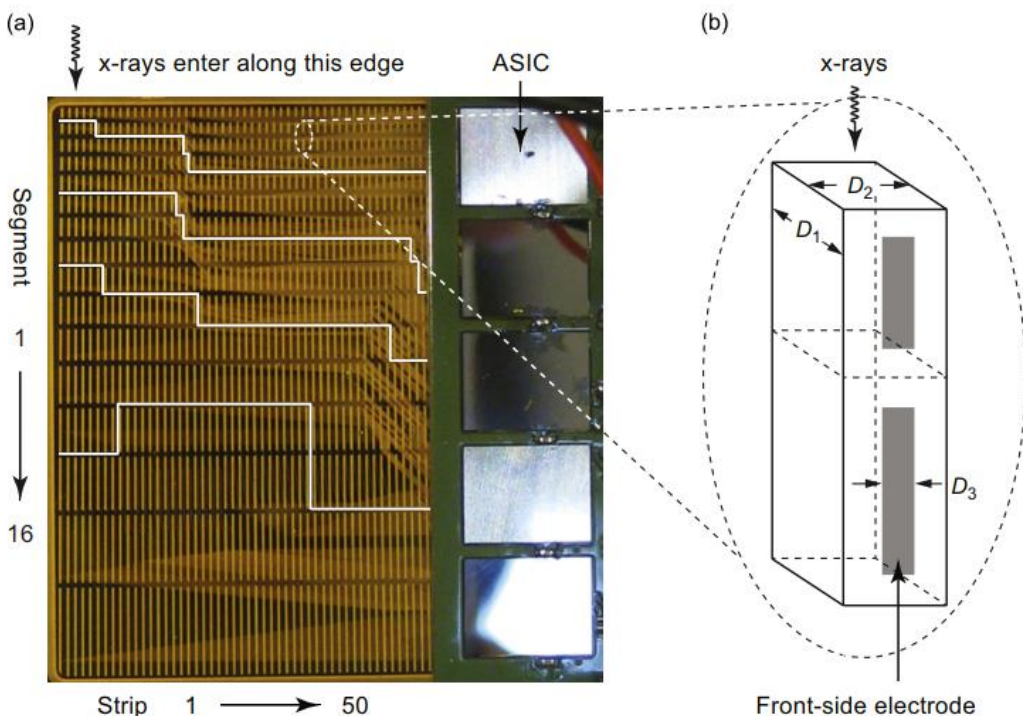
Maximum count rates (Mcps/mm²) vs pixel size (μm)



A High-Rate Energy-Resolving Photon-Counting ASIC for Spectral Computed Tomography

Mikael Gustavsson, *Member, IEEE*, Farooq Ul Amin, Anders Björklid, Andreas Ehliar, Cheng Xu, and Christer Svensson, *Fellow, IEEE*

- 0.4x0.5mm detector element size
- 1 detector module has 50 Si strips (edge-on-geometry)
- 1 strip is divided into 16 segments
- 800 channels per module (8 thresholds/channel)
- 1500 modules in a full system
- **Segmentation in the direction of the X-rays increases the maximum flux the system can deal with**
- **Longer segments (~4.8mm) together with complicated wiring increase the input capacitance of the readout channel (~3pF)**

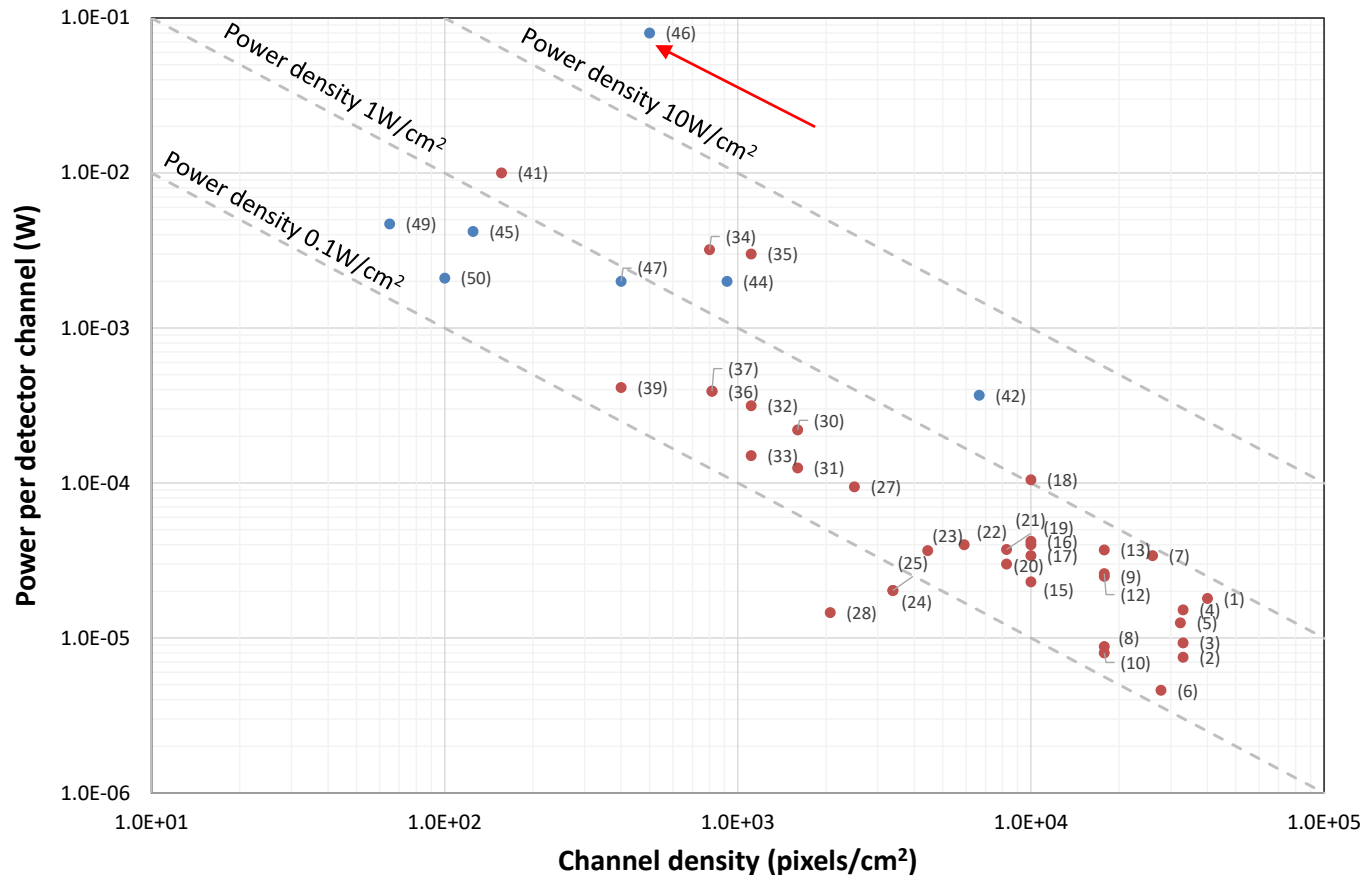


30mm depth

ASIC: M. Gustavsson et al. "A high-rate Resolving Photon Counting ASIC for Spectral Computed Tomography", *IEEE Trans Nucl. Sci*, Vol. 59, No. 1, Feb 2012.

Module description and characterization: C. Xu et al. "Energy resolution of a segmented silicon strip detector for photon-counting spectral CT" *NIMA* 43 715 (2013) 11–17

Power consumption



- Power consumption versus channel density
- Edge-on configuration: An effective sensor channel is read out by 16 electronics channels
 - Interconnection scheme adds input capacitance
 - Requirement to achieve low minimum thresholds to account for primary Compton interactions to improve the detection efficiency

A linear array silicon pixel detector: images of a mammographic test object and evaluation of delivered doses

F Arfelli†‡, V Bonvicini†, A Bravin†§, G Cantatore†§, E Castelli†§, L Dalla Palma||, M Di Michiel†§, R Longo†§¶, A Olivo†§, S Pani†‡, D Pontoni†‡, P Poropat†§, M Prest†§, A Rashevsky†, G Tromba†‡ and A Vacchi†

† Istituto Nazionale di Fisica Nucleare, Sezione di Trieste, via Valerio 2, 34127 Trieste, Italy

‡ Società Sincrotrone, Basovizza, 34012 Trieste, Italy

§ Dipartimento di Fisica dell'Università di Trieste, via Valerio 2, 34127 Trieste, Italy

|| Istituto di Radiologia dell'Università di Trieste, Ospedale di Cattinara, Strada di Fiume, 34100 Trieste, Italy

Received 30 January 1997

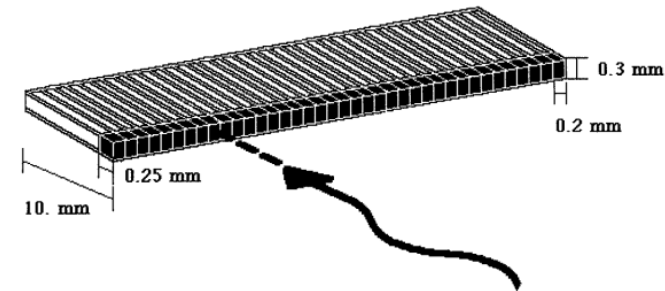


Figure 1. The photon detector geometry (see the text).

[...] A 1.4 cm length linear array detector was developed with a pixel size of $200 \times 300 \mu\text{m}^2$. It consists of a silicon microstrip device used in a configuration in which radiation impinges on the side rather than on the surface of the chip (Arfelli et al 1996). Due to the way the beam impinges on the detector, the radiation must traverse 1 cm of silicon. If the incident radiation has an energy lower than 30 keV it is fully absorbed. Figure 1 illustrates the detector geometry. [...]

Techniques for increasing the count rate

Experimental evaluation of the Pile-Up Trigger method in a revised quantum-counting CT detector

E. Kraft*^a, F. Glasser^b, S. Kappler^a, D. Niederloehner^a, P. Villard^b

^aSiemens AG, Healthcare Sector, Siemensstr. 1, 91301 Forchheim, Germany;

^bCEA-LETI-MINATEC, Recherche Technologique, 17 rue de martyrs, 38054 Grenoble Cedex 09, France

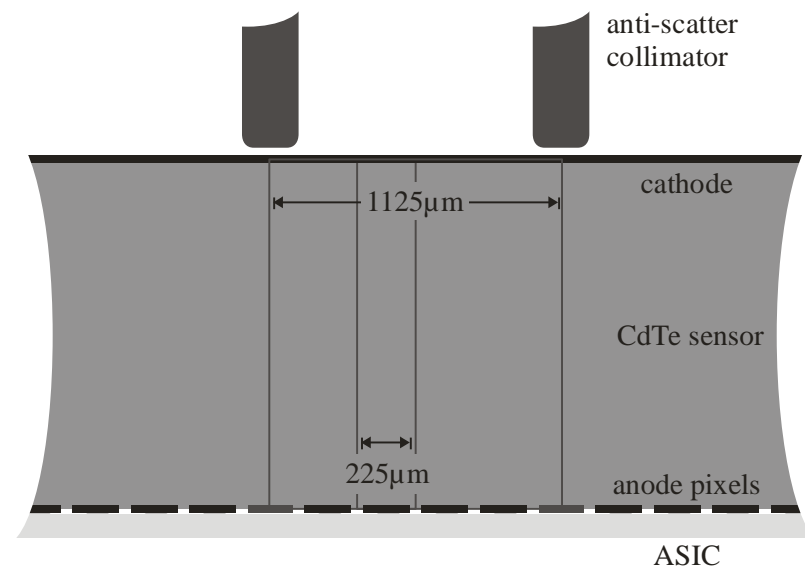
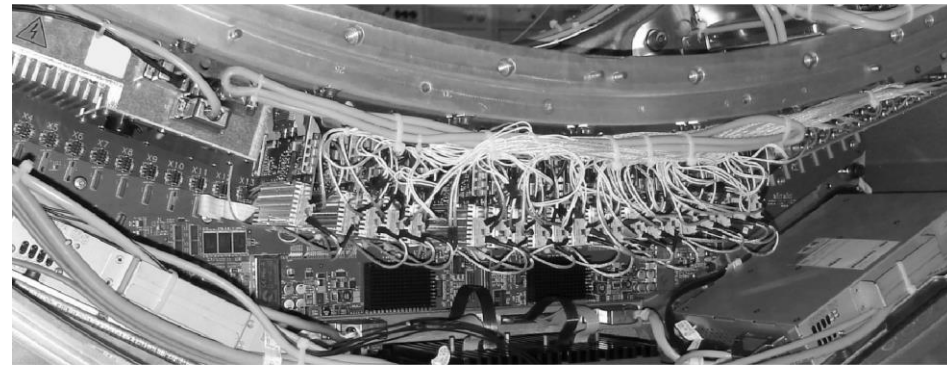
The Counting Detector

Basic Geometry:

- CdTe sensor, 1.6mm thick
- 225 μ m sub-pixel pitch
- Macro-pixel mode (4x4) fits to geometry of anti-scatter grid
- 24 modules \rightarrow 22cm FOV
- z-coverage up to 32x0.5mm

ASIC:

- Fast pulse shaping < 20ns
- Counter thresholds 20keV ... 160keV
- Two counters per sub-pixel

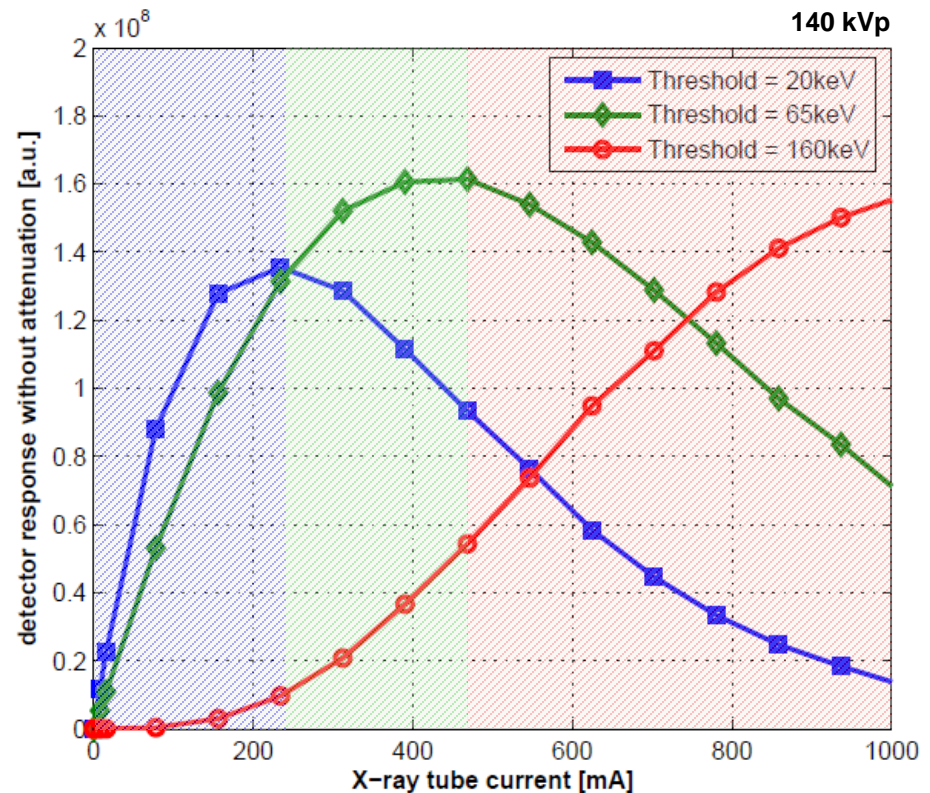


Siemens Photon Counting ASIC (pileup trigger method)

- 64x64 pixel matrix, 225 μ m pixel pitch
- Pile-up trigger method
- Observation: higher thresholds paralyze at higher count rates
- Combine spectral counter signal with pile-up counter signal

$$N = N_s + w \cdot N_p$$

- Advantages
 - Unambiguous up to the highest fluxes
 - Full spectral sensitivity in the low-flux regime inside the patient ($N_p \ll N_s$)



E. Kraft et al. "Experimental evaluation of the pile-up trigger method in a revised quantum-counting CT detector" Proc. SPIE 8313, Medical Imaging 2012: Physics of Medical Imaging, 83134A (2012).

The New PILATUS3 ASIC with Instant Retrigger Capability

Teddy Loeliger, *Member, IEEE*, Christian Brönnimann, *Member, IEEE*, Tilman Donath, Matthias Schneebeli, Roger Schnyder, *Member, IEEE*, and Peter Trüb

Pilatus3 (Dectris)

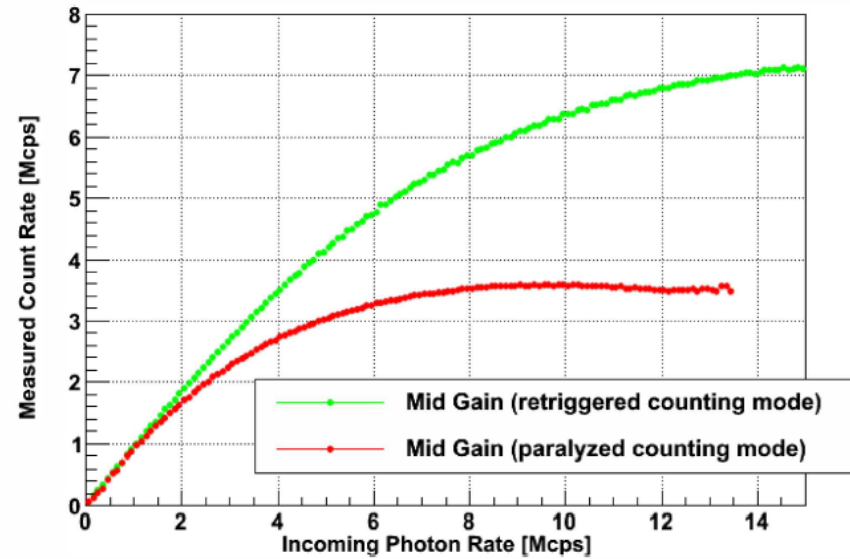
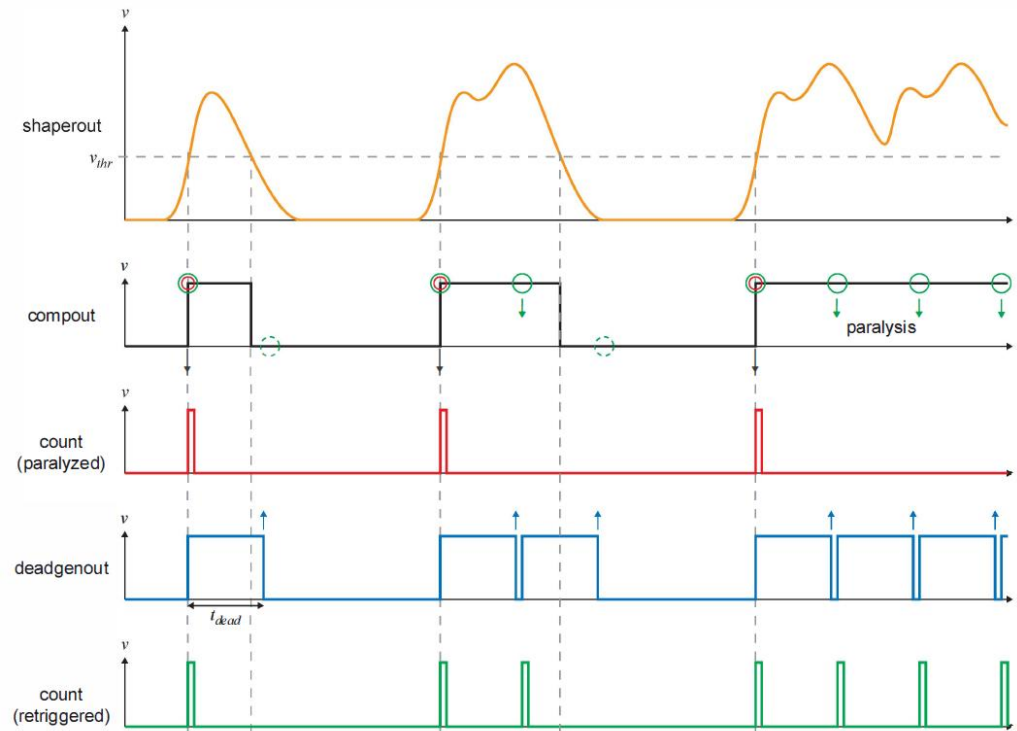
- 60x97 pixel matrix, 172 μ m pixel pitch
- 1 Threshold level
- 0.25 μ m CMOS technology
- Radiation hardness by design

(IBEX includes also the instant retrigger functionality)

TABLE I
PERFORMANCE SUMMARY OF THE PILATUS3 ASIC.

Parameter	Value
power consumption	80 mW (static) 90 mW/MHz count rate (dynamic)
pixel size	172 μ m \times 172 μ m
number of pixels	60 \times 97 = 5280
threshold energy range (typical)	2 to 20 keV
counter size	20 bit
max. count rate (pixel)	> 10 Mcps incoming rate
max. photon rate	> 3 \cdot 10 ⁸ photons/s/mm ²
absolute count rate error (with count rate correction; preliminary)	< 1 % @ 1 Mcps incoming rate < 10 % @ 10 Mcps incoming rate
readout time	0.95 ms
max. frame rate	500 Hz

Pilatus 3 ASIC (Instant retrigger)



Measurement 8keV photons, Threshold @4keV

T. Loeliger et al. Nuclear Science Symposium and Medical Imaging Conference (NSS/MIC), 2012 IEEE Conf. Record. pp. 610-615 (2012).

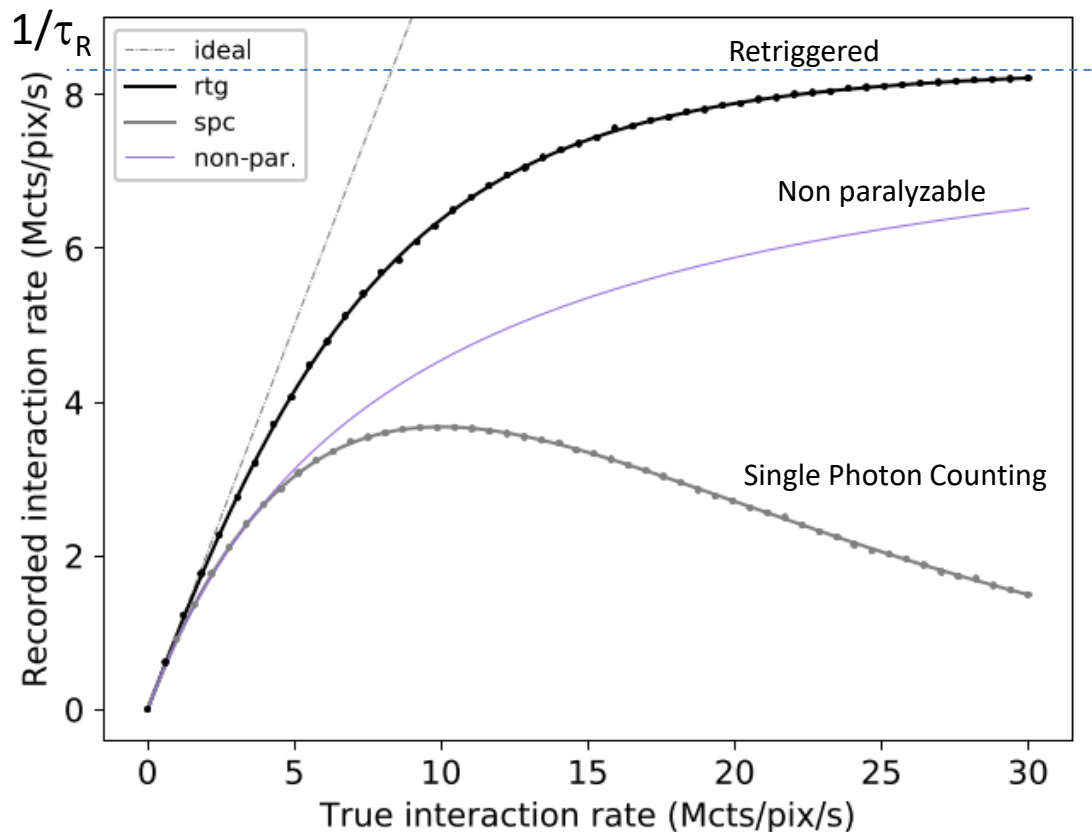
*After increasing counter, re-evaluation of the pulse after a pre-determined time interval
Very accurate for monochromatic light (synchrotrons)*



Dead time model for X-ray photon counting detectors with retrigger capability

P. Zambon

DECTRIS Ltd., Taefernweg 1, 5405 Baden-Daettwil, Switzerland



$\tau_p = 100\text{ns}$ (pulse width)
 $\tau_R = 120\text{ns}$ (retrigger time)

$$m = \frac{n}{e^{-n\tau_p} + n\tau_R}$$

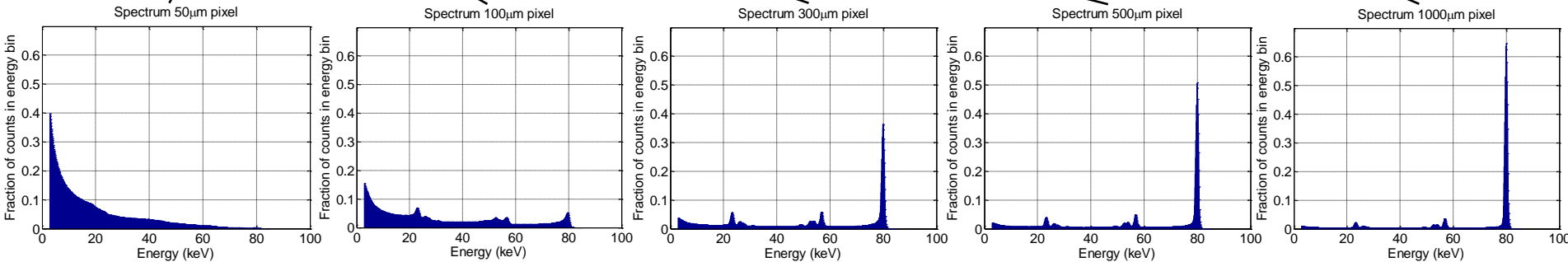
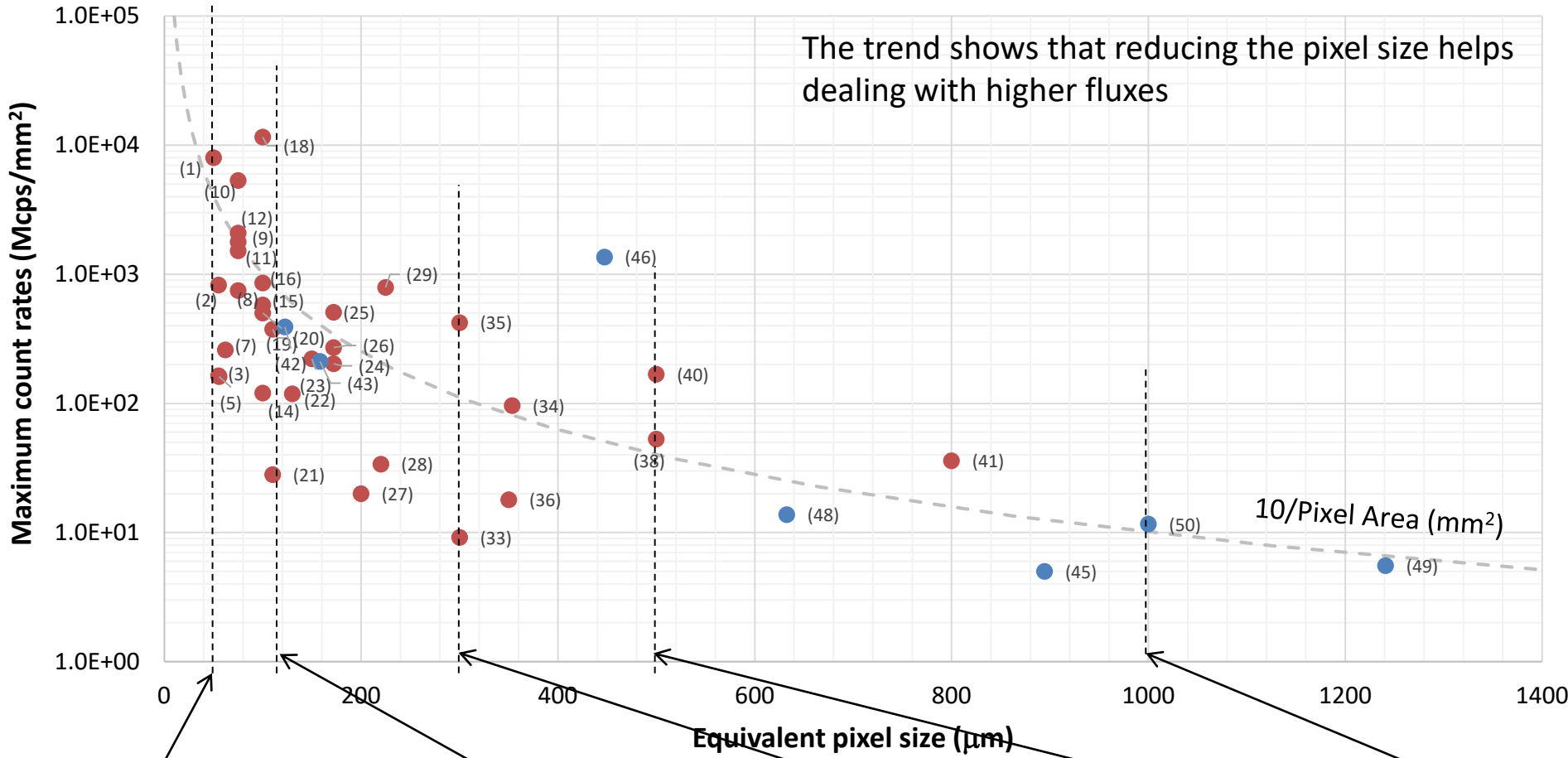
m : recorded rate

n : true rate

τ_p : pulse width

τ_R : retrigger time

Techniques for allowing spectroscopic information at fine pixel pitch



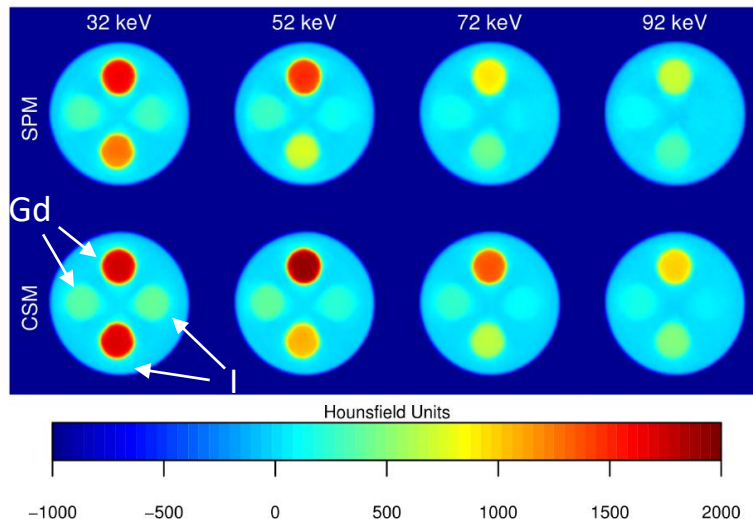
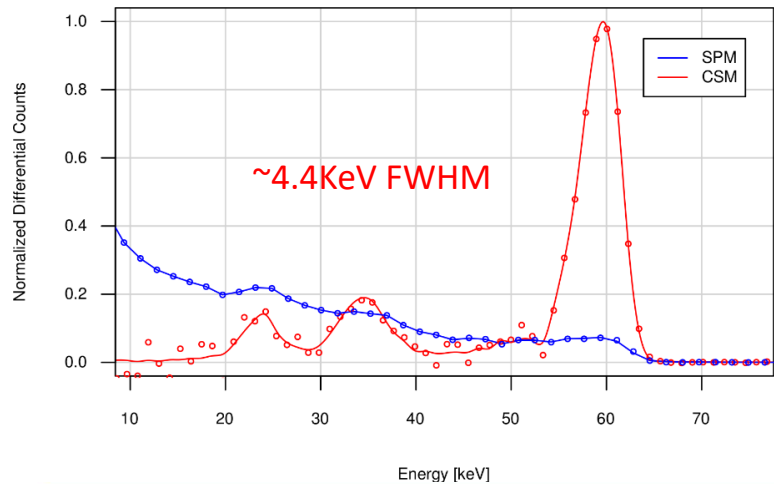
Simulation 80keV photons, 2mm CdTe, -800V, 100e- r.m.s. noise (no threshold dispersion, no charge trapping)

In order to do spectroscopy at fine pitches a charge reconstruction and hit allocation architecture is required.

The Medipix3RX: a high resolution, zero dead-time pixel detector readout chip allowing spectroscopic imaging

(2013 JINST 8 C02016)

R. Ballabriga,^{a,1} J. Alozy,^a G. Blaj,^a M. Campbell,^a M. Fiederle,^d E. Frojdh,^a
E.H.M. Heijne,^{a,b,c} X. Llopart,^a M. Pichotka,^d S. Procz,^d L. Tlustos^d and W. Wong^a



- Energy spectrum in Single Pixel Mode and in Charge Summing Mode (sum of all the pixels in the chip ~16k pixels)
- 60keV, 2mm CdTe, 110 μ m pitch
- Fluorescence photons are included in charge sum if their deposition takes place within the volume of the pixels neighbouring the initial deposition
- Ga K-edge (50.2keV) can be identified in CSM images
- SNR higher in CSM for the higher energy thresholds

PIXIE III: a very large area photon-counting CMOS pixel ASIC for sharp X-ray spectral imaging

2015 JINST 10 C01032

R. Bellazzini,^{a,b} A. Brez,^{a,b} G. Spandre,^{a,b,1} M. Minuti,^{a,b} M. Pinchera,^{a,b} P. Delogu,^{a,c}
P.L. de Ruvo^{a,c} and A. Vincenzi^b

ERICA: An Energy Resolving Photon Counting Readout ASIC for X-Ray In-Line Cameras

Jose-Gabriel Macias-Montero^{a,*}, Maher Sarraj^b, Mokhtar Chmeissani^a, Thomas Moore^c, Raimon Casanova^a, Ricardo Martinez^d, Carles Puigdemengoles^a, Xavier Prats^a, and Machiel Kolstein^a.

Photon counting, dual energy X-ray imaging at CT count rates: measurements and implications of in-pixel charge sharing correction

Christer Ullberg, Mattias Urech, Charlotte Eriksson, Alexander Stewart, Niclas Weber
XCounter AB, Svärdvägen 23, S-182 33 Danderyd, Sweden

2018 SPIE

IEEE TRANSACTIONS ON NUCLEAR SCIENCE, VOL. 62, NO. 1, FEBRUARY 2015

359

Measurements of Matching and Noise Performance of a Prototype Readout Chip in 40 nm CMOS Process for Hybrid Pixel Detectors

P. Maj, *Member, IEEE*, P. Grybos, *Member, IEEE*, R. Szczygiel, *Member, IEEE*, P. Kmon, *Member, IEEE*,
R. Kłeczek, *Member, IEEE*, A. Drozd, *Member, IEEE*, P. Otińowski, *Member, IEEE*, and
G. Deptuch, *Senior Member, IEEE*

Towards large area fine pixel pitch detectors



Work carried out in the framework of the development of the NAEOTOM Alpha by Siemens Healthineers

Image: <https://www.siemens-healthineers.com/en-uk/computed-tomography/photon-counting-ct-scanner/naeotom-alpha>

FDA NEWS RELEASE

FDA Clears First Major Imaging Device Advancement for Computed Tomography in Nearly a Decade

[f Share](#) [t Tweet](#) [in LinkedIn](#) [✉ Email](#) [🖨 Print](#)

[↻ More Press Announcements](#)

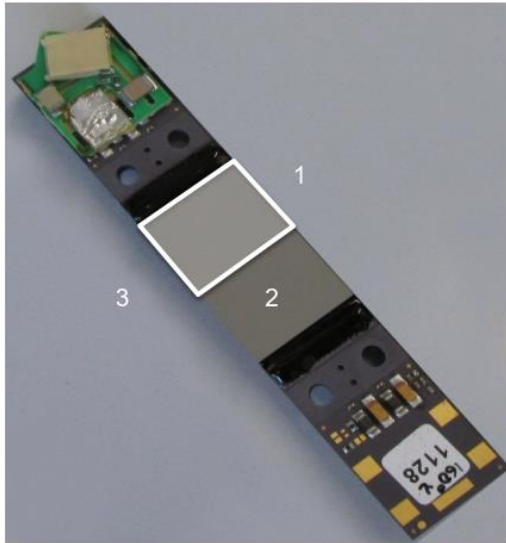
For Immediate Release: September 30, 2021

Today, the U.S. Food and Drug Administration cleared the first new major technological improvement for Computed Tomography (CT) imaging in nearly a decade.

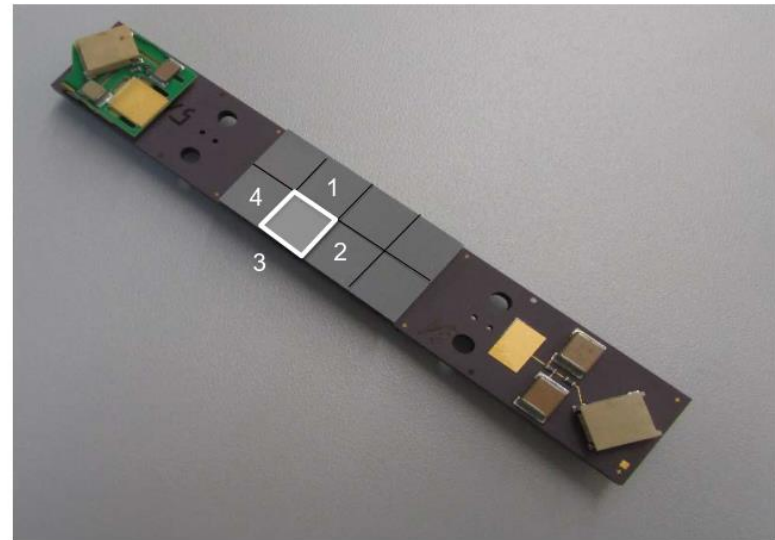
“Computed tomography is an important medical imaging tool that can aid in diagnosing disease, trauma or abnormality; planning and guiding interventional or therapeutic procedures; and monitoring the effectiveness of certain therapies,” said Laurel Burk, Ph.D., assistant director of the Diagnostic X-ray Systems Team in the FDA’s Center for Devices and Radiological Health. **“Today’s action represents the first major new technology for computed tomography imaging in nearly a decade and underscores the FDA’s efforts to encourage innovation in areas of scientific and diagnostic progress.”**

<https://www.fda.gov/news-events/press-announcements/fda-clears-first-major-imaging-device-advancement-computed-tomography-nearly-decade>

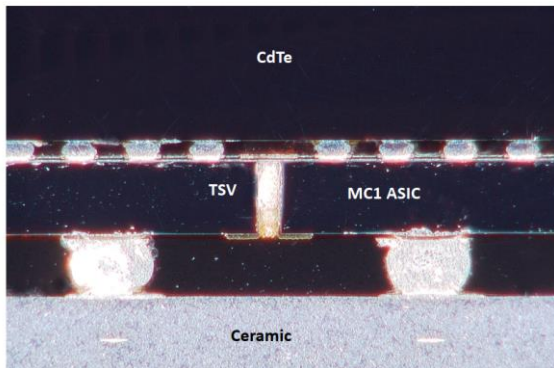
Towards large and seamless detector areas (Siemens Healthineers)



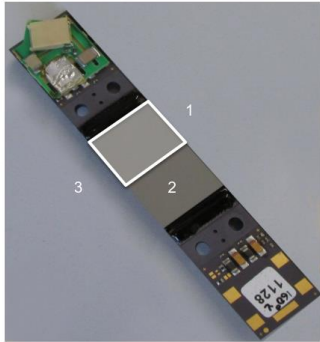
3 side buttable



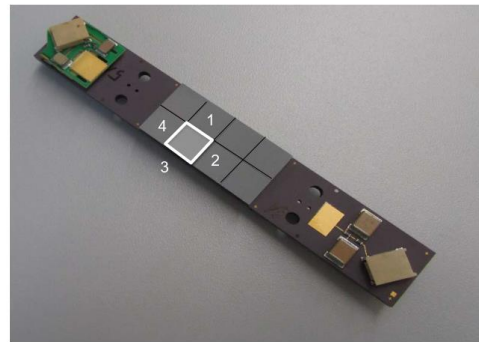
4 side buttable



MC3 ASIC, Siemens Healthineers



3 side buttable



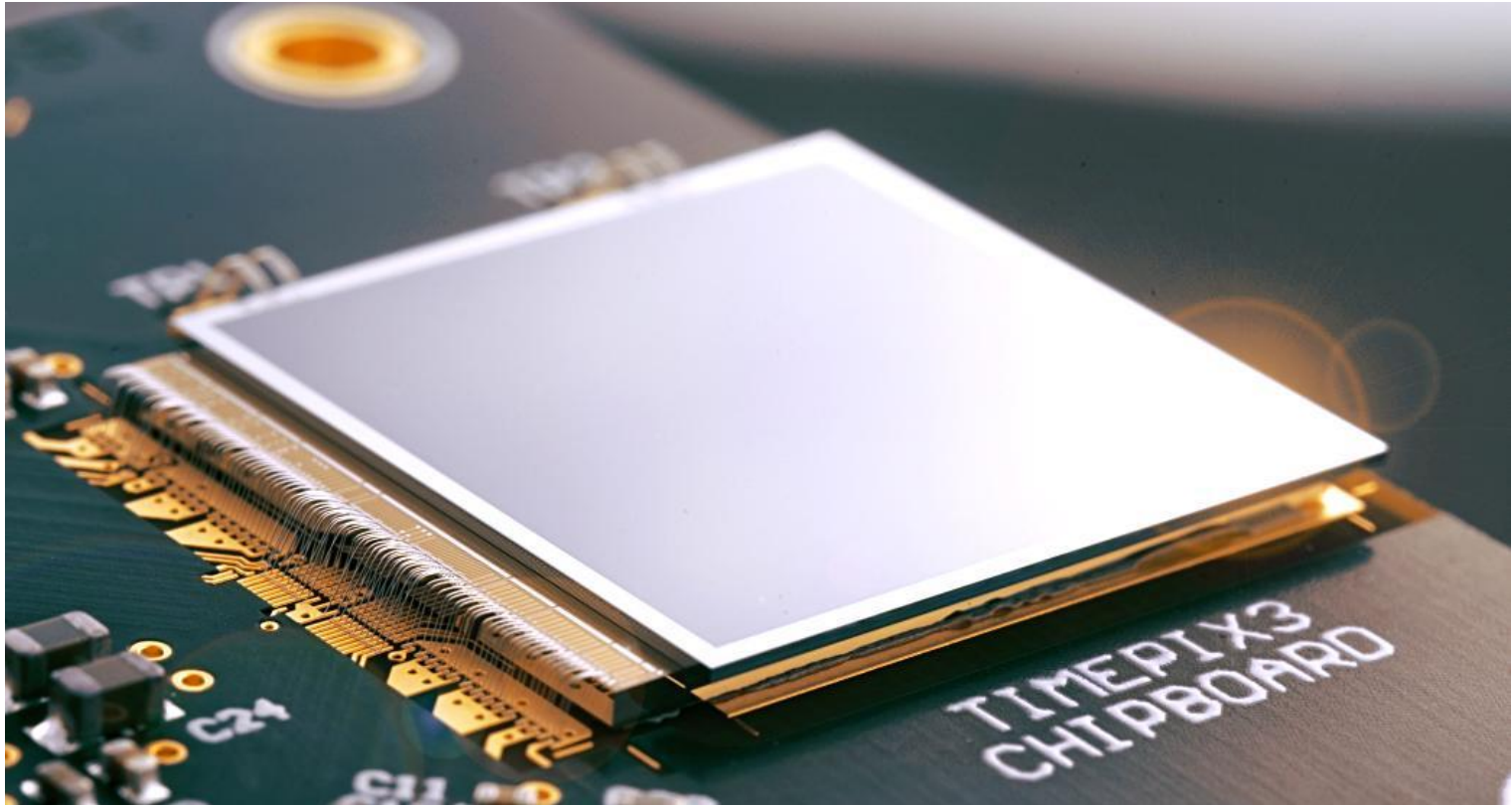
4 side buttable



MC3 ASIC, Siemens Healthineers

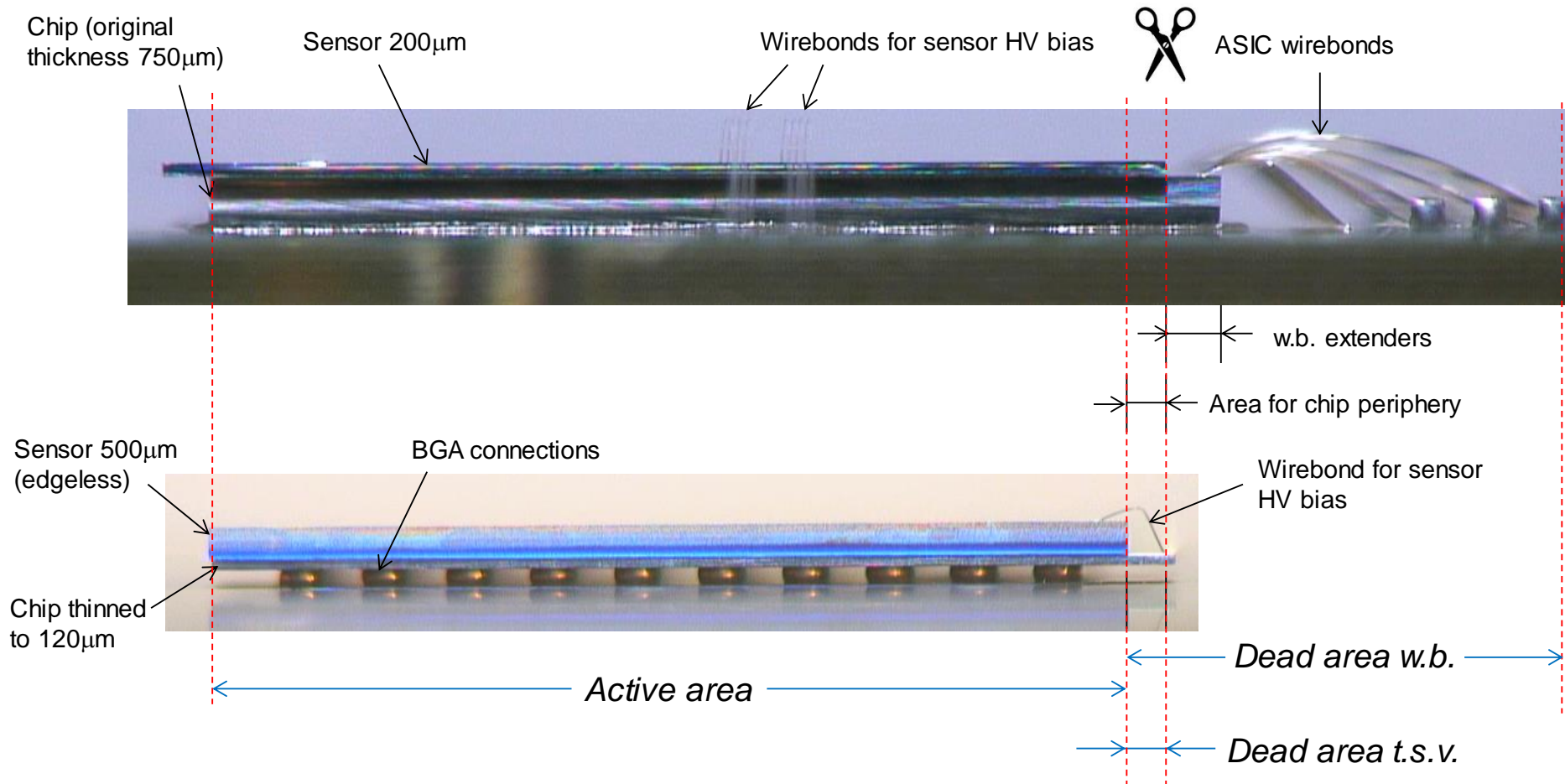
- CT application
- $275 \times 322 \mu\text{m}^2$ pixels, 4 side buttable
- 32×24 pixels
- Die size $\sim 10.5 \times 8.4 \text{mm}^2$
- 4 thresholds (Range 0-95keV)
- 16 bit counters
- 300Mbit/s readout speed (i.e. $< 200 \mu\text{s}$ per frame)
- 12ns FWHM signal
- Non paralyzable
- 2.5keV (FWHM @60keV)
- $1 \text{mV}/\text{mm}^2$ i.e. $125 \mu\text{W}$ per pixel

Towards large detector areas: Medipix collaborations developments

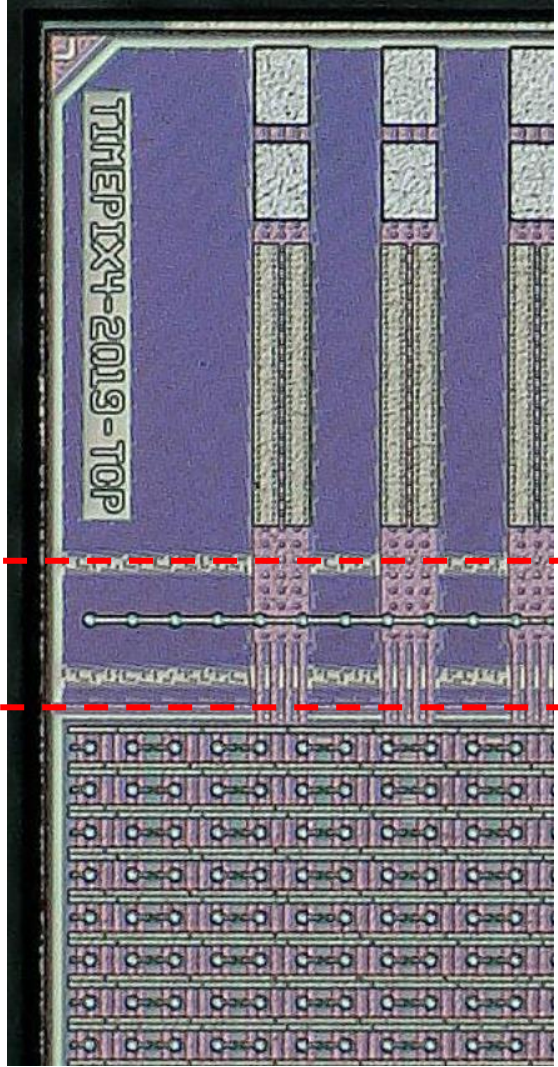
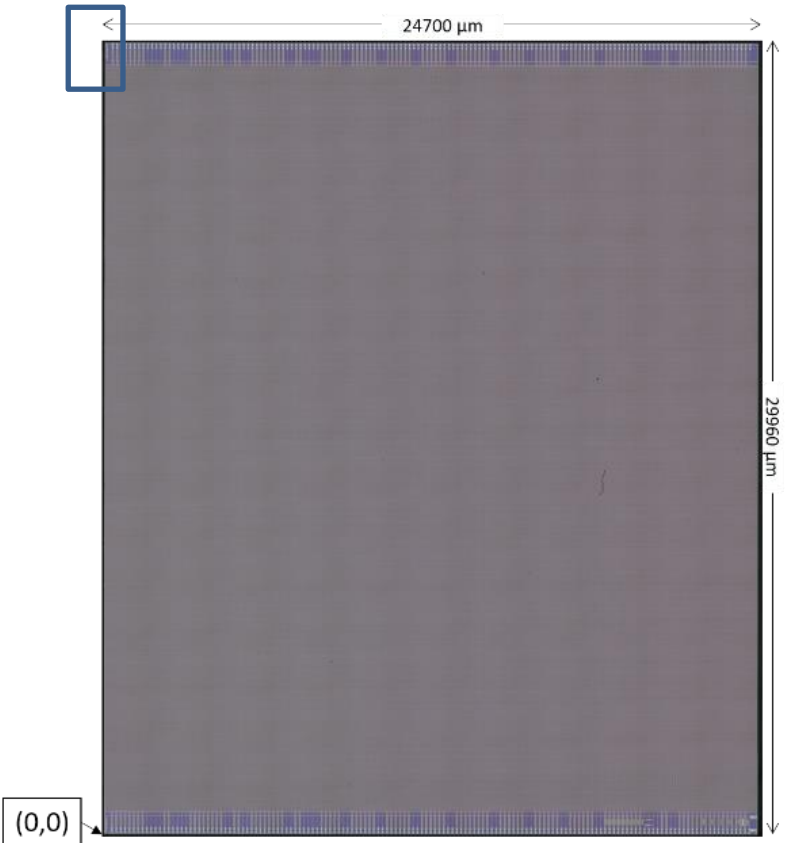


The fill factor in the active pixel matrix is 100 %
However the systems have traditionally been designed to be tiled
seamlessly on 3 sides (i.e. active area <100%)

Through Silicon Vias on the Medipix3RX ASIC

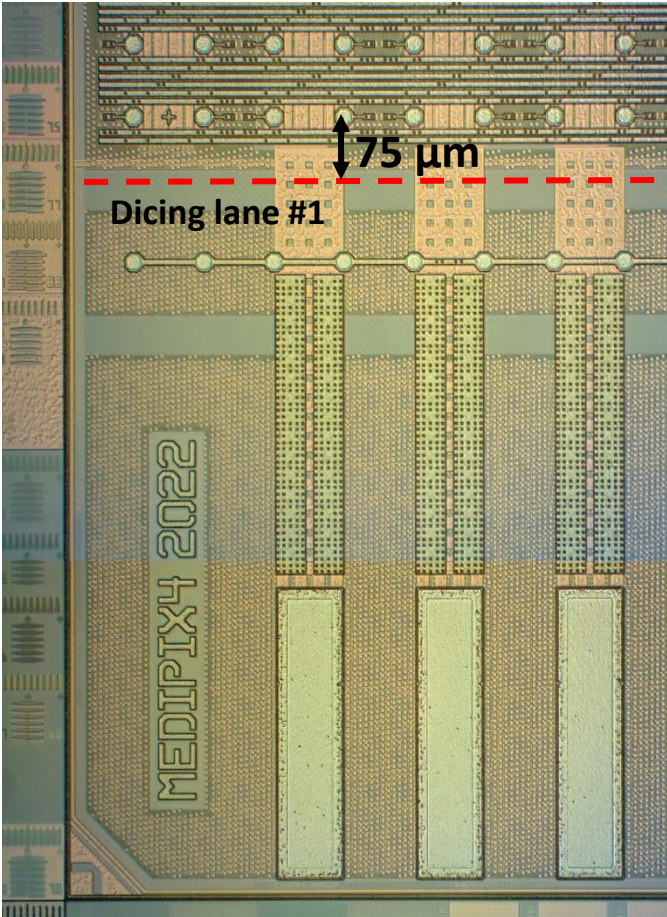
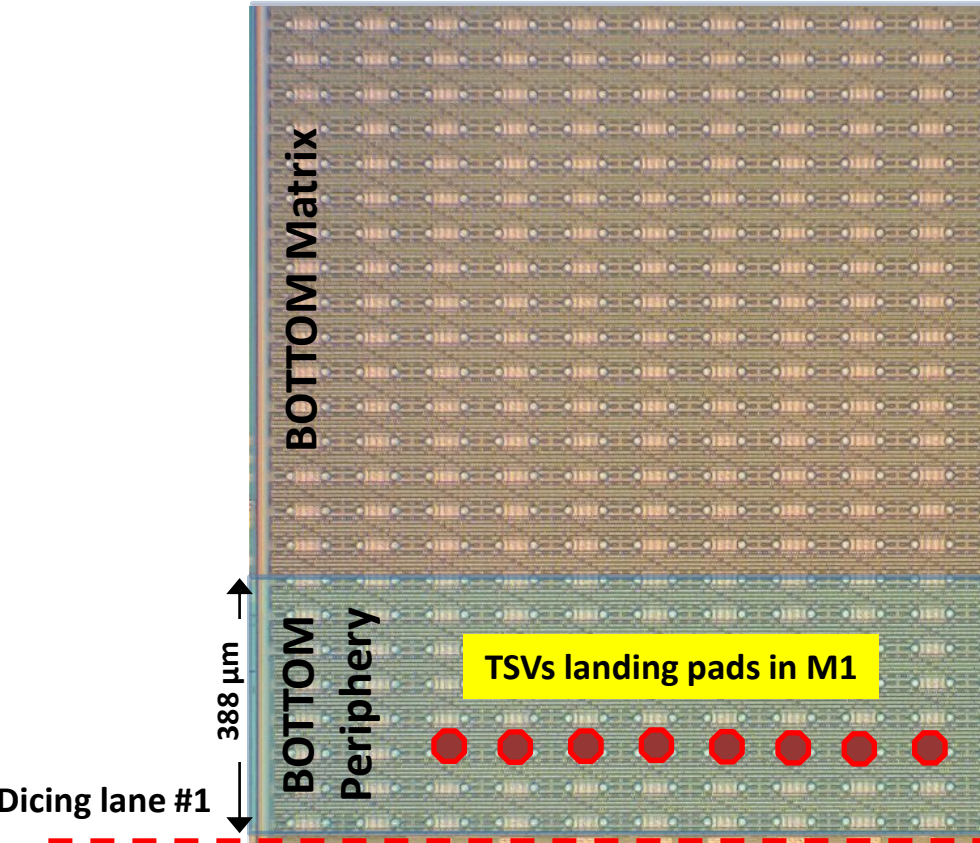


Through Silicon Vias on the Timepix4 ASIC



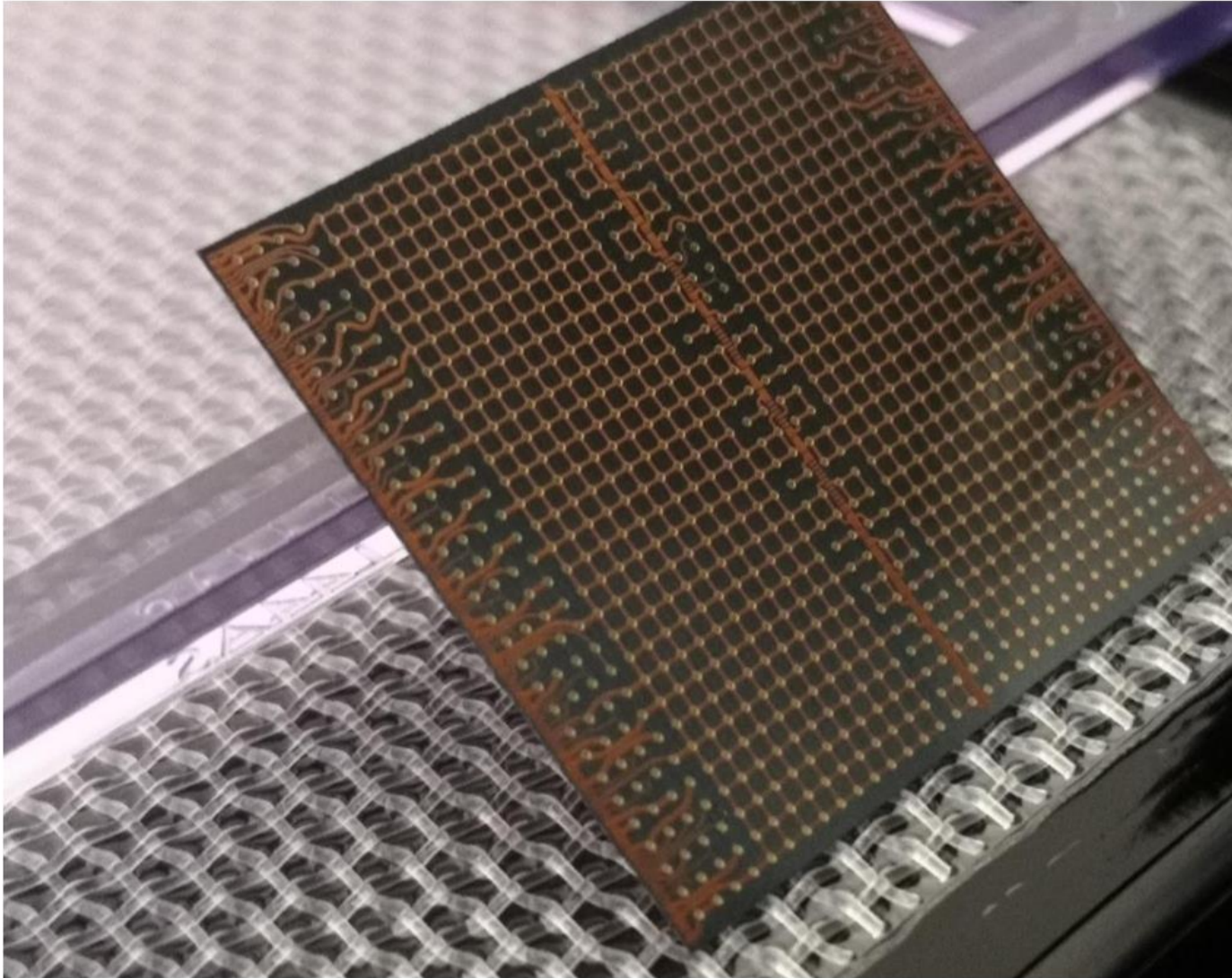
Timepix4 chip image, 448 x 512 pixels, 55μm pitch
First wafers sent for TSV processing

Through Silicon Vias on the Medipix4 ASIC



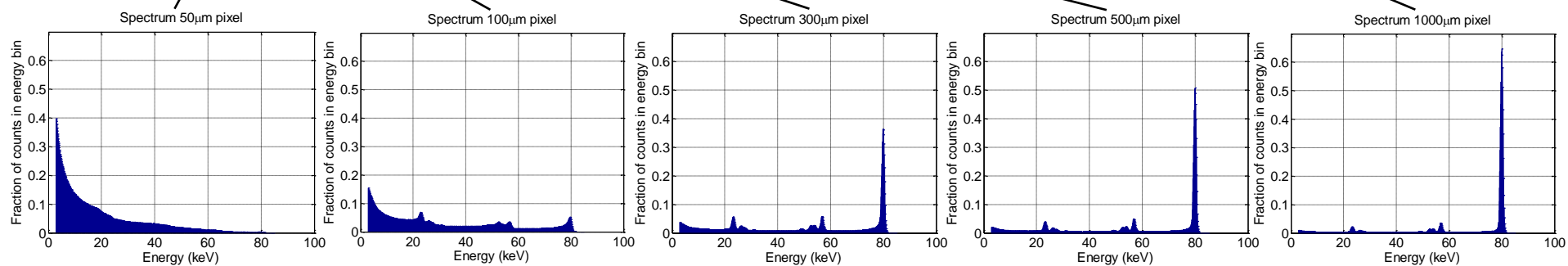
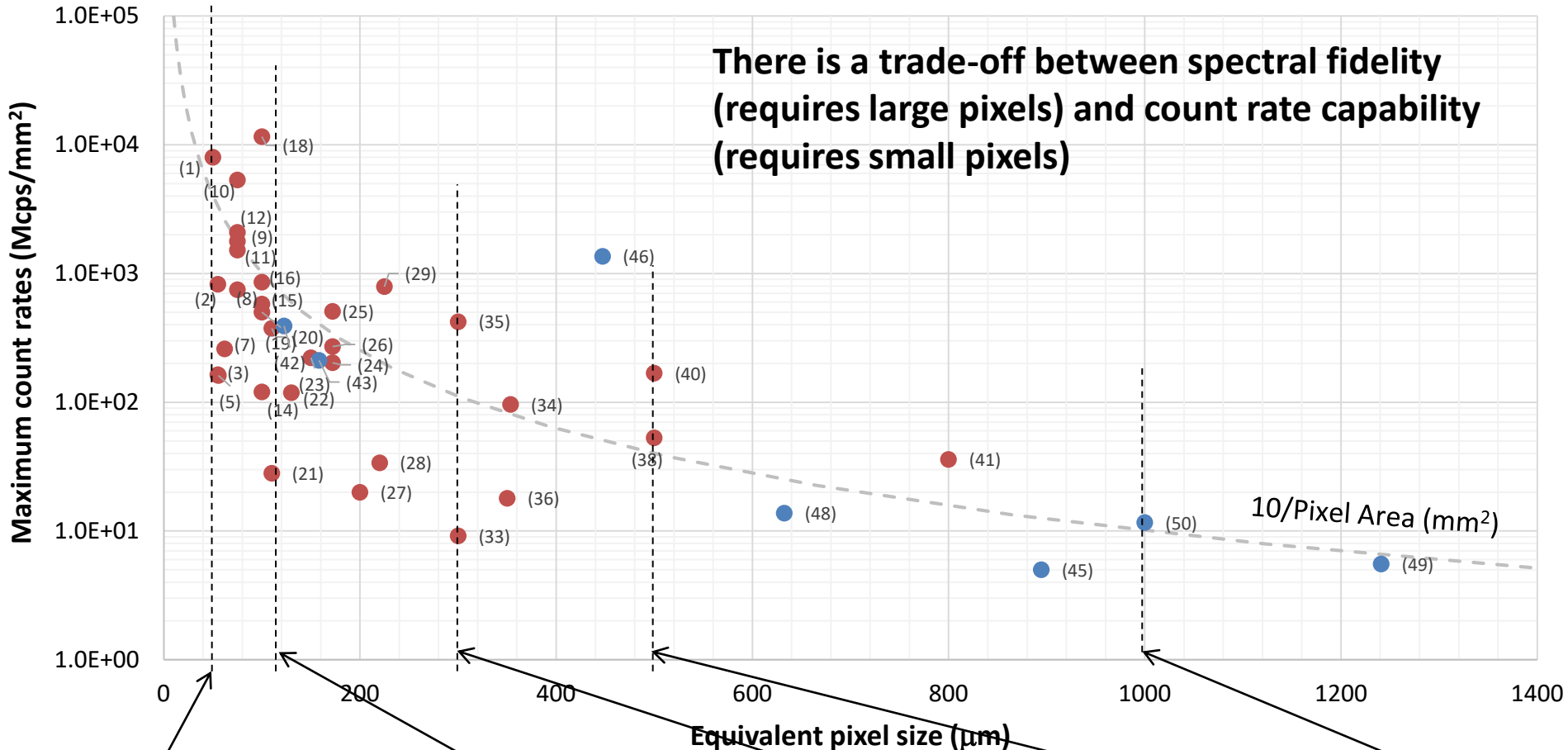
*Picture courtesy: J. Alozy.

RDL view of the Timepix4 chip processed for TSVs

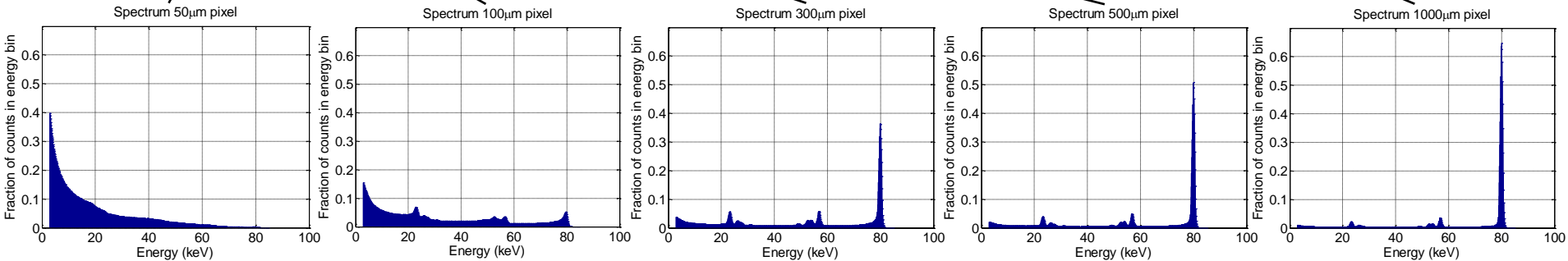
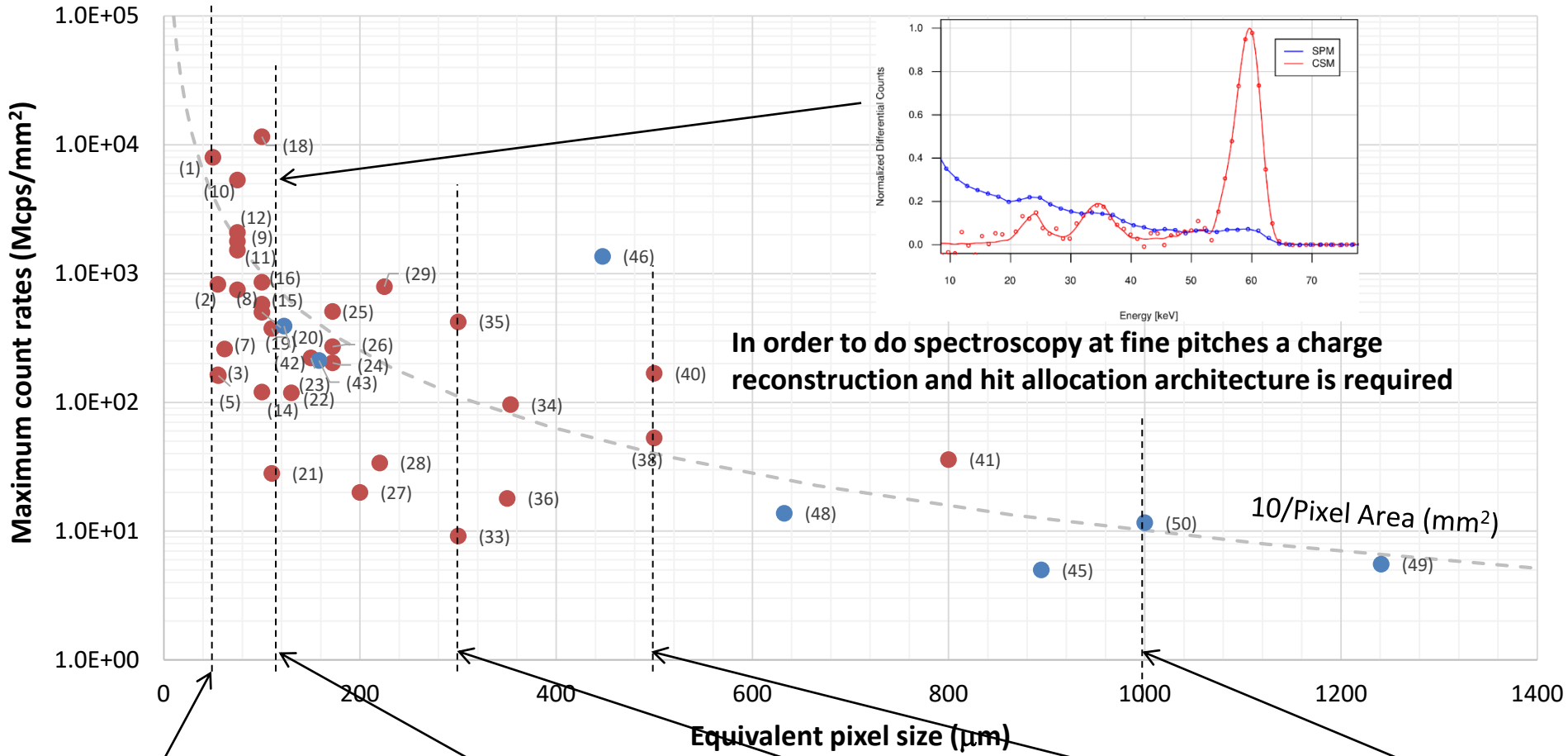


Summary and conclusions

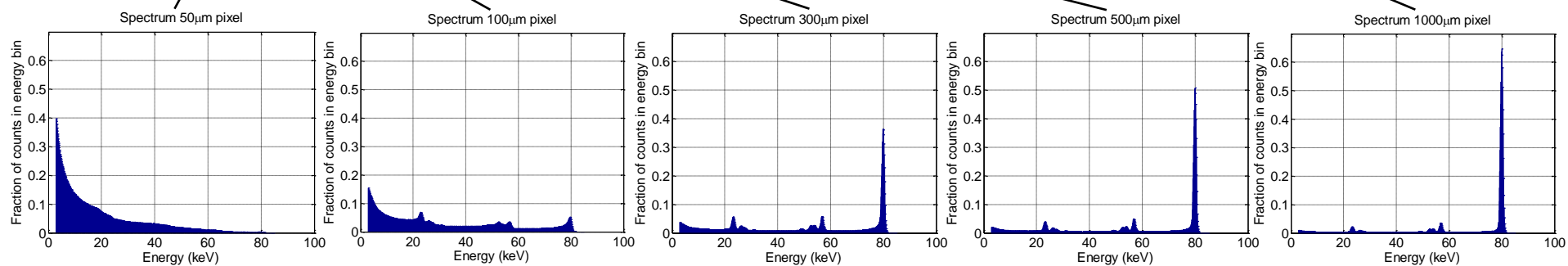
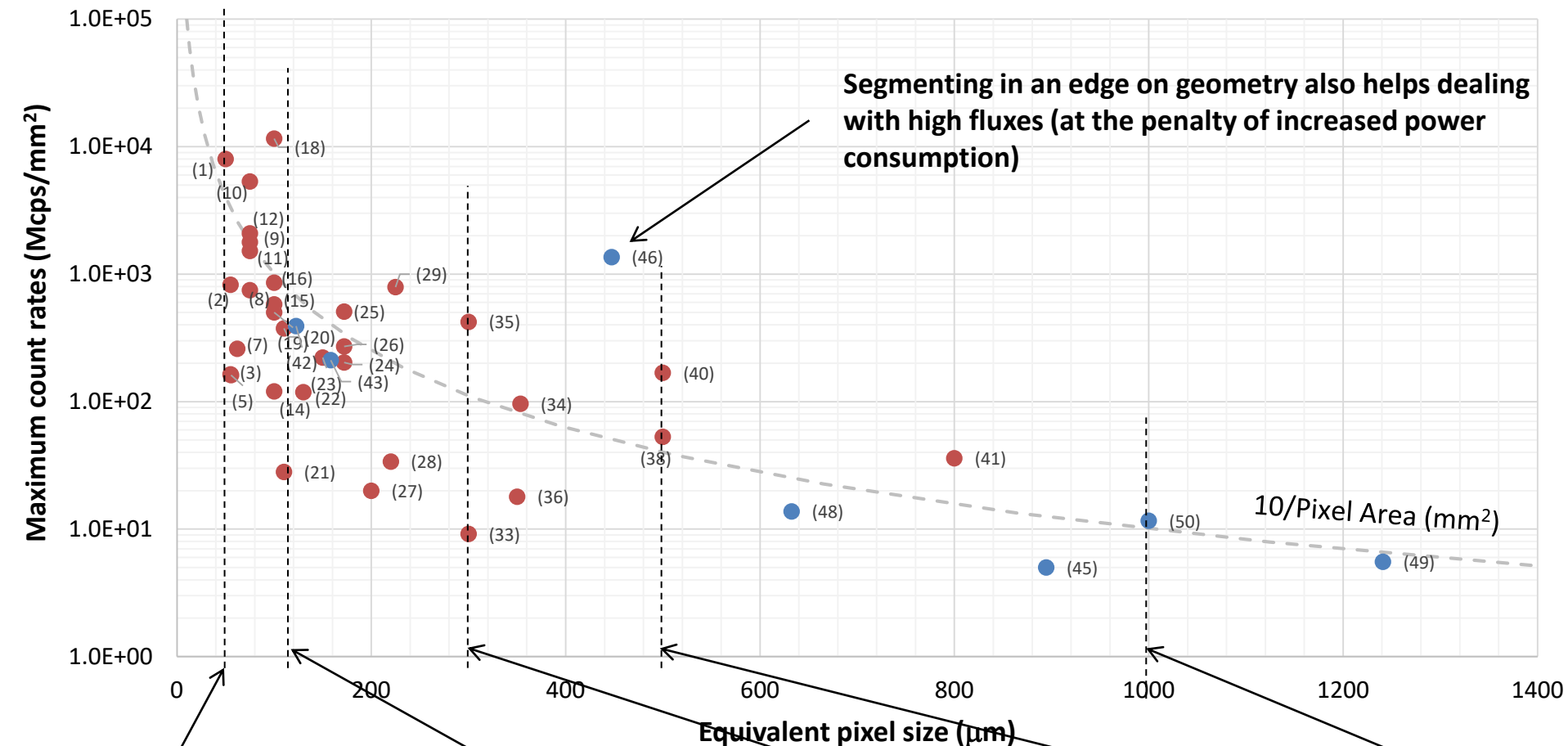
There is a trade-off between spectral fidelity (requires large pixels) and count rate capability (requires small pixels)



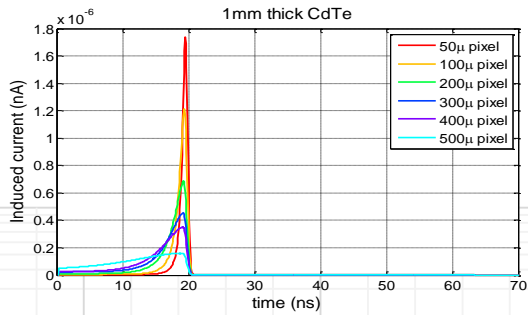
Simulation 80keV photons, 2mm CdTe, -800V, 100e- r.m.s. noise (no threshold dispersion, no charge trapping)



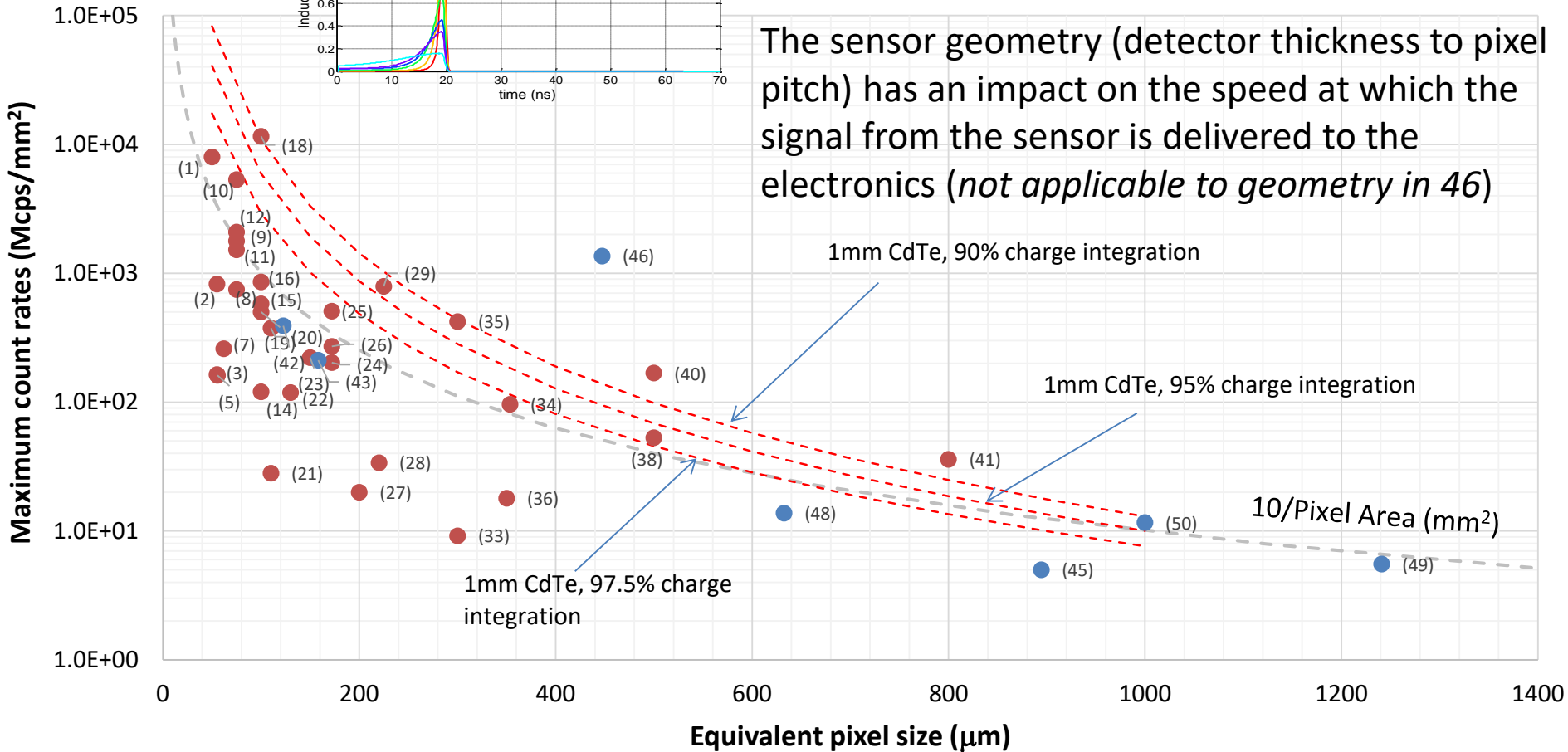
Simulation 80keV photons, 2mm CdTe, -800V, 100e- r.m.s. noise (no threshold dispersion, no charge trapping)



Simulation 80keV photons, 2mm CdTe, -800V, 100e⁻ r.m.s. noise (no threshold dispersion, no charge trapping)

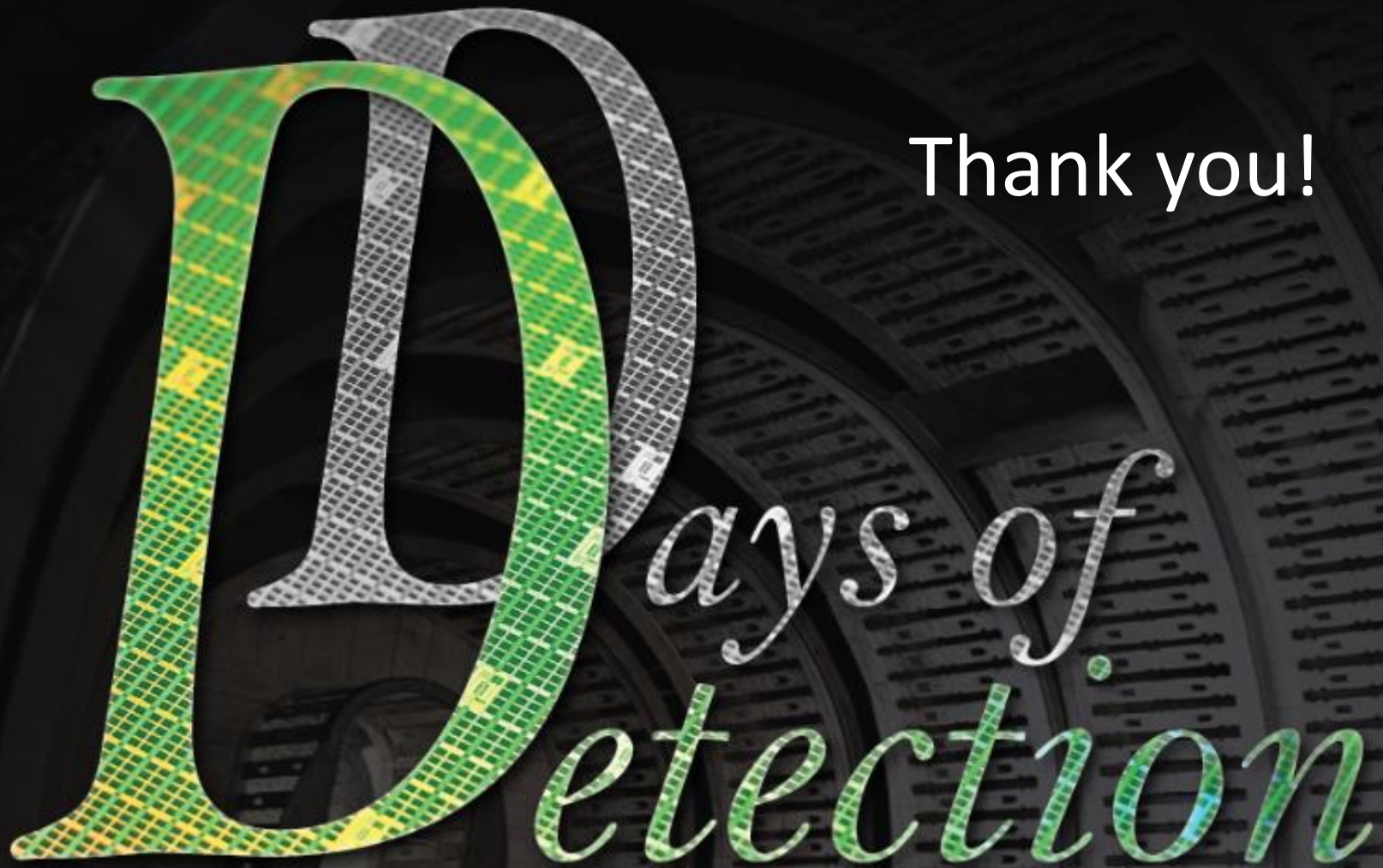


The sensor geometry (detector thickness to pixel pitch) has an impact on the speed at which the signal from the sensor is delivered to the electronics (*not applicable to geometry in 46*)



- We saw techniques for increasing the count rate
- TSVs are a technology enabling to achieve seamless large areas even at fine pixel pitches

Thank you!

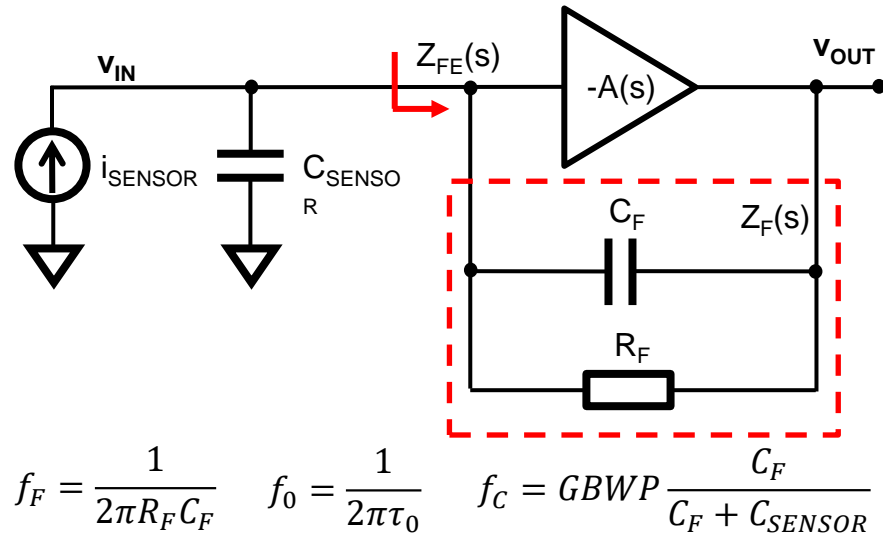
The image features a large, stylized letter 'D' on the left, filled with a green and yellow grid pattern. To its right, the words 'Days of Detection' are written in a cursive font. 'Days of' is in white, and 'Detection' is in green. The background is a dark, circular pattern of microelectronics components.

*Days of
Detection*

1st international school on microelectronics for solid state detectors design, manufacturing, and application

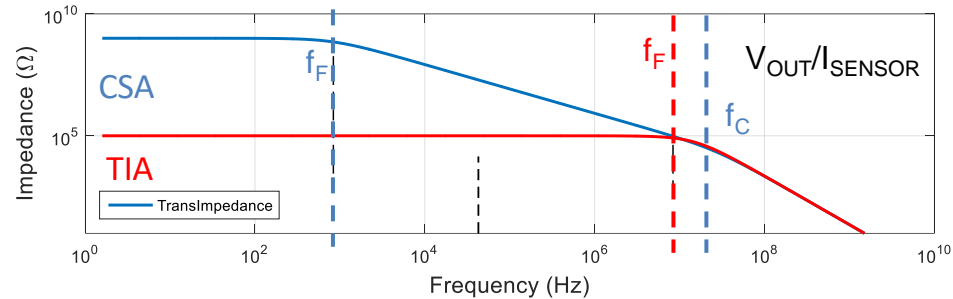
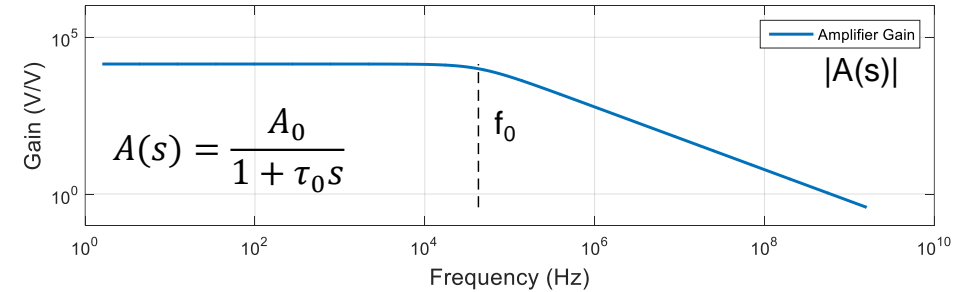
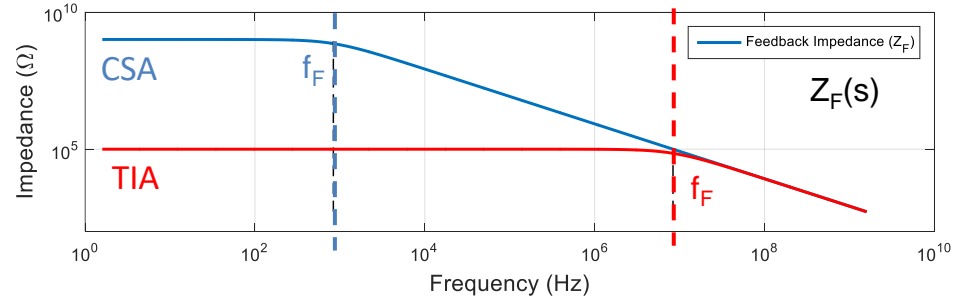
Additional

General case



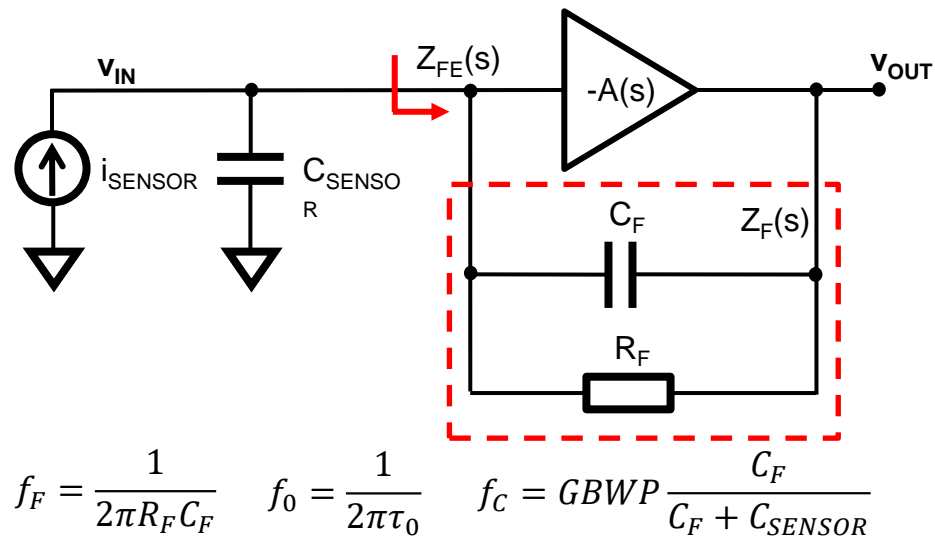
$$\frac{v_{OUT}}{i_{SENSOR}}(s) \cong Z_F(s)$$

$$Z_{FE}(s) \cong \frac{Z_F(s)}{A(s)}$$



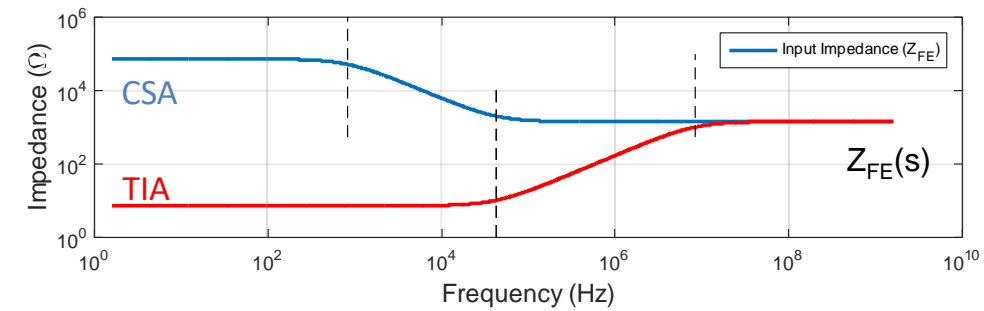
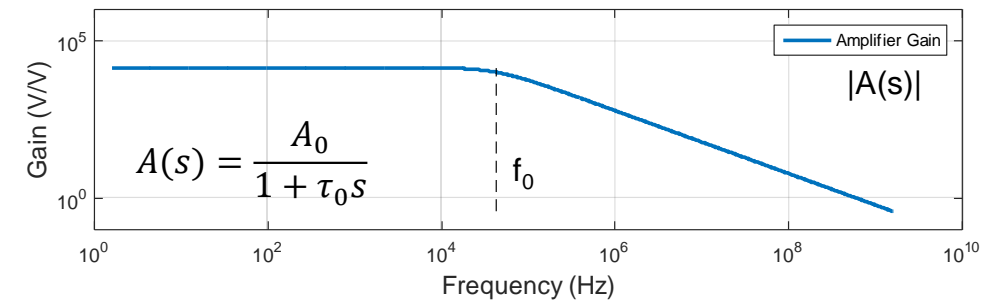
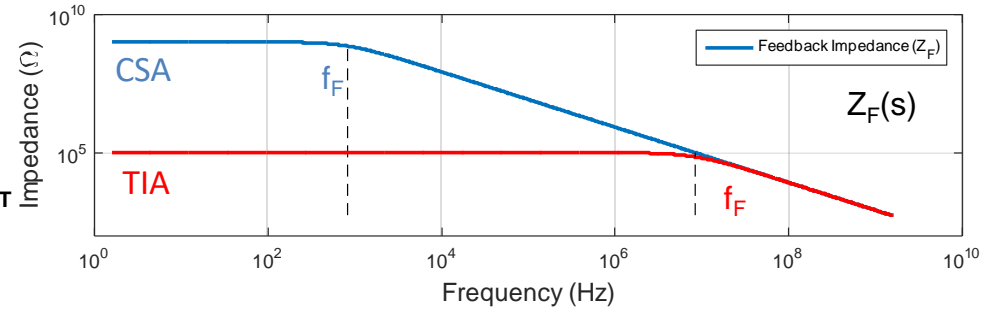
CSA configuration: $C_F=190\text{fF}$, $R_F=1\text{G}\Omega$
 TIA configuration: $C_F=190\text{fF}$, $R_F=100\text{k}\Omega$
 Amplifier: $A_0=14000$ (83dB), $f_0=42.8\text{kHz}$, $GBWP=600\text{MHz}$

General case



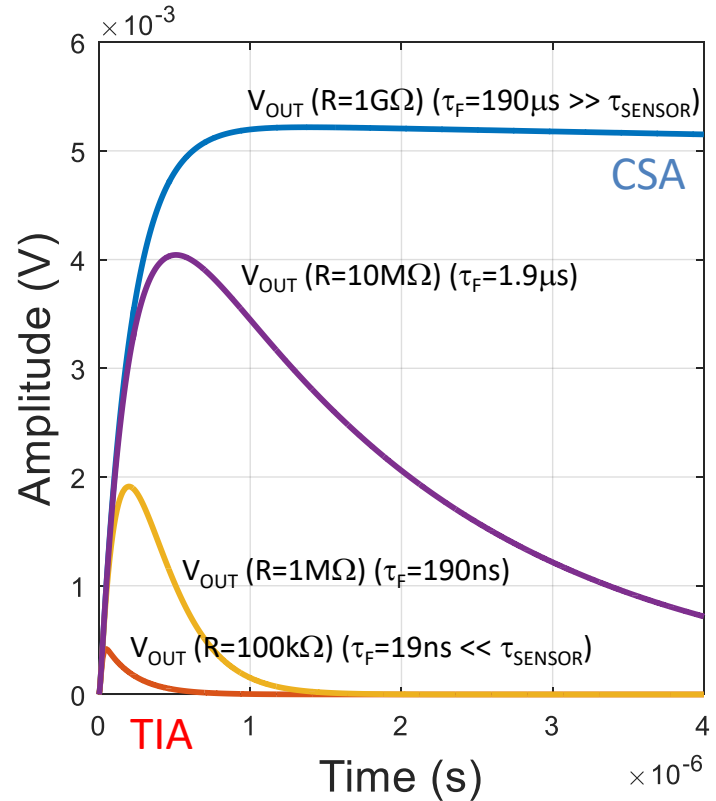
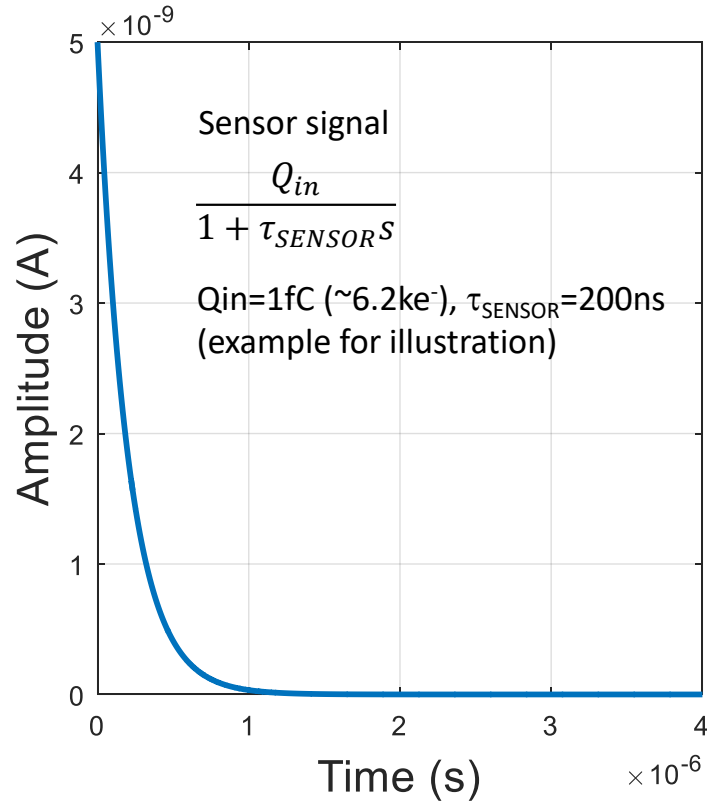
$$\frac{v_{OUT}}{i_{SENSOR}}(s) \cong Z_F(s)$$

$$Z_{FE}(s) \cong \frac{Z_F(s)}{A(s)}$$



CSA configuration: $C_F=190\text{fF}$, $R_F=1\text{G}\Omega$
 TIA configuration: $C_F=190\text{fF}$, $R_F=100\text{k}\Omega$
 Amplifier: $A_0=14000$ (83dB), $f_0=42.8\text{kHz}$, $GBWP=600\text{MHz}$

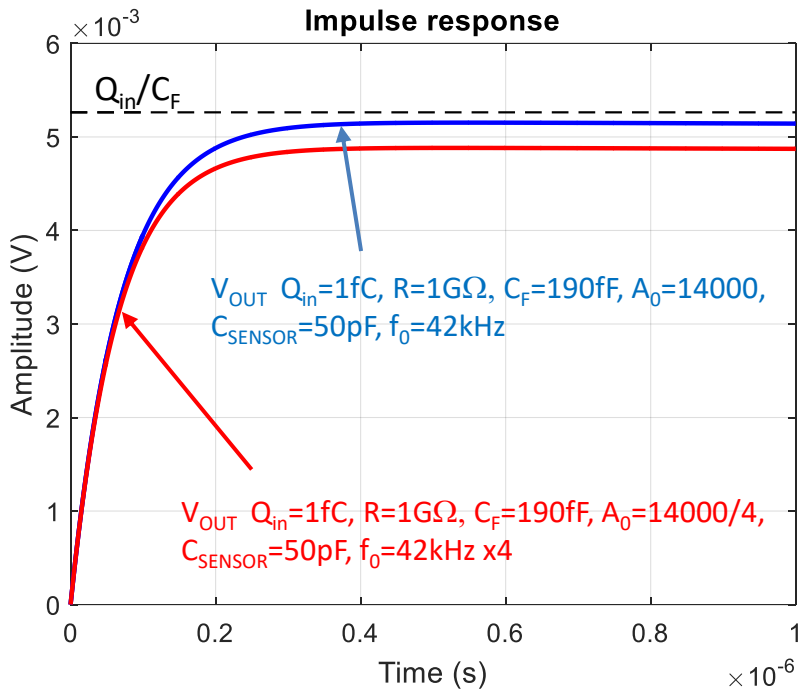
General case



CSA: Signal integration. The circuit has higher gain and longer tails (limitation for high flux applications).

TIA: Signal shape is preserved. Lower gain i.e. higher dynamic range, shorter tails.

Time expressions (CSA)



Same GBWP for the two amplifiers but different gain

Increasing the open loop gain allows decreasing C_{FB} and increase the charge gain. This is important from the perspective of optimizing the system's noise-power. High gain is also important for low PSRR.

Transfer function when $R_F \rightarrow \infty$

$$\frac{v_{OUT}}{i_{IN}}(s) = \frac{1}{\left(C_F + \frac{C_{SENSOR}}{A_0}\right)s \left(1 + \frac{\tau_0}{1 + A_0 \frac{C_F}{C_{SENSOR}}}\right)s}$$

Impulse response $i_{IN}=Q_{IN}\delta(t)$

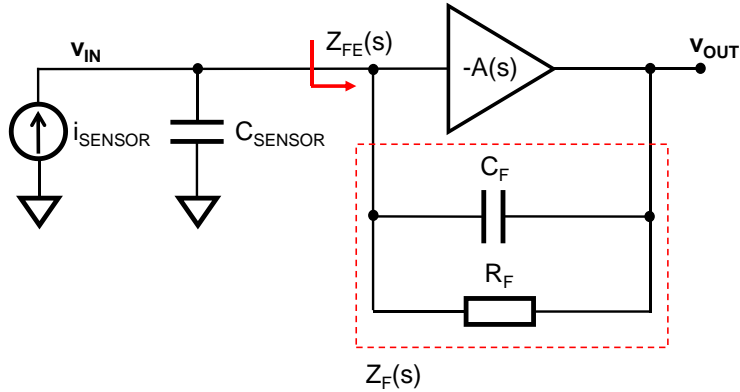
$$v_{OUT}(t) = \frac{Q_{IN}}{\left(C_F + \frac{C_{SENSOR}}{A_0}\right)} \left(1 - e^{-t/\tau}\right)$$

Importance of driving up the gain and the bandwidth of the amplifier in order to obtain a fast response of the amplitude independently of the capacitive load of the sensor (C_{SENSOR}).

By design:

$$C_F A_0 \gg C_{SENSOR}$$

Input impedance



CSA configuration: $C_F=190\text{fF}$, $R_F=1\text{G}\Omega$

TIA configuration: $C_F=190\text{fF}$, $R_F=100\text{k}\Omega$

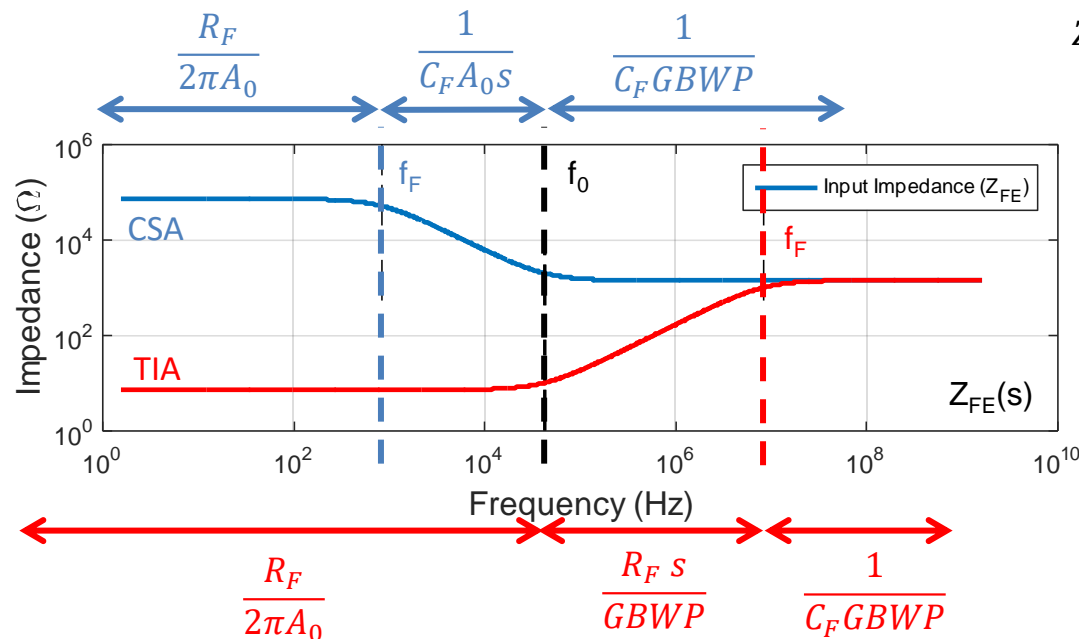
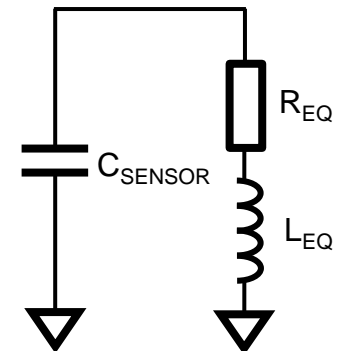
Amplifier: $A_0=14000$ (83dB) $f_0=42.8\text{kHz}$

$$Z_{FE} = \frac{Z_F(s)}{A(s) + 1} \cong \frac{Z_F(s)}{A(s)} = \frac{R_F}{(1 + R_F C_F s)} \frac{(1 + \tau_0 s)}{A_0}$$

$$f_F = \frac{1}{2\pi R_F C_F}$$

$$f_0 = \frac{1}{2\pi \tau_0}$$

Inductive behaviour for the transimpedance configuration

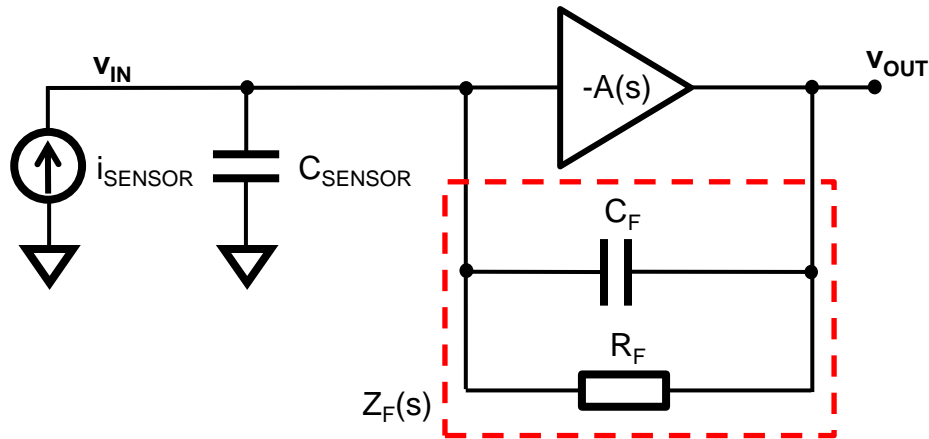


$$\frac{R_F}{2\pi A_0}$$

$$\frac{R_F s}{GBWP}$$

$$\frac{1}{C_F GBWP}$$

Stability



- The expression for $v_{\text{OUT}}/i_{\text{SENSOR}}$ is that of a second order system
- In the case of a transimpedance amplifier we can calculate the minimum value for C_F required for stability

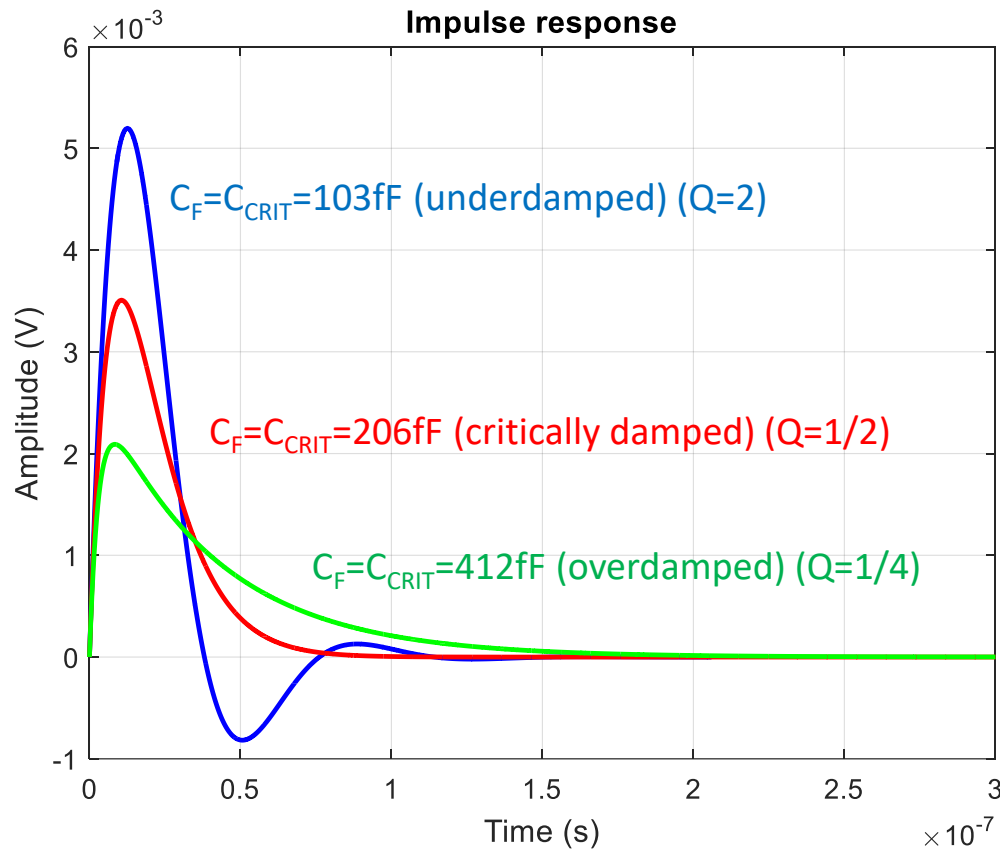
$$C_F = \frac{1}{Q} \sqrt{\frac{C_{\text{SENSOR}}}{\text{GBWP} \cdot R_F}} \quad \text{GBWP} = \frac{A_0}{\tau_0}$$

- $Q < 1/2$ (Overdamped system)
- $Q = 1/2$ (Critically damped system)
- $Q > 1/2$ (Underdamped system)

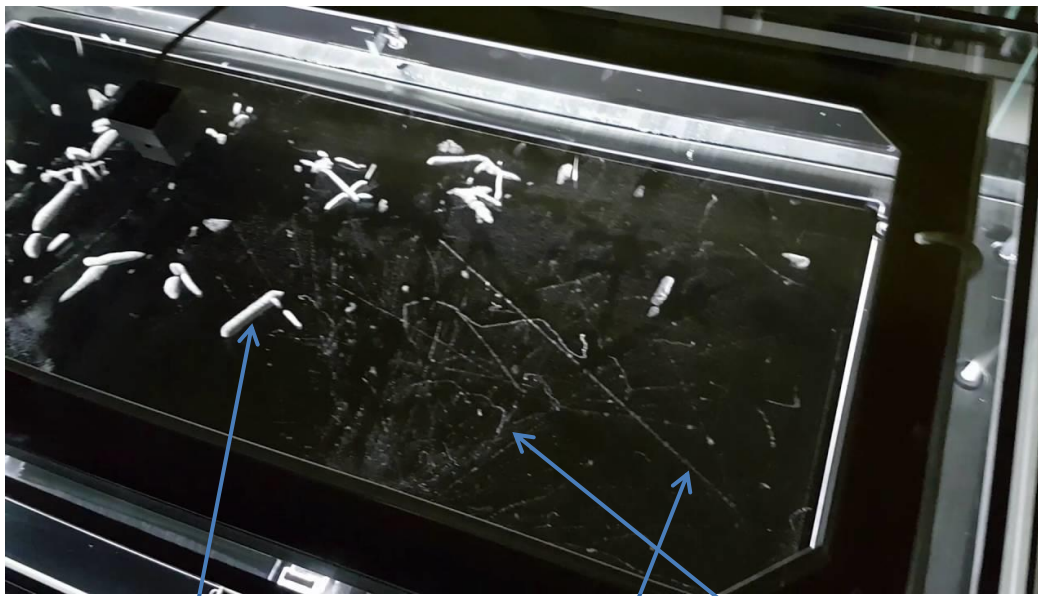
$$C_F > 2 \sqrt{\frac{C_{\text{SENSOR}}}{\text{GBWP} \cdot R_F}}$$

- For overdamped system
- High GBWP amplifiers are easier to compensate
- Trade off stability-closed loop bandwidth

Stability

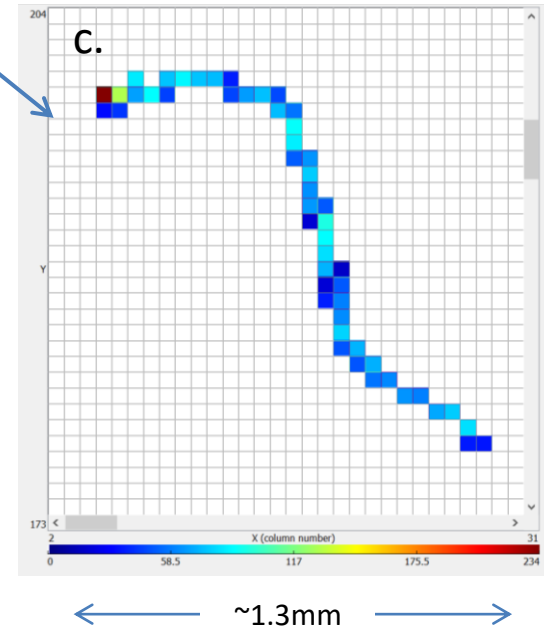
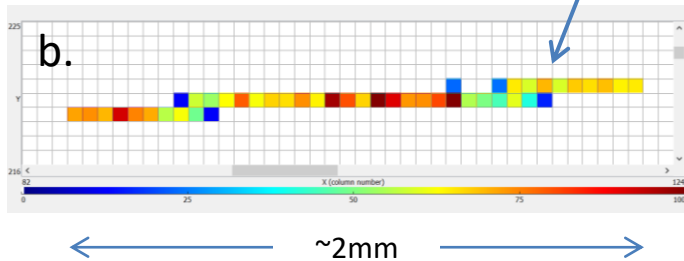
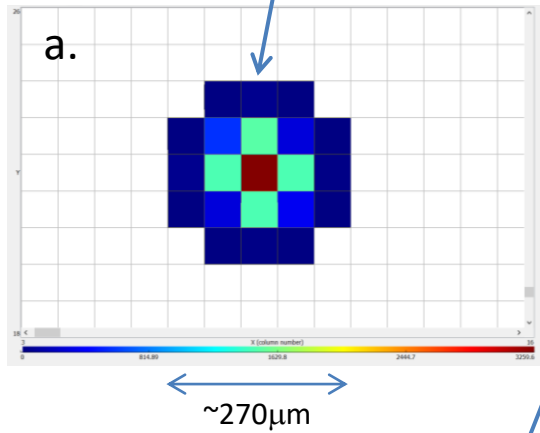


TIA configuration: $C_F = 120\text{fF}$, $R_F = 100\text{k}\Omega$
Amplifier: $A_0 = 14000$ (83dB) $f_0 = 42.8\text{kHz}$
 $Q_{in} = 1\text{fC}$

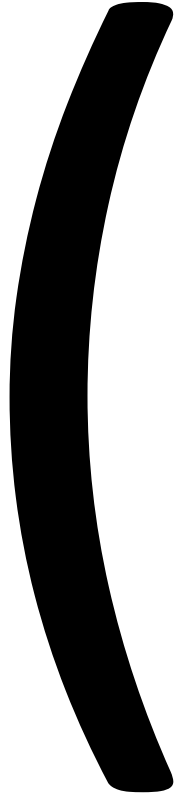


Cloud Chamber
(Wilson Chamber)
(1920-1950)

“Different particles have a different “signature” in their interaction with the detector material”



a. Alpha particle, b. Muon, c. Electron
Timepix data, 55 μ m pixels



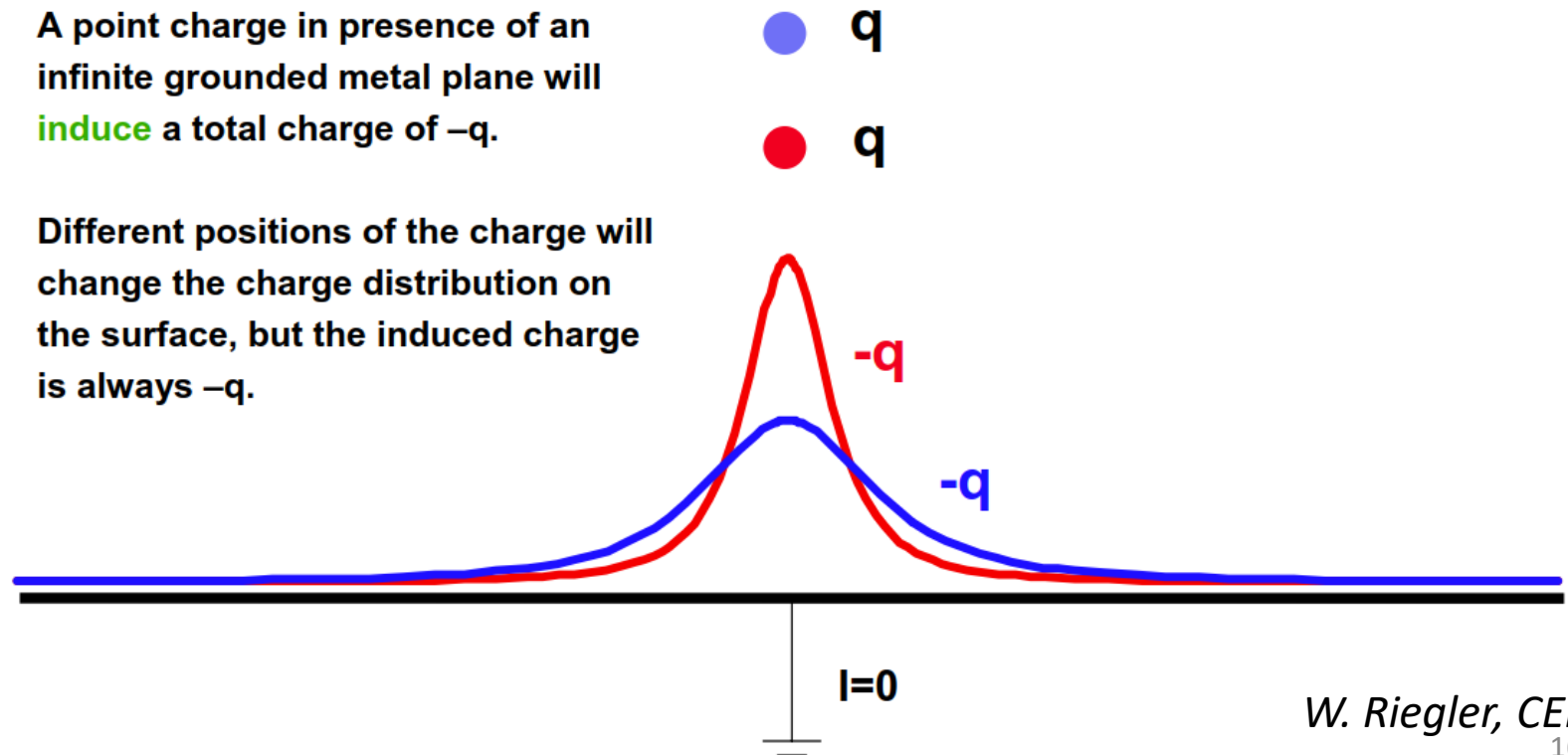
Signal induction

Induced charge on detector electrodes

- Signals on detector electrodes arise from motion of charge carriers
- Induced current is derived from laws of electrostatics

A point charge in presence of an infinite grounded metal plane will induce a total charge of $-q$.

Different positions of the charge will change the charge distribution on the surface, but the induced charge is always $-q$.



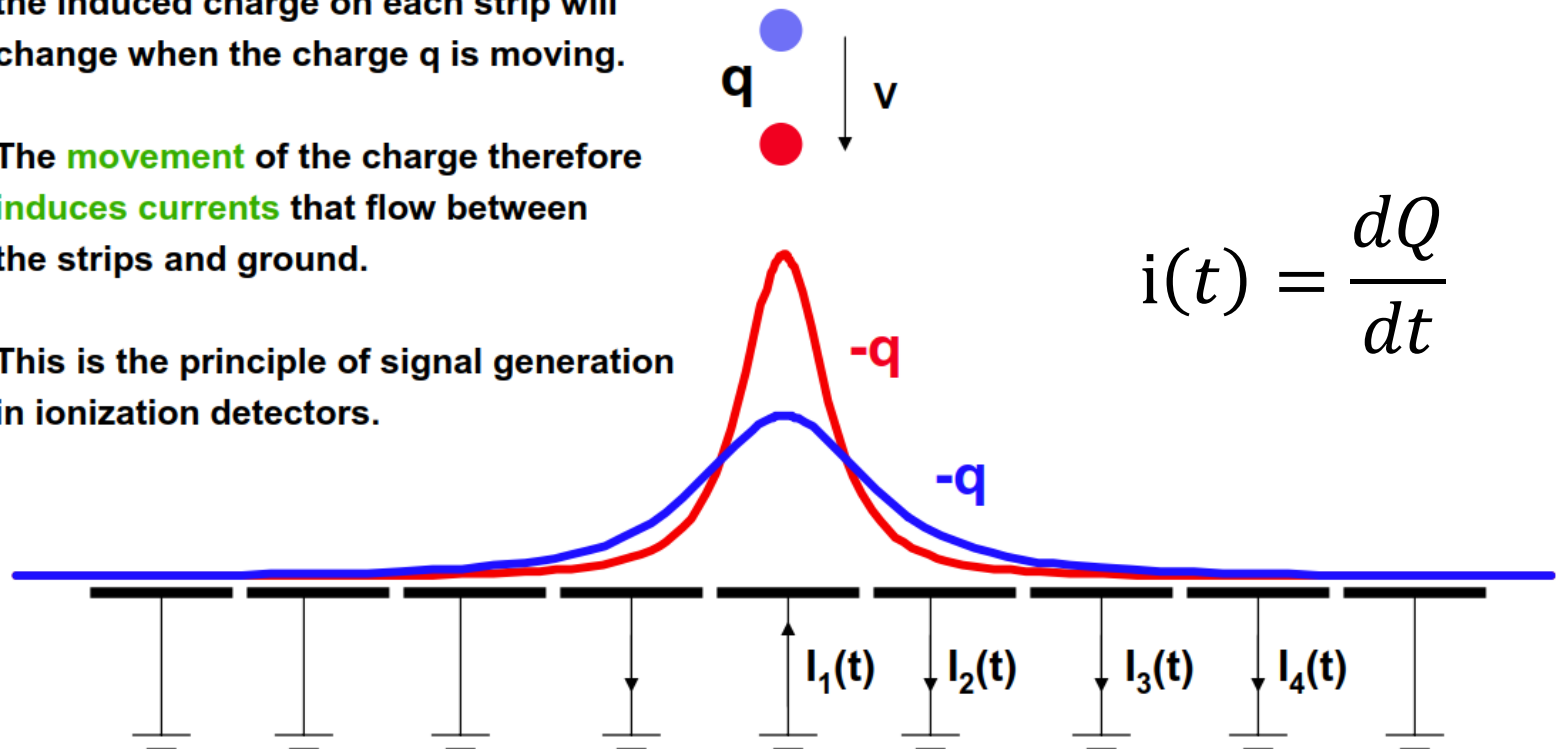
Induced charge on detector electrodes

- Signals on detector electrodes arise from motion of charge carriers
- Induced current is derived from laws of electrostatics

In case the strips are segmented, the induced charge on each strip will change when the charge q is moving.

The **movement** of the charge therefore **induces currents** that flow between the strips and ground.

This is the principle of signal generation in ionization detectors.



$$i(t) = \frac{dQ}{dt}$$

Induced charge on detector electrodes

- Method: Shockley-Ramo theorem: the instantaneous current induced on a given electrode is equal to

$$i(t) = q\vec{v} \cdot \vec{E}_w \qquad \vec{v} = \mu\vec{E}_d$$

where q is the charge of the carrier, v is its velocity, E_w is the weighting field and E_d is the drift field

- The induced charge (Q) on the electrode is given by

$$Q = q\Delta\varphi_0$$

where $\Delta\varphi_0$ is the weighting potential from the beginning to the end of the carrier path

S.Ramo, Proc. IRE, 27 (1939) p.584

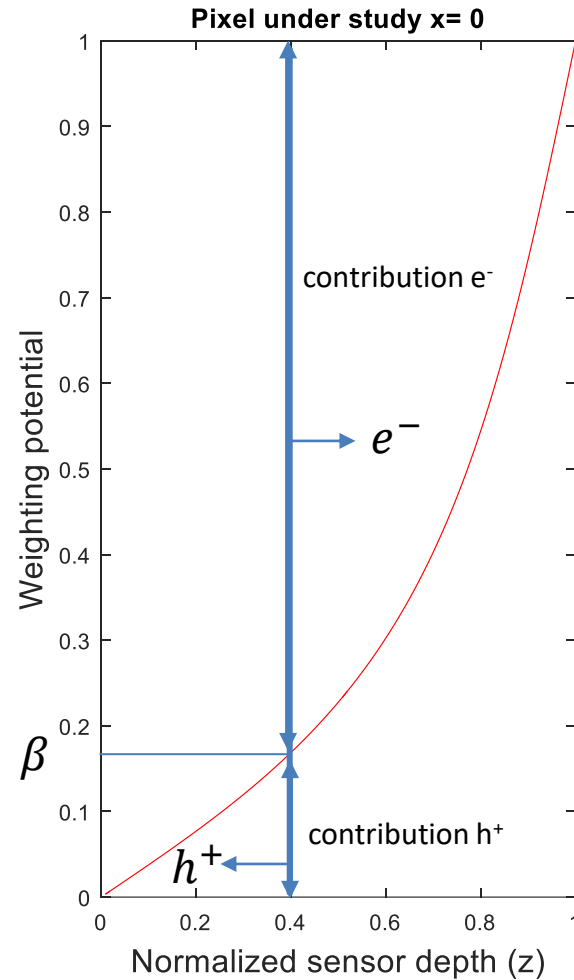
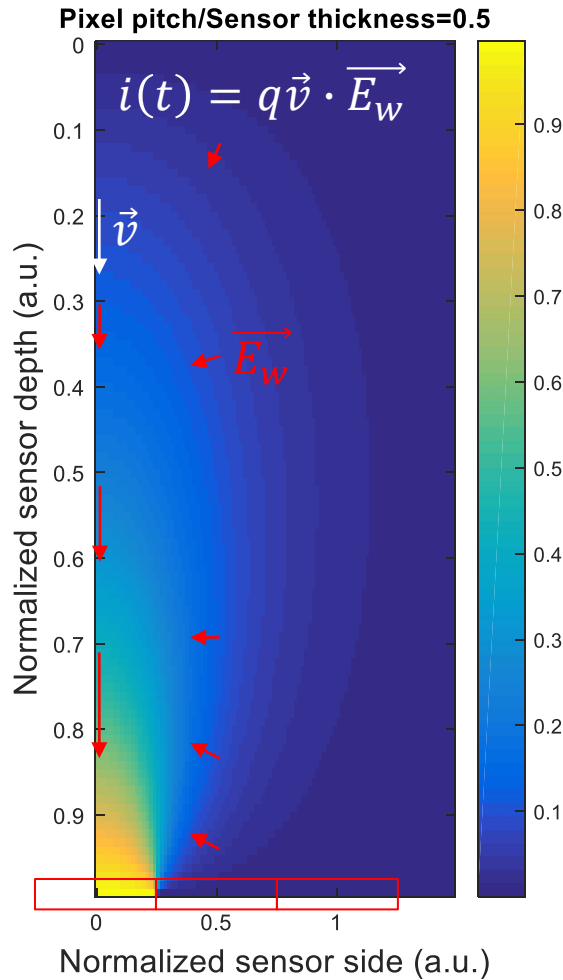
W.Shockley, J. Appl. Phys. 9, 635 (1938)

V. Radeka Ann. Rev. Nucl. Part. Sci. 1988 38: 217-277

Gatti et al., NIMA 193 (1982) 651

Induced signal on detector electrodes

Example of calculation of the weighting potential in pixelated system (Pitch/Thickness=0.5)



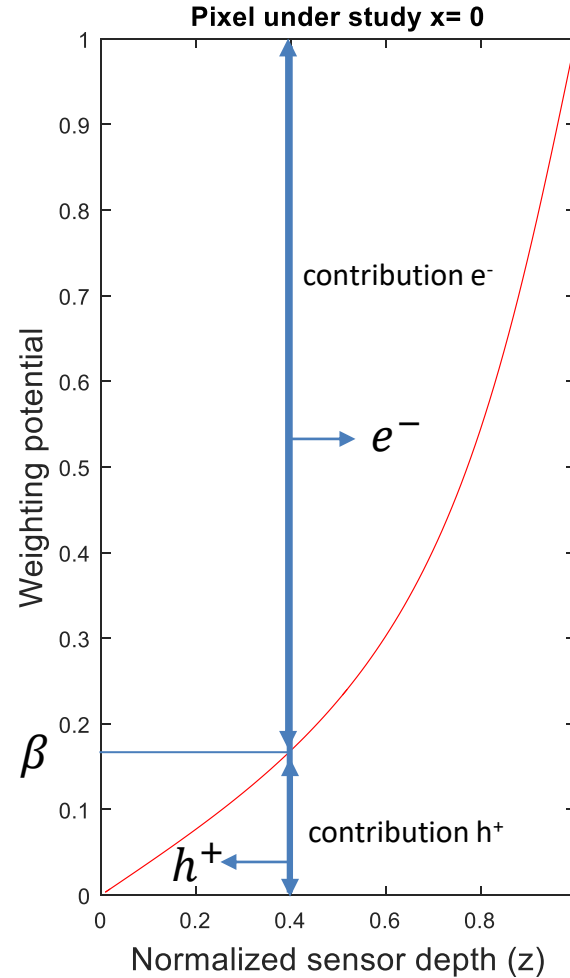
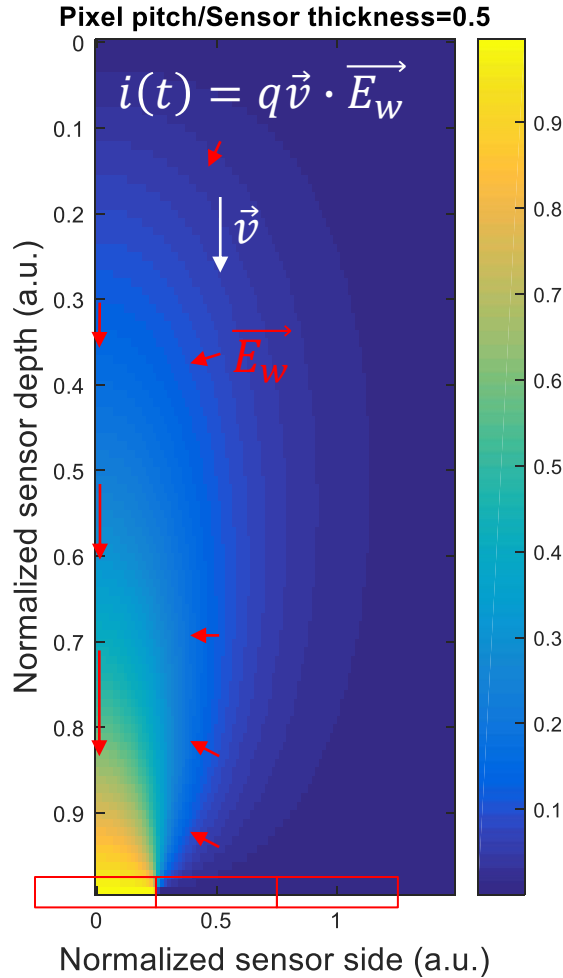
Electron motion contribution: $-n_0q(1-\beta)$

Hole motion contribution: $n_0q(0-\beta)$

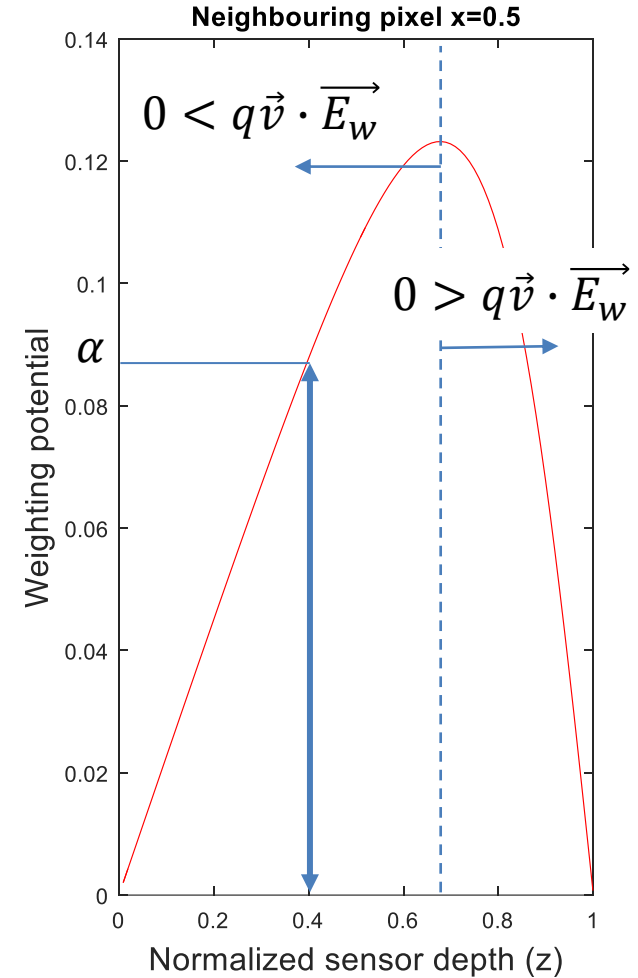
Total induced charge: $-n_0q$

Induced signal on detector electrodes

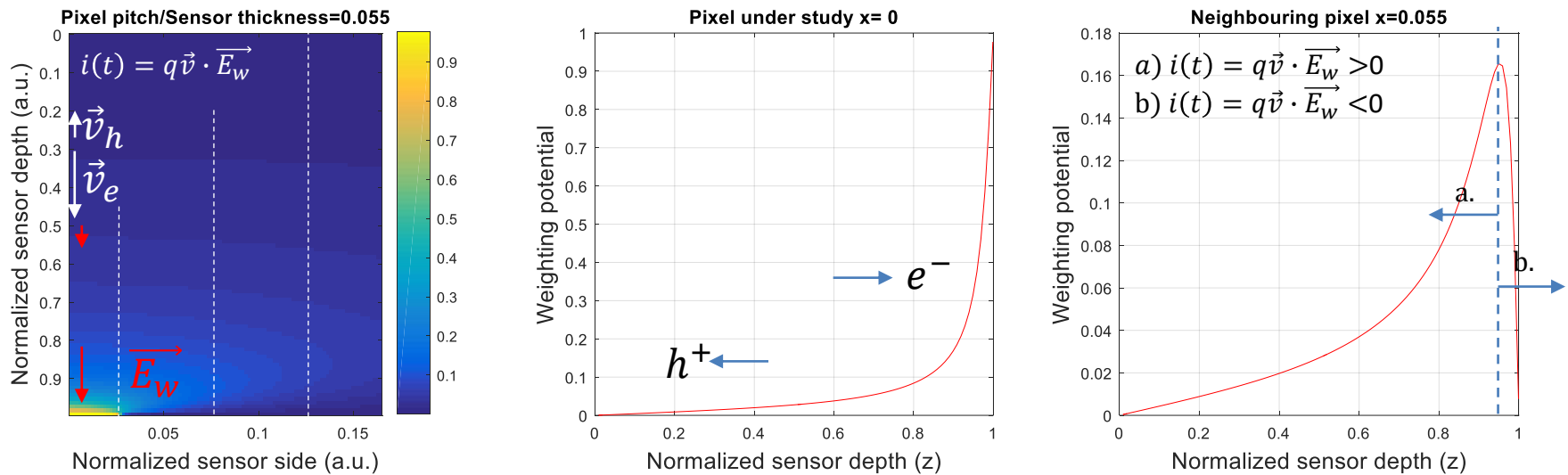
Example of calculation of the weighting potential in pixelated system (Pitch/Thickness=0.5)



Electron motion contribution: $-n_0q(1-\beta)$
 Hole motion contribution: $n_0q(0-\beta)$
 Total induced charge: $-n_0q$



Electron motion contribution: $-n_0q(0-\alpha)$
 Hole motion contribution: $n_0q(0-\alpha)$
 Total induced charge: 0
 But there is a transient induced signal!

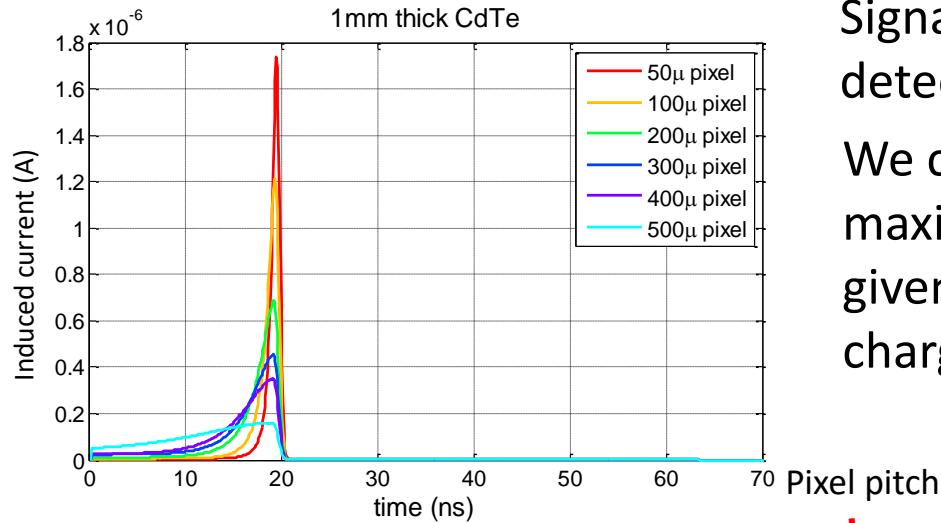
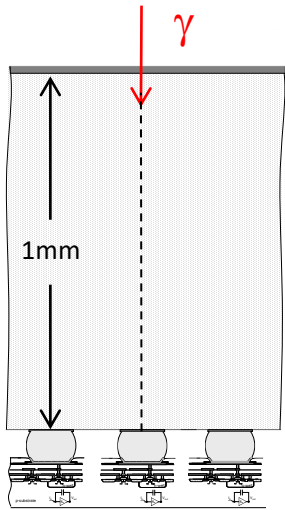


The carrier that drifts towards the pixel electrodes will contribute to most of the charge induced on the pixel electrode. Furthermore, it is the motion close to the pixel surface that contributes most strongly to the induced charge.

For detectors in which electrons are much more mobile than holes, deriving the signal from a small pixel rather than from a large-area anode can help improve energy resolution by minimizing sensitivity of the pulse amplitude to the motion of the positive charges that may not be completely collected.

The **small pixel effect** is the consequence of signal induction process in a segmented detector.

Signal induction in the pixel electrodes



Signal shape depends on detector geometry

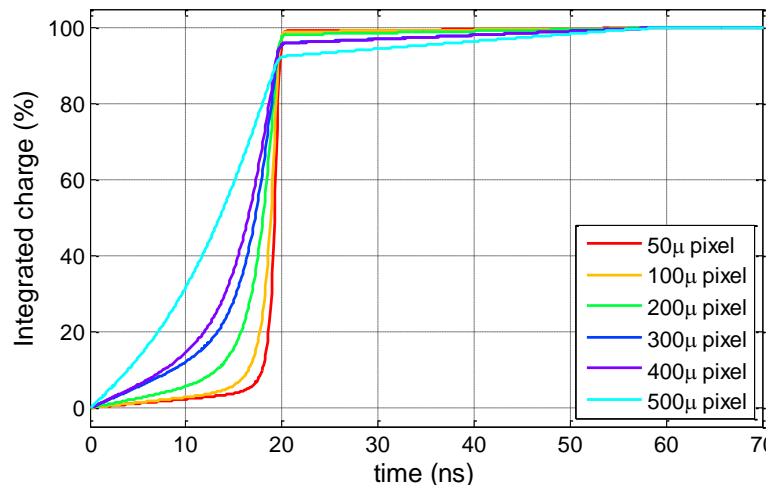
We calculate the maximum count-rate for a given pixel size for a given charge integration time

Time to integrate a given percentage of the charge

Pixel pitch	$t_{90\%}$	$t_{97.5\%}$
50 μm	2.4ns	13.5ns
300 μm	14.7ns	38.2ns

We assume $t_{x\%} = t_p$ and $\tau = 2t_p$

$$\frac{1}{\tau} \frac{1}{\text{pixel area}} \left[\text{Mcps} / \text{mm}^2 \right]$$



- 1mm CdTe
- 60keV photon
- 600V sensor bias
- Energy deposition at $z=240\mu\text{m}$
- (No charge trapping, charge sharing included in simulation)

Message: The geometry of the sensor (pitch/thickness) determines the shape of the induced current pulse (and puts a lower limit on the electronics integration time)

